Sunlight-based Passive VLC

Utilizing the sun to establish wireless connections

Chavez Tapia, M.A.

DOI
10.4233/uuid:5e9bee9e-16fa-427e-bae0-5a65525c098e

Publication date
2025

Document Version
Final published version

Citation (APA)
Chavez Tapia, M. A. (2025). *Sunlight-based Passive VLC: Utilizing the sun to establish wireless connections*. [Dissertation (TU Delft), Delft University of Technology].
https://doi.org/10.4233/uuid:5e9bee9e-16fa-427e-bae0-5a65525c098e

Important note
To cite this publication, please use the final published version (if applicable).
Please check the document version above.

SUNLIGHT-BASED PASSIVE VLC

UTILIZING THE SUN TO ESTABLISH WIRELESS CONNECTIONS

SUNLIGHT-BASED PASSIVE VLC

UTILIZING THE SUN TO ESTABLISH WIRELESS CONNECTIONS

Proefschrift

ter verkrijging van de graad van doctor
aan de Technische Universiteit Delft,
op gezag van de Rector Magnificus Prof.dr.ir. T.H.J.J. van der Hagen,
voorzitter van het College voor Promoties,
in het openbaar te verdedigen op maandag 27 januari 2025 om 12:30 uur

door

Miguel Antonio CHAVEZ TAPIA

Master of Research,
University of Cambridge, Cambridgeshire, United Kingdom,
geboren te Lima, Perú.

Dit proefschrift is goedgekeurd door de promotoren

Samenstelling promotiecommissie:

Rector Magnificus,	voorzitter
dr. ir. M.A. Zuñiga Zamalloa	Technische Universiteit Delft, promotor
prof. dr. K.G. Langendoen	Technische Universiteit Delft, promotor
Onafhankelijke leden:	
Prof. dr. P. Casari	University of Trento, Italy
Prof. dr. M. Katz	University of Oulu, Finland
Prof. dr. F.A. Kuipers	Technische Universiteit Delft
Dr. J. Liang	Technische Universiteit Einhoven
Overige leden:	
Prof. dr. G. Smaragdakis	Technische Universiteit Delft

The work in this dissertation has been part of the *LuxSenz* project, a *TOP-Grant, Module 1, Physical Sciences* with project number 612.001.854, which is financed by the Dutch Research Council (Nederlandse Organisatie voor Wetenschappelijk Onderzoek, NWO).

Keywords:	Passive Visible Light Communication, Embedded Systems, Internet-of-Things, Sunlight Communications
Printed by:	Johannes Gutenberg
Front & Back:	Beautiful cover art that captures the entire content of this thesis in a single illustration.

ISBN 000-00-0000-000-0

An electronic version of this dissertation is available at
http://repository.tudelft.nl/.

Nothing in science has any value to society
if it is not communicated.

Anne Roe

CONTENTS

SUMMARY

Nowadays, wireless connectivity is ubiquitous: humans use smartphones, smartwatches, laptops and other devices, while at the same time, the Internet of Things (IoT) is adding millions of connected objects. This large number of devices uses mainly the radio frequency (RF) spectrum for communication. And a direct consequence of this exponential growth is the scarcity of free RF bands to cope with this demand.

To tackle this challenge, researchers have proposed using a different carrier: visible light. With *Visible Light Communications* (VLC), devices communicate with each other by modulating the intensity of their light-emitting diodes (LEDs) and demodulating it using light sensors. The key advantage of VLC is the utilization of the visible light spectrum, with free bands that do not interfere with traditional RF systems. Nonetheless, despite the efficiency of LED technology, luminaries still require several Watts to generate light. The need for this considerable amount of energy has triggered interest in a new research area: *Passive VLC*. The fundamental principle of Passive VLC is to exploit *ambient light* to create wireless links, thus reducing the energy required by transmitters to generate their own light.

Passive VLC is a promising area, but poses a daring challenge: modulate light without any control over the source. The research community has proposed using optical surfaces that block or reflect light dynamically as modulators, but these platforms provide limited data rates, ranging from a few tens of bps to a few kbps. Moreover, using the sun as the source of ambient light introduces another challenge: variations in position and intensity.

This dissertation aims to improve the performance of Passive VLC systems operating with sunlight, with a particular focus on increasing the data rate and resilience to the changing sun's position.

Our first contribution is a short-range wireless link using a tiny screen as a transmitter and a camera as a receiver. The screen is a reflective surface, adapted to work with ambient light. The sunlight reaching the screen is modulated to transmit information to a smartphone's camera, creating a stream of optical data. This screen-to-camera link using sunlight attains up to 10 kbps, ten times faster than previous similar systems, working from sunrise to sunset - independent of the sun's position.

Inspired by the concept of Li-Fi, which combines illumination and VLC, our second contribution envisions the creation of a *natural* light bulb with wireless communication capabilities. Our design combines optical modulators, optical filters and sunlight collectors to track the sun's position during the day and radiate modulated beams of sunlight in indoor scenarios. These beams of natural light provide illumination and communication and are the first to divide sunlight into two color channels to double the data rate.

Our third contribution proposes a novel link for robots to communicate using sunlight. We leverage a material used in solar technology, the Luminescent Solar Concentrator (LSC). An LSC surface absorbs light from its top and emits it on its edges. We place

LSCs on top of robots, together with liquid crystal cells (LCs), so sunlight arriving from the top can be modulated into data packets transmitted toward the edges. This novel communication system allows task coordination between robots using sunlight.

Overall, this dissertation presents new *Passive VLC* systems focusing on applications that exploit the sun as the light source. Within this scenario, our focus has been to increase the data rate, with the first two contributions, and on making the systems resilient to the sun's position, with all three contributions.

1

INTRODUCTION

There is a crack in everything,
that's how the light gets in.

Leonard Cohen

1

WIRELESS connectivity is an essential component of people's daily interactions and there is a growing demand for faster and more pervasive wireless communication. The arrival and advances of the *smartphone* changed how humans study, work, manage their finances, shop, listen to music, watch films and interact socially, among other tasks. The demand for these devices is evident: mobile network subscriptions have grown from less than 2 billion in the early 2000s to almost 9 billion in 2023 [1]. But users do not only demand more wireless network connections: applications such as media streaming, video-conferencing, social media and gaming leverage higher connection speeds provided currently by LTE (60 % of mobile subscriptions in 2023) and it is projected that by 2028 5G will surpass LTE as the major technology for mobile connectivity while providing speeds 100 times faster [2]. People crave fast and ubiquitous mobile wireless connectivity.

There is, however, a relative newcomer in the market with its own demand for wireless connectivity and growing at an astonishing rate: the *Internet of Things* (IoT). IoT devices, which are embedded systems featuring sensors and network connectivity, are used to collect and share different types of data. Due to their ease of installation, IoT devices are currently used in various industries such as smart cities/homes, supply chain, agriculture, wearables, smart factories, utility supply and healthcare among others. The rapid rise of these devices is clear: the number of IoT connections increased from less than 2 billion in the early 2010s to 15 billion in 2023 with a forecast to increase to ~30 billion by 2030 [3, 4]. The current IoT demands significant wireless connectivity and the deployment of more devices in the future will only push this demand up.

A consequence of the increasing demand for wireless systems, aside from the increased research interest in the topic, is the high demand for energy required to operate them: mobile networks account for around 66 % of the total transmission networks' power [5]. The energy transition to *greener technologies* is transversal to, and impacts, multiple industries, if not all. Therefore, wireless technologies should also explore the possibilities of more energy-friendly solutions to reduce their energy footprint.

1.1. WIRELESS COMMUNICATIONS

Sending messages over the air is an activity that humans have performed since ancient times. Thousands of years ago, people signaled each other using torches, smoke signals, and flags. These rudimentary ways of communication are still used nowadays, for instance in airports to give indications to pilots while taxing. However, around 100 years ago, a pivotal event in wireless communication took place: the spawn of *radio frequency technology*.

1.1.1. RADIO FREQUENCY SYSTEMS

In 1873, Charles Maxwell published four equations explaining the behavior of electric and magnetic (or *electromagnetic*) fields. Based on the principles outlined by these equations, Heinrich Hertz expanded the *electromagnetic theory* and, between 1885 and 1889, Hertz transmitted *electromagnetic waves* over the air at a short distance, which were converted into electricity at the receiver. But it was in 1895 when Guillermo Marconi transmitted wireless telegraphy messages using radio over a distance of 2.4 km, that radio frequency wireless communication was born.

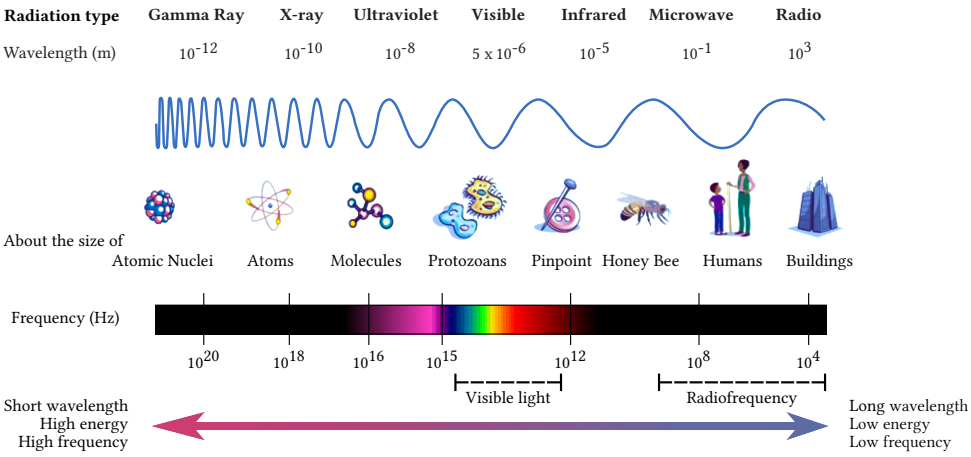

Figure 1.1: Electromagnetic Spectrum. Modified from [6].

Radio frequency has been the dominant technology for wireless communication, constantly evolving for the last 100 years. The early applications of radio wireless were in maritime, military and transatlantic communications. During its history, radio systems were and are still used for audio broadcasting (AM and FM radio), television (TV) broadcasting, navigation, satellite communication, and mobile telephony, among other services. However, during the last 30 years, the appearance of mobile devices such as portable personal computers and smartphones spawn a new application of radio: ubiquitous data access. Whether using a wireless local area network (WLAN), commercially known as WiFi, or cellular networks for smartphones, radio provides the last-mile connection to such devices. Finally, the more recent development of IoT devices has also triggered new radio-based links, such as LoRaWAN, BLE, Zigbee or NB-IoT, to provide network access to these devices. Nowadays, radio wireless connectivity is a ubiquitous asset for humans and mobile computing systems.

CURRENT STATE OF RADIOFREQUENCY COMMUNICATION

The popularity of services based on radio wireless systems has created a critical drawback: a **spectrum crunch**. The *radio frequency spectrum* spans from 3 Hz to 3 THz in the electromagnetic spectrum (Figure 1.1) and within this range, each service is allocated a specific frequency band. The large number of services requiring radio bands has occupied most of this spectrum and as an example Figure 1.2 presents the US radio frequency spectrum allocation, showing almost no free bands available to allocate new services.

We can list two direct consequences of the scarcity of radio bands:

1. **The decommission of services or the borrowing of RF bands from existing services.** During the London 2012 Olympics, the demand for wireless connections was so high that the British communication regulator had to decommission analog TV signal bands and borrow bands from the Ministry of Defense to increase the capacity of wireless systems [7].

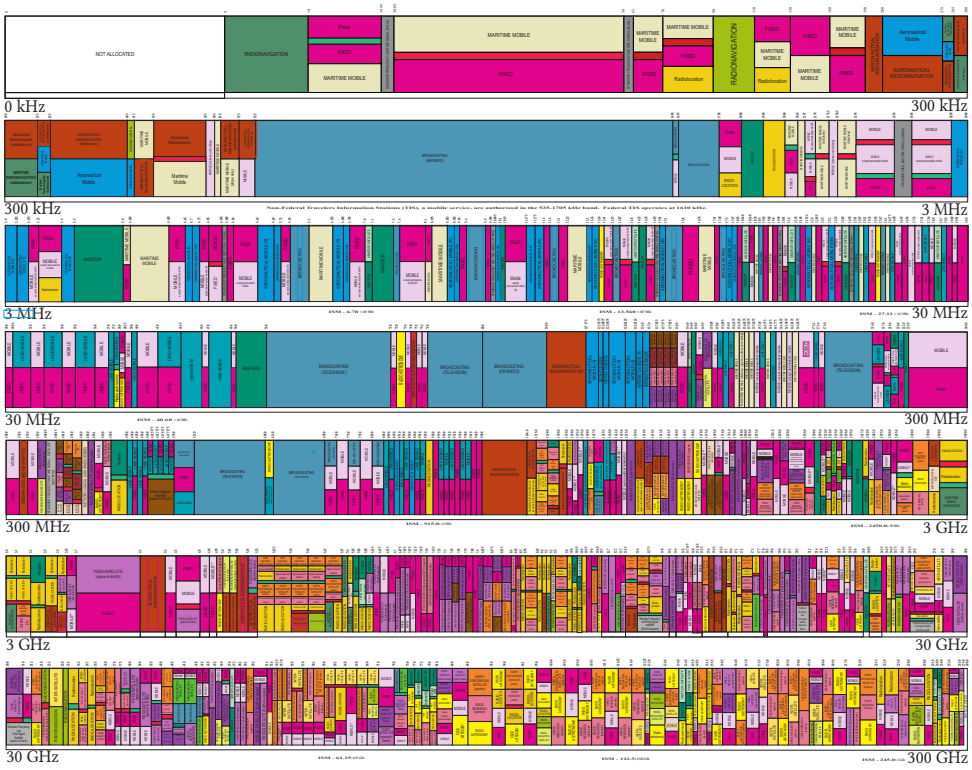

Figure 1.2: RF spectrum allocation in the US[10]. Each colored box represents a service.

2. **A high price for RF band auctions.** A recent bid for 5G bands in the US led to the highest auction cost in history, adding up to 81 billion US dollars for a spectrum of 280 MHz in the 3.70–3.98 GHz band [8]. To put this amount in perspective, one could buy the 3 most profitable airlines in the world with the amount paid in that spectrum auction [9].

To tackle the so-called spectrum crunch, the research community has explored alternatives to radio frequency to create wireless links. In the next section, we explore one popular solution.

1.1.2. VISIBLE LIGHT COMMUNICATION (VLC)

Light is the fastest physical carrier to transfer information between two points: the internet backbone is underpinned by links of optical fibers connecting computing devices separated by large distances. The use of light to create wireless connections was explored by Alexander Graham Bell in the 1880s with the invention of the photophone, which transmitted voice by modulating sunlight over a distance of a few hundred meters[1]. However, it was not until the early 2000s [11] that the research community started

[1] Note that this predates the transmission of speech by radio.

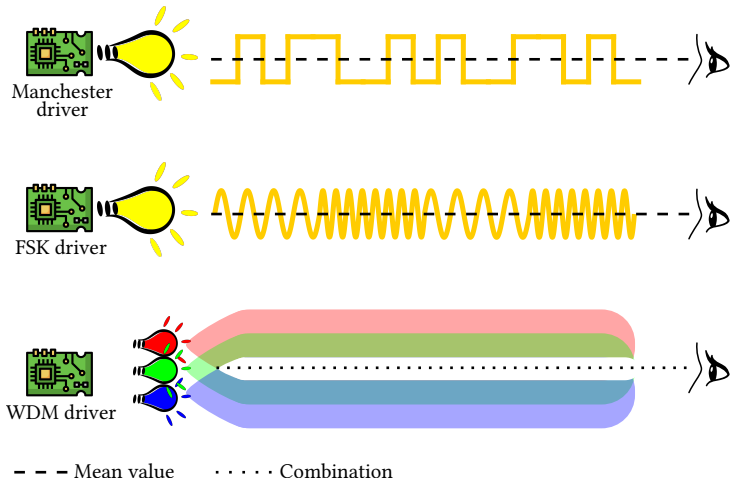

Figure 1.3: Types of VLC modulations and multiplexing techniques. A key aspect of VLC output is that it should not disturb the human eye. The dashed line represents the average intensity and the dotted line is the combination of colours. FSK: frequency shift keying, WDM: wavelength division multiplexing. Using icons from *Flaticon*.

to explore again the use of visible light using light-emitting diodes (LEDs), which can be directly modulated to send data, a technique called *visible light communication* (VLC).

Visible light and radio are electromagnetic waves[2], and they are both located within the electromagnetic spectrum. Nonetheless, the visible light spectrum is located outside of the already crowded RF spectrum, as shown in Figure 1.1. VLC systems have the potential to increase the capacity of wireless communication by creating links using a different carrier, light, located in a *free band* of the electromagnetic spectrum.

VLC MODULATION

One key difference in the nature of light compared to radio waves is its visibility: the human eye can perceive visible light. Thus, while modulating a light source, special attention needs to be considered to avoid distressing people's perception due to flickering. To avoid this effect, we can leverage the fast response of LEDs in combination with various modulation techniques[3]. Figure 1.3 presents some of these modulation techniques. For instance, intensity modulation using Manchester encoding balances the high- and low-intensity symbols equally, maintaining a constant average intensity of 50 %. Another type of modulation is frequency shift keying (FSK) in which each symbol is represented by a different frequency, while the average intensity is kept constant. The evolution of VLC in the last two decades has led to attaining speeds in the order of Gbps, leveraging sophisticated optical methods such as wavelength division multiplexing (WDM), which

[2] Light is considered both a wave and a particle according to quantum mechanics.
[3] Due to the relatively slow response of human vision, for light oscillations higher than ~200 Hz, the human eye perceives the oscillation's average intensity.

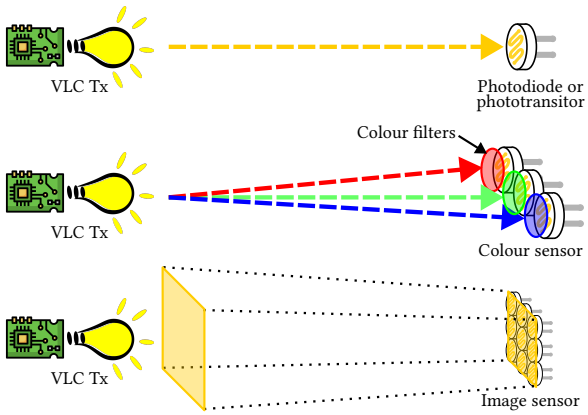

Figure 1.4: Different types of devices used as receivers in VLC. Using icons from *Flaticon*.

divides light into independent color channels to increase link capacity while still rendering a white light when the channels are combined.

VLC DEMODULATION

The nature of a VLC carrier requires the use of a light sensor for detection and demodulation, a device that plays a similar role as an RF receiving antenna. The light sensor performs an optoelectrical conversion: it gathers photons and produces electrons or changes electrical properties. Some of the most popular light sensors are:

- Photodiode. A current, the reverse flow of electrons, is created depending on the intensity of light reaching the PN junction.
- Phototransistor. Similar to a regular transistor, an electrical signal is produced and amplified proportionally to the photons reaching the base/gate of the transistor.
- Color sensor. An array of photodiodes with color filters, thus each single device can only detect the part of the light spectrum corresponding to the color.
- Image sensor. By implementing more complex optical elements, image sensors or cameras capture an area using an array of single photodetectors.

Figure 1.4 shows these types of devices within a VLC link.

1.2. ENERGY COST OF WIRELESS SYSTEMS

All over the world, there is a general trend to switch to *green technologies* rapidly. Due to the large amount of electricity used in mobile networks, reducing the energy footprint of wireless communications can play a significant role and the research community can also contribute to *greener* solutions: wireless systems with reduced power consumption.

A subtype of wireless systems, aimed at reducing energy consumption, is known as *passive systems*. These systems leverage energy already present in the environment to create wireless links and send information.

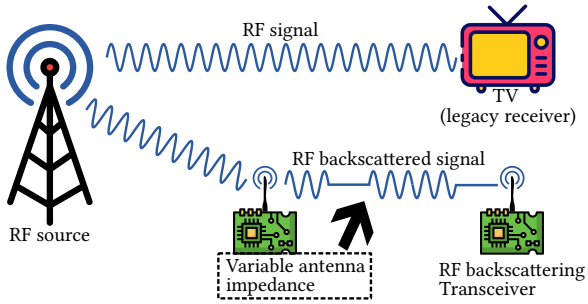

Figure 1.5: RF ambient backscattering system. An RF source, such as a base station, generates RF waves for systems, such as TV broadcasting, and a small device harvests this RF energy for power and modifies the impedance of an RF antenna to modulate the original RF waves. Using icons from *Flaticon*.

1.2.1. PASSIVE WIRELESS SYSTEMS

RF AMBIENT BACKSCATTERING SYSTEMS

The pervasiveness of RF signals (such as radio and TV) allows the creation of links that harvest these radio waves and convert them to electricity. While the amount of harvested electricity is limited, it can provide enough energy to power a simple modulator that changes an antenna's impedance. These changes in impedance reflect (or backscatter) the radio waves present in the environment but are embedded with the modulated information. A schematic of an RF ambient backscattering system is presented in Figure 1.5.

PASSIVE VLC SYSTEMS

Whether by artificial or natural means, light is a ubiquitous resource because human activity requires its presence. The almost omnipresence of light has triggered research interest in using ambient light to create VLC links. These systems, known as *Passive VLC*, utilize two types of light sources:

1. **Artifical light.** Several of these passive VLC links implement a type of backscattering reflection towards the source, such as ceiling lights [12, 13] or vehicle head-

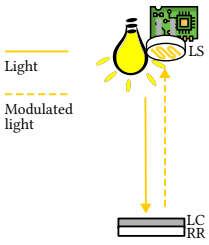

(a) Passive VLC using artificial light only.

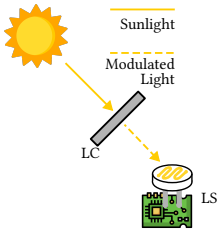

(b) Passive VLC using sunlight passing through an LC.

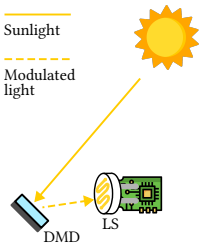

(c) Passive VLC using sunlight being reflected by a DMD.

Figure 1.6: Passive VLC systems using different sources. LC: liquid crystal, RR: retro-reflector, LS: Light sensor, DMD: digital micro-mirror device. Using icons from *Flaticon*.

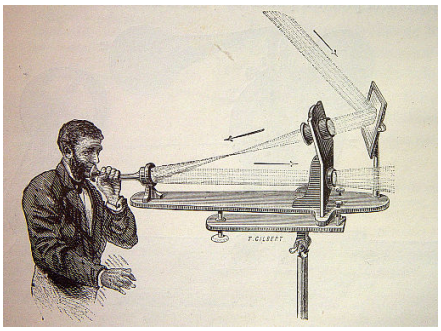

(a) Photophone transmitter [19].

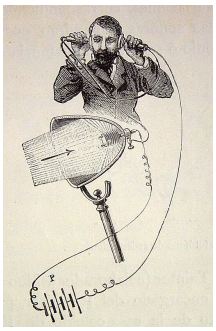

(b) Photophone receiver [19].

(c) Heliograph [20].

Figure 1.7: Early systems employing sun for wireless communications.

lights [14, 15], using special reflecting surfaces (retro-reflector). For example, by using a liquid crystal (LC) shutter, an optical device that dynamically blocks light or allows it to pass through, the reflected light is modulated and later captured by a light sensor close to the light source, as depicted in Figure 1.6a.

2. **Sunlight.** In the 1800s, systems like the photophone and the heliograph, depicted in Figure 1.7, leveraged mirrors or reflective surfaces to modulate sunlight. While the idea of using sunlight for communication was not further explored after this period, more recent *Passive VLC* studies employ a similar system using novel optical modulators, such as LC shutters to modulate light coming through a window [16, 17], or Digital Micro-Mirror Devices (DMDs) to reflect sunlight towards the light sensor [18], as depicted in Figure 1.6b and Figure 1.6c, respectively.

Comparison among passive wireless systems. While both the passive RF and VLC systems outlined in this section use energy from the environment to create wireless links, only *Passive VLC* systems can exploit *natural* resources. Radio waves are naturally generated by cosmic sources, but they cannot be harnessed for communications. Passive RF requires human-made signals, such as those created for TV, radio, WiFi, and LoRa. *Passive VLC*, on the other hand, is the only one able to leverage a vast source of natural light, such as the sun, enabling *sunlight communications*. Using a natural resource potentially reduces energy consumption because no power is required to generate light to backscatter. Nonetheless, advances in *Passive VLC* using sunlight have been limited mostly by the speed of the light modulators available. To briefly capture this situation, Table 1.1 compares different passive wireless systems.

1.3. PROBLEM STATEMENT

Overall, most active wireless systems, including RF and VLC, achieve high speeds, rendering links in the order of Mbps or even Gbps. If we focus our attention towards power consumption, passive systems consume less power but their adoption has focused mainly on low data rate links. *Passive VLC* systems attract attention due to their ability to reuse the vast and free energy provided by the sun. However, these systems have two main

	Source	Power
Ambient radio	TV tower	0.1 kW to 11 kW [21]
	Radio tower	0.5 kW to 20 kW [22]
	Cellular tower	40 W to 160 W [23]
Ambient light	Ceiling light (LED)	4 W to 22 W [24]
	Car headlights (LED)	13 W to 24 W [25]
	Sun	0 W

Table 1.1: Electrical power required by *sources* of passive wireless communication systems.

limitations. First, the attainable data rates of most *Passive VLC* systems are limited to a few kbps, due to the slow speed of the light modulators. Second, the position of the sun has a dramatic effect on the performance of the system. This occurs because changes in the sun's position require (re)aligning the link between the transmitter and receiver, affecting the link's reliability. This dissertation aims to address these gaps by answering the following research question:

What new optical devices and methods can be implemented in *Passive VLC* to improve its performance?

1.3.1. THE APPROACH AND OUTLINE OF THIS THESIS

For this dissertation, we aim at improving *Passive VLC* in two main ways: higher data rates and independence from the sun's position. Our vision is straightforward: leverage devices, materials or methods developed in other optical fields, and use them to build *Passive VLC* systems that can work with artificial light sources, such as ceiling lights, but must also work using the sun as the source of light. The structure of the dissertation is described next and Figure 1.8 depicts each contribution.

Sunbox. Previous works in *Passive VLC* use liquid crystal as the light modulator. The most common type of liquid crystal used is the nematic liquid crystal (or a sub-variant) with a particularly slow optical switching speed between its transparent and opaque states. The slow response, in the order of ms, stems from the chemical properties of the nematic liquid crystal material. In Chapter 2, we explore the use of a different type: a ferroelectric liquid crystal (FLC) that has a faster response, in the order of µs. However, the commercial availability of FLC is limited to the projection technology in the form of small FLC pixel arrays that cast images using sophisticated optical components and control electronics. Using one small FLC, part of a micro-projector, we implement a system dubbed Sunbox that manages to backscatter both ceiling light and sunlight towards a smartphone camera to convey information, creating a short-range passive VLC link with several kbps.

Sol-Fi. In 20112, Prof. Harald Haas coined the term *Li-Fi* in his TED talk *"Wireless Data from Every Lightbulb"*, demonstrating the potential of using VLC lightbulbs that can provide illumination and wireless connectivity simultaneously. In Chapter 3, we combine

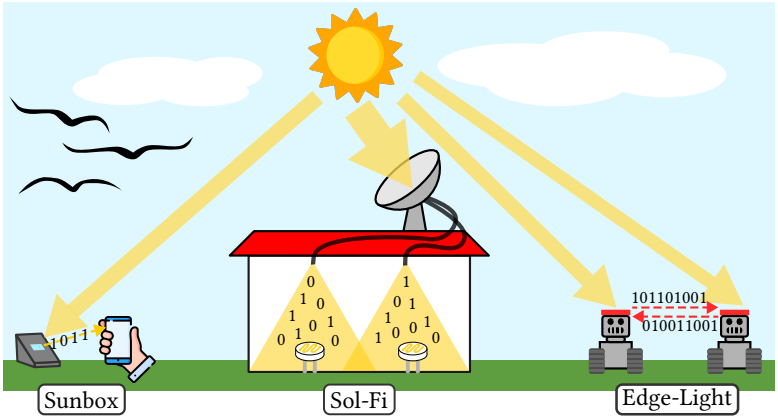

Figure 1.8: Summary of contributions of this dissertation.

the concept of *Li-Fi* and *Passive VLC* by using daylighting systems in combination with light modulators to create a *natural VLC light bulb*. This novel light bulb renders indoor sunlight illumination and wireless connectivity using a single phototransistor as a receiver. Furthermore, expanding on the concept of WDM, vastly used in optical networks, our system implements a *multichannel Passive VLC* system, modulating two colors independently and recombining them into white light used for illumination while doubling the attainable data rate.

Edge-Light. The development of solar technologies is a source of inspiration for *Passive VLC*. A particularly valuable technology is the luminescent solar concentrator (LSC), which has been used for around 40 years in combination with solar cells. An LSC absorbs a part of the sunlight spectrum (or color band) and re-emits light in a different spectrum on its edges. The spectrum emitted at the edges is captured by solar cells to harvest energy. In Chapter 4, we explore the possibilities of implementing a *Passive VLC* link using LSC layers in combination with liquid crystals as modulators. The light modulated in different spectrum bands is decoded by color sensors on the receiver. We demonstrate a potential application of this system in short-range robot-to-robot communications that exploits sunlight-fueled wireless communication to coordinate tasks between two robots.

RELATED PUBLICATIONS

Chapters 2, 3 and 4 are based on the following publications:

- **Miguel Chávez Tapia**, Talia Xu, Zehang Wu, Marco Zúñiga Zamalloa (2022). SunBox: Screen-to-Camera Communication with Ambient Light. *Proceedings of the ACM on Interactive, Mobile, Wearable and Ubiquitous Technologies (IMWUT).*
- **Miguel Chávez Tapia**, Talia Xu, Marco Zúñiga Zamalloa (2024). Sol-Fi: Enabling Joint Illumination and Communication in Enclosed Areas with Sunlight. *Proceedings of the ACM/IEEE International Conference on Information Processing in Sensor Networks (IPSN).*

- **Miguel Chávez Tapia**, Diego Palma Rodríguez, Marco Zúñiga Zamalloa (2024). Edge-Light: Exploiting Luminescent Solar Concentrators for Ambient Light Communication. *Proceedings of the ACM on Interactive, Mobile, Wearable and Ubiquitous Technologies (IMWUT).*

Additionally, the following publications are also a result of the doctorate program, but are not part of the dissertation:

- Talia Xu, **Miguel Chávez Tapia**, and Marco Zúñiga (2022). "Exploiting Digital Micro-Mirror Devices for Ambient Light Communication". *Proceedings of USENIX Symposium on Networked Systems Design and Implementation (NSDI).*
- Talia Xu, Mirco Muttillo, **Miguel Chávez Tapia**, Patrizio Manganiello, Harald Haas, Marco Zúñiga Zamalloa (2024). Sunlight-Duo: Exploiting Sunlight for Simultaneous Energy Harvesting & Communication. *Proceedings of the International Conference on Embedded Wireless Sensor Networks (EWSN).*
- **Miguel Chávez Tapia** Daniel Tomas Menacho Ordoñez, Kiara Micaela Rodriguez Bautista, Talia Xu, Davorka Medvedović, Marco Zúñiga Zamalloa (2024). T-light: A Platform Based on Flashlights and Robots to Teach Wireless Communication to Children and Teenagers. *Proceedings of the International Conference on Embedded Wireless Sensor Networks (EWSN).*

2

SunBox: Screen-to-Camera Communication with Ambient Light

In this chapter, our exploration of Passive VLC begins by analyzing the use of a camera as a receiver, which has the advantage of being a ubiquitous device. However, as a receiver, an average smartphone camera is slow, sampling frames at 30 FPS or 240 FPS for high-speed video recording. Its use in Passive VLC has been limited to single-pixel transmitters, an LC cell, with speeds of a few bps. Inspired by screen-to-camera communication of Active VLC systems, which use both multi-pixel transmitter and receiver, we design a system that adapts a small reflective screen to backscatter ambient light. The screen embeds information into the reflected light, and the smartphone's camera captures and decodes it.

Our final prototype is tested under different conditions and light sources: artificial ambient light and natural sunlight, reaching speeds between 2 kbps and 10 kbps using a low-end camera with just 30 FPS.

2.1. INTRODUCTION

While VLC systems leverage the free light spectrum, they can also leverage the pervasiveness of various types of LEDS in our environments, as transmitters, and cameras on mobile devices, as receivers. Broadly speaking, there are two kinds of optical links using light sources as transmitters and smartphones as receivers: LED-to-camera and screen-to-camera. In these two systems, the light sources transmit information by modulating their intensity at relatively high speeds (hundreds of Hz), and smartphones capture these patterns with cameras that usually operate between 30 to 120 frames-per-second (FPS). When a single LED is used for transmission, every captured frame contains one bit or at most a few bits of information. LED-to-camera links are simple to implement but result in low data rates. Depending on the type of modulation, binary or rolling shutter, those systems achieve from less than 100 bps [26, 27] to 100 kbps [28, 29, 30]. Screens, on the other hand, contain millions of tiny LEDs (pixels). With those pixels, displays can create more complex patterns, similar to QR codes, containing thousands of bits on every frame. This property enables screen-to-camera links to reach data rates beyond 100 kbps [31, 32, 33, 34, 35].

The above systems are enabling a wide range of new applications, from indoor positioning [36, 37] and human-computer-interaction [27, 26], to streaming services [35, 38]. The *transmitters* of these systems, however, have two limitations. First, they require modifying the operation of the light source (LED or screen), which is not always possible. Second, they often require a significant amount of power. For example, a standard LED bulb can consume several watts, and a simple monitor requires several tens of watts.

To overcome the above limitations, researchers are proposing *passive* methods that use *ambient light* for communication. Contrary to the aforementioned *active* systems, which require direct control of the light source to modulate its intensity, *passive* methods work with any ambient light, natural (coming from the sun) or artificial (coming from a light bulb). The basic principle of most *passive* systems is to modulate the intensity of ambient light using liquid crystals. A liquid crystal (LC) cell placed between two polarizers can be seen as an optical shutter that switches between opaque and semi-transparent states to transmit logical 0s and 1s. In these novel *LCD-to-camera* systems, the LCD transmitters consume power in the order of a few tens of mW and do not require any modification of the light source [17].

Challenge. Similar to LED-to-camera systems, the main limitation of current LC-to-camera links is their low data rate. The problem of using a single LED (or a single LC cell) is that the transmitter only has a single pixel to send information. To increase the data rate, we require a multi-pixel modulating surface, similar to a screen but operating with the surrounding ambient light.

Contributions. Motivated by advances in reflective display technology, which backscatters sunlight to create images [39], we propose the first screen-to-camera system that works solely with ambient light. The aim is to deploy small screens, a few millimeters in size, so users can place their phone near the screen to receive data: *such a system implements an optical wireless link with a range similar to near-field communication (NFC) technology but using ambient light as the carrier and the smartphone's camera as a receiver.* Our system, called *SunBox*, will enable all types of smartphones, from low- to high-end, to rely only on their camera to obtain a near-field optical link. Overall, our

work provides three main contributions.

Contribution 1 [section 2.3]: A system that achieves secure screen-to-camera communication with ambient light. Taking as a basis a tiny projector designed for near-eye applications (short-range projection), we propose a novel optical design that removes the embedded LEDs of the original system so it can operate solely with ambient light. The system is enclosed in a custom-designed 3D box that prevents eavesdropping.

Contribution 2 [section 2.4]: A robust optical link under varying lighting conditions. SunBox is designed to work indoors, with different types of artificial lighting; and outdoors, where the spectrum and intensity of sunlight change constantly. This wide range of conditions affects the performance of the optical link. We combine various signal processing and error-correcting methods to provide reliable ambient light communication.

Contribution 3 [section 2.5 and section 2.6]: A prototype implementation and a thorough evaluation. We build a prototype and test it with different types of phones, data densities and ambient light. Considering all these variables, our results show that the goodput reaches between 2 and 10 kpbs, providing reliable connections indoors and outdoors, even with low-end phones.

2.2. BACKGROUND

2.2.1. SHORT-DISTANCE WIRELESS TECHNOLOGY

Traditional short-distance wireless links, like NFC or Bluetooth Low Energy (BLE) use radio waves as their carrier and their hardware modules consume low power. BLE is widely adopted and NFC hardware is available in around 60% of smartphones[1]. However, both are prone to interference with other signals in the radio-frequency spectrum.

To overcome this limitation, the research community has proposed the use of magnetic fields, such as Pulse[40] and MagneComm[41]. These approaches exploit the magnetic sensor present in all smartphones, but it has a limited data rate and it is exposed to the magnetic field created by different appliances. Our work presents SunBox. An approach that uses the free and open spectrum provided by ambient light and requires only a camera as a receiver, which is present in virtually all smartphones. SunBox achieves data rates that are orders of magnitude higher than magnetic approaches while consuming less power than some of them. Table 2.1 positions the pros and cons of SunBox with respect to other short-distance wireless technologies. In the next sections, we analyze different types of displays to find the best fit for our screen-to-camera approach.

2.2.2. IDENTIFYING THE RIGHT TYPE OF DISPLAY

Display technology offers different options for various kinds of scenarios. A popular option is e-ink, but it is too slow, as it offers refresh rates of ~3 Hz. Among other low-power display technologies, two types have (partial) properties suitable for SunBox: microdisplays and reflective displays.

Microdisplays are small, a few mm in size, and they are designed to work in enclosed near-eye applications, such as virtual reality headsets. This setup is similar to the one envisioned for SunBox, where the enclosed environment provides a secure optical link

[1] NFC Forum: https://nfc-forum.org/fresh-smartphone-statistics-and-what-they-mean-for-you-nfc-and-the-world/

Table 2.1: Wireless short-distance communications

Protocol	Throughput	Power	Band	Presence in phones	Interference in the same band
BLE	2 Mpbs	~50 mW	Radio	~100%	WiFi, Zigbee, microwave oven
NFC	424 kbps	~30 mW	Radio	~60%	RFID
Pulse[40]	44 bps	~0.83 mW	Magnetic field	~100%	Appliances with high magnetic induction
Magne-Comm[41]	110 bps	~5.2 W	Magnetic field	~100%	Appliances with high magnetic induction
Sunbox	(2–10) kbps	~110 mW	Visible Light	~100%	-

because the image is projected only to the intended receiver. The main limitation is that microdisplays require embedded LED lights to operate. *Reflective displays*, on the other hand, do not need embedded artificial lights, they simply reflect ambient light to render an image. Reflective displays are particularly suitable for outdoor deployments because they achieve a high contrast under sunlight. The shortcomings of reflective displays are their *size*, there are no micro-display versions, and their inherent *broadcast nature*, the field of view is broad. These two shortcomings would allow eavesdropping.

Our application, secure short-range communication using ambient light, requires a microdisplay but with reflective properties. Next, we describe various microdisplay technologies and identify one that will allow us to remove the embedded LEDs and re-design the optical enclosure to work as a reflective display with ambient light.

2.2.3. MICRODISPLAYS FOR SHORT-RANGE COMMUNICATION

Microdisplay technologies include micro-OLED, Digital Micro-mirror Devices (DMDs) and Liquid Crystal over Silicon (LCoS). We are looking for two properties in their optical designs, the possibility to disconnect the LEDs and the ability to backscatter light. Micro OLED displays have tightly integrated organic LEDs. DMD and LCoS displays, on the other hand, work as reflective surfaces with hundreds of thousands of pixels. Embedded LEDs radiate light onto the pixels, which either reflect or absorb light to render the image.

DMD and LCoS are, in principle, suitable for our application. Their embedded lights can be removed, they use backscattering surfaces, and they have similar low-power consumption. Their main difference is the reflective material. DMDs use an array of micro-mirrors that are moved mechanically between two fixed angles: towards the intended receiver or towards a light absorber. These micro-mirrors work well with custom-designed LEDs that provide constant illumination at the same incidence angle, but sunlight is variable and changes its direction throughout the day. LCoS do not have strong constraints for the incoming light. Instead of mechanical movements, they use liquid crystals above a layer of reflective coating with a wide incident angle. This property makes them suitable to operate with various types of light.

The more relaxed requirement for the incident angle is a key factor for our system to work indoors and outdoors. Next, we describe in more detail the operation of LCoS, and the difference with other types of LCs used in the SoA. This background is necessary to understand the optical modifications required to make LCoS work with ambient light, as will be discussed in section 2.3.

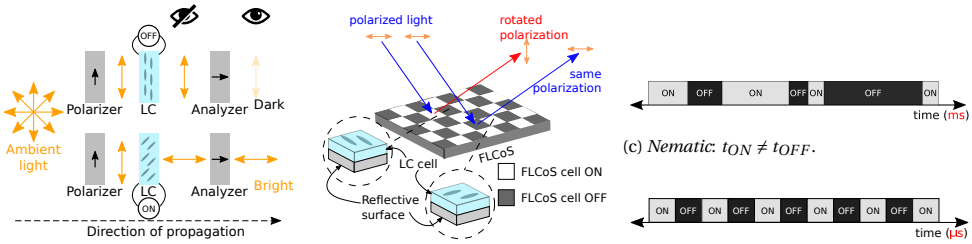

(a) Single cell with two polarizers. (b) Reflective display (array of LC cells). (c) *Nematic*: $t_{ON} \neq t_{OFF}$. (d) *Smectic*: $t_{ON} = t_{OFF}$

Figure 2.1: (a, b) Basic LC modulation and (c,d) the operational difference of LCs. ON and OFF are polarization states set by the control voltage.

2.2.4. TYPES OF LCOS MICRODISPLAYS

LCs have the ability to change the polarization of light and are commonly used as optical shutters, as shown in Figure 2.1a. First, a light source emits unpolarized light, which passes through a first polarizer. Then, depending on the applied voltage on the LC, the polarization direction remains the same or rotates 90°. A second polarizer, called *analyzer*, either blocks or allows the passing of light. Microdisplays have hundreds of thousands of tiny LC cells, each a few microns in size, and every cell (pixel) exploits the above principle. The important difference of LCoS is the presence of the reflective layer under the LC cell, as shown in Figure 2.1b. LCoS has the potential to work with external sources (like sunlight) because the light rays are reflected off the surface[2].

A central property of an LC cell is the switching speed between its two states. The faster the speed, the more colors a display can convey[3]. The pixels are manufactured with different types of LCs, called *mesophases*, and the two main are *nematic* and *smectic*, depicted in Figure 2.1c and Figure 2.1d, respectively.

Nematic LCs have slow and asymmetric response times but allow a flexible control. The rise and fall times are in the order of ms and the fall time is slower than the rise time. On the positive side, any status of the cell (on or off) can be maintained for an arbitrary period, which allows flexibility in the modulation process.

Smectic LCs have symmetric and fast response times, in the order of tens of µs, which allow refresh rates as high as 360 Hz. On the negative side, they have a relatively rigid operation. Due to their internal molecular alignment, the modulation has to switch constantly between the two polarization states and needs to maintain, on average, a 50 % duty cycle.

Current research in ambient light communication focuses on *big nematic* LCs [13, 12, 14, 15, 17, 42]. Those LCs lead to designs that are simple and low-cost, but *bulky* (the area of a single cell is bigger than 10 cm^2) and *slow* (the data rate of *single-pixel transmitters* using cameras as receivers is below 100 bps, and around 1 kbps when photodiodes are

[2] Note that sunlight, like artificial light, is unpolarized. Thus, reflective displays still need the polarizers shown in Figure 2.1a to operate.

[3] Displays create colors by duty-cycling their pixels. For example, an image transmitted at 60 Hz is decomposed into its RGB components (180 Hz). Denoting the period of each primary color as $T = \frac{1}{180\ Hz}$, the colors red and white are conveyed by keeping a pixel ON for T and 3T, respectively. But a shade of red, say at 10%, requires a pixel to be ON only for 0.1T. Hence, faster pixels can render more color combinations.

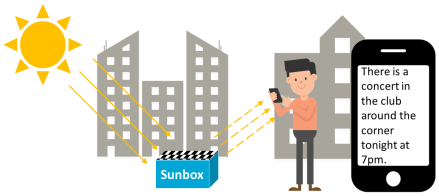

Figure 2.2: Overview of SunBox. A microdisplay reflects encoded ambient light to a smartphone camera placed at close range.

used as receivers). We use a microdisplay based on Ferroelectric LCoS (FLCoS), a type of smectic LC, that is designed to work with tightly synchronized LEDs. In section 2.3, we show that, after removing the embedded LEDs, the duty-cycling requirement of smectic LCs poses non-trivial challenges to make them work with ambient light.

2.2.5. DATA REPRESENTATION

Having a screen at the transmitter enables the modulation of 2D codes. The design of these codes needs to balance range, reliability, and throughput. SunBox aims at short-distance communication in the range of centimeters, hence our main trade-off is between reliability and throughput. Prior studies using traditional screens as transmitters have either used well-known standards [43], such as QR codes, or defined their own customary code [35, 44]. We use standard codes because they are designed to have high-density capabilities, error correction, and resilience to image distortion.

Two standards are widely used for 2D codes: QR and Datamatrix. The pixels in 2D codes are divided into two main areas: recognition (masks, alignment, etc.) and data (information plus error correction). A Datamatrix can carry more information because fewer pixels are used for *recognition*[4], but we select QR codes for two main reasons. First, Datamatrices have a fixed 30% error correction overhead, while QR codes are more flexible, allowing 7%, 15%, 25%, and 30%. Second, QR technology is more mature and widely deployed in mobile applications, which eases the code generation and decoding processes. In our evaluation, however, we also present results with Datamatrices to showcase the generality of our approach to different formats and data densities.

2.3. PASSIVE MICRODISPLAY-TO-CAMERA COMMUNICATION

We propose a passive communication system, depicted in Figure 2.2, that has three main components: an emitter (any type of light source, natural or artificial), a transmitter (a screen that backscatters 2D patterns with ambient light), and a receiver (a smartphone camera). To provide a user interface, a keyboard could be added to allow the user to enter a specific code. In this section, we focus on the design of the transmitter. First, we describe the original off-the-shelf microdisplay, which contains various optical and lighting components in addition to the microdisplay itself, and then, we present our design which removes all these components and proposes a novel design that works solely with ambient light.

[4] Approximately, a Datamatrix uses 15% of the area for recognition, while QR codes use 25%.

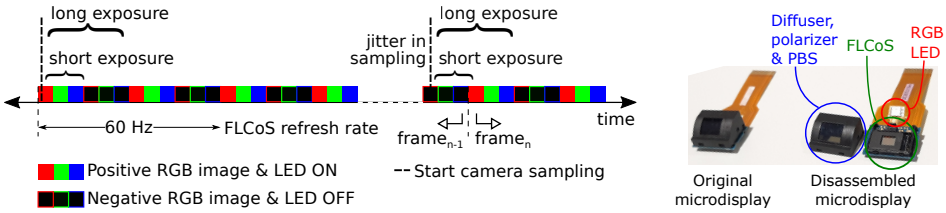

(a) Time sequence of the FLCoS RGB-color sub-framing and the camera exposure time. (b) Disassembly of microdisplay.

Figure 2.3: Operation and components of the microdisplay. In(b), the black cap contains a polarizer and a diffuser for the RGB LED, and a polarizing beam splitter (PBS), which works as the analyzer. Removing this cap gives access to the FLCoS

2.3.1. OFF-THE-SHELF MICRODISPLAY

We build our system based on the LCOS720 micro-projector from Control Electronic [45]. It has a small microdisplay with a diagonal size of 5 mm and is used for short-range near-eye applications, such as augmented reality headsets. The microdisplay is based on FLCoS technology and has a resolution of 720x540 pixels, a video refresh rate of 60 Hz, and costs 70€.

The LCOS720 micro-projector works in the following manner. Inside the projector, embedded RGB lights are integrated with polarizer screens. Polarized rays reach the microdisplay and are reflected with either the same polarization (pixel on) or with a rotated polarization that is blocked by the analyzer (pixel off), similar to the design in Figure 2.1b. In principle, the ability to backscatter the incident light allows the microdisplay to be used with any ambient light, instead of dedicated RGB lights.

However, in spite of the backscattering property, transforming the FLCoS display into an ambient light display is not as trivial as simply removing the 'unnecessary' components of the original micro-projector (LED lights, Polarized Beam Splitters, etc.). The intrinsic 50% duty cycle of the smectic LCs requires a fundamentally different system design to work with ambient light.

2.3.2. BENCHMARK WITH ORIGINAL DISPLAY

The FLCoS display renders color by dividing each frame into six sub-frames for red, green, and blue: $RGBRGB$. To satisfy the duty cycle requirement of smectic LCs, every time a pixel is *on* for a given color, it has to be *off* for the same period. Hence, the frames also need to include the negative states: $RGB\overline{RGB}RGB\overline{RGB}$. To project the intended image, the device tightly synchronizes its RGB LED to illuminate *only* the *positive* pulses (RGB), as shown in Figure 2.3a. To capture the radiated image, cameras average the light intensity received over the *exposure time*, as illustrated in Figure 2.3a. Depending on the exposure time, a camera may capture only part of the RGB pulses (resulting in a colored code) or a full RGB period (resulting in a black&white code), as shown in Figure 2.4b. The exposure time can be set initially via the exposure value (EV) parameter, but it changes in time according to the amount of ambient light. In general, the darker the environment, the longer the exposure time.

(a) Setup.

(b) Sample captures of the QR sequence

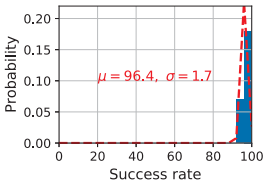

(c) The QR success rate.

Figure 2.4: Results using COTS microdisplay

SETUP

The setup we use to test the micro-display is depicted in Figure 2.4a. The display transmits QR codes at 15 FPS, and it is positioned 10 cm away from a Xiaomi Redmi 5A (a low-end phone), which captures the frames at 30 FPS. To recreate an enclosed casing, we carry out the experiments in a dark environment.

PROCESSING

SunBox requires tailored signal processing and error correction methods to work reliably (section 2.4). However, to set a baseline for our evaluation, we use a basic processing toolchain. An *OpenCV* script is used to identify the area of the FLCoS screen, and the *ZXing* library is used to decode the QR codes.

RESULTS

We transmit 100 messages, each containing 100 QR codes. Figure 2.4c shows the statistical distribution of the *success rate*, which is defined as the percentage of QR codes decoded in a message. As expected, most QR codes are decoded, with a success rate of 96.4 %±1.7 %. Occasionally the camera misses a frame, which can be caused due to jitter or because the exposure time is long and gets close to the frame rate of the transmitter [46, 47].

We will see next that the high success rate of the original projector gets severely affected when the embedded lights are removed and the system operates with ambient light.

2.3.3. FLCOS WITH AMBIENT LIGHT

The operation with ambient light is different from the operation with the embedded RGB LED in two key aspects: a lack of synchronization with the positive pulses and a shorter exposure time due to a more illuminated environment. Both effects, combined with the inherent jitter of the camera, mean that the exposure time can cover positive pulses (RGB), negative pulses ($\overline{RGB}$), or their combination, rendering a low contrast QR, its negative version, or gray images, respectively. To highlight these effects, we assess the modified system with ambient light.

SETUP

After removing the embedded RGB LED (Figure 2.3b), we consider two setups. The first setup is used to capture the reflection properties of all pulses: $RGB\overline{RGB}$. This setup uses

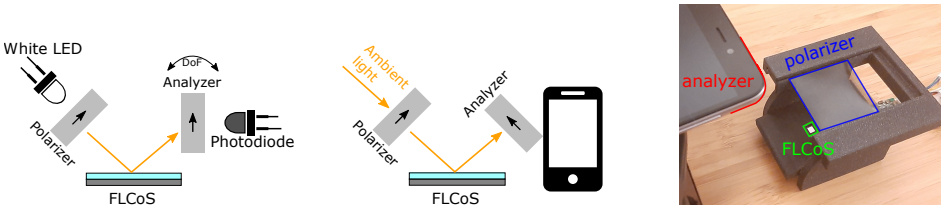

(a) Photodiode (PD) setup. (b) Phone setup. (c) Phone physical setup.

Figure 2.5: Setups for experiments using the FLCoS. For each setup, the second polarizer (analyzer) has a degree of freedom (DoF) to change its orientation w.r.t the first polarizer.

an external flashlight as the light source and a photodiode as a receiver (Figure 2.5a), which has a higher sampling rate and allows capturing in detail the pulses' trend. The second setup is used to capture the success rate (Figure 2.5b). This setup uses the phone as a receiver and considers only the ambient light present in the room, around 500 lx, which is the average illuminance in an office space. Since the FLCoS requires two polarizers to work, c.f. Figure 2.1, a polarizer is placed on top of the FLCoS and an analyzer in front of the photodiode or camera.

RESULTS

For the first setup (flashlight & photodiode), we send a series of white and black screens. Figure 2.6a shows the results. The top plot depicts the pulses for the white screen and the bottom for the black screen. In both cases, we can see the $RGB\overline{RGB}$ trend. Note that both screen colors need to maintain an average duty cycle of 50%. Below the plots, we place sample exposure times to showcase the possibility of getting positive, negative, or gray images. For the second setup (ambient light & camera), we send 100 messages with 100 QR codes each. A few samples of the captured frames are displayed in Figure 2.7a, showing (as expected):

- *Positive (normal) image:* when the exposure time covers only (mainly) the regular

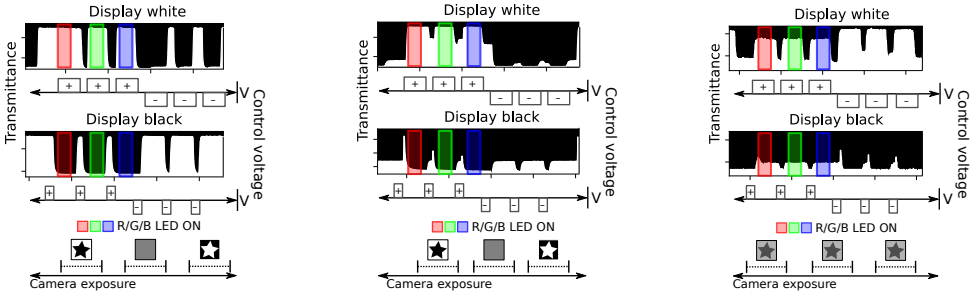

(a) COTS FLCoS with cross polarizers. (b) FLCoS with cross polarizers and no alignment layer. (c) FLCoS with analyzer at 135° and no alignment layer.

Figure 2.6: Output of the photodiode for the setup in Figure 2.5a. Each plot shows the sequence of voltage pulses. And, at the bottom of each figure, we show the expected images (positive, negative or gray) for different exposure times.

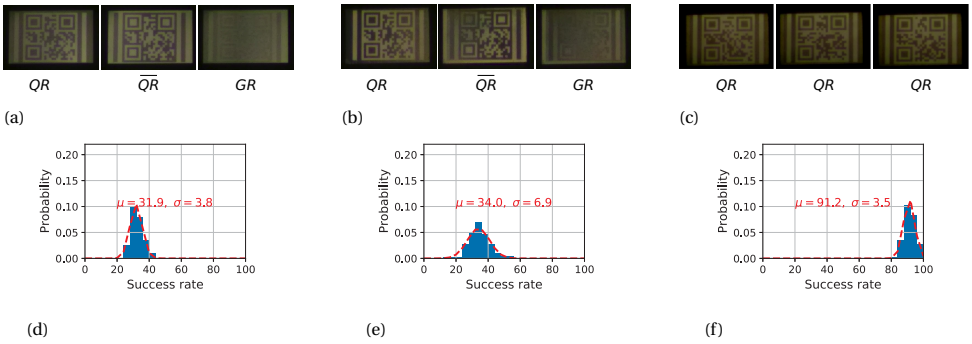

Figure 2.7: Output of the camera for the setup in Figure 2.5b. FLCoS and cross polarizers: (a) & (d). FLCoS with cross polarizers and no alignment layer: (b) & (e). FLCoS with analyzer at 135° and no alignment layer: (c) & (f). The left column shows sample QR codes and the right column the QR success rate.

pulses RGB. Note that even in this "optimal" case, the contrast is lower than the one obtained with embedded LEDs (c.f. Figure 2.4).

- *Negative image:* when the exposure time covers only (mainly) the negative pulses $\overline{RGB}$. In this case, the color of the image is inverted.
- *Gray image:* when the exposure time covers partially the regular and negative pulses, the intensity of the colors averages out, rendering an unreadable gray screen.

The negative and gray images, which the system cannot decode, cause the success rate to drop drastically to 31.9 %±3.8 %, as illustrated in Figure 2.7d. Next, we propose two methods to eliminate these types of images.

2.3.4. FLCoS WITHOUT THE "ALIGNMENT LAYER"

A unique (and counter-intuitive) feature of smectic LCs is that rendering both, black and white screens, require providing and blocking illumination, c.f. Figure 2.6a. This behavior is widely different from the nematic LCs used in the SoA [17, 13, 42, 35, 12, 15, 14]: the white state, set by V_+, provides illumination, and the black state, set by V_0 (ground voltage), blocks it. Smectic LCs, on the other hand, need to balance the polarization states by using three voltages: V_+, V_-, and V_0, and an *alignment layer*. Due to the effect of the *alignment layer*, the transitions from V_+ to V_0 block illumination and from V_- to V_0 provide it. With these transitions, the positive pulses (RGB) require sending a series of (V_+, V_o), and the negative pulses ($\overline{RGB}$) require sending a series of (V_-, V_o), as depicted in the voltage plots of Figure 2.6a.

The *alignment layer* simplifies the control signals required by the smectic LC because switching between the orthogonal states requires only removing the driving voltages. For our purposes, this continuous switching makes it highly probable for a camera to capture low-contrast or gray images. Motivated by research studies that analyze the properties of smectic FLCs [48, 49, 50], we hypothesize that by releasing the FLCoS from the alignment layer, we could get illumination patterns that will increase the contrast between the black and white states across time.

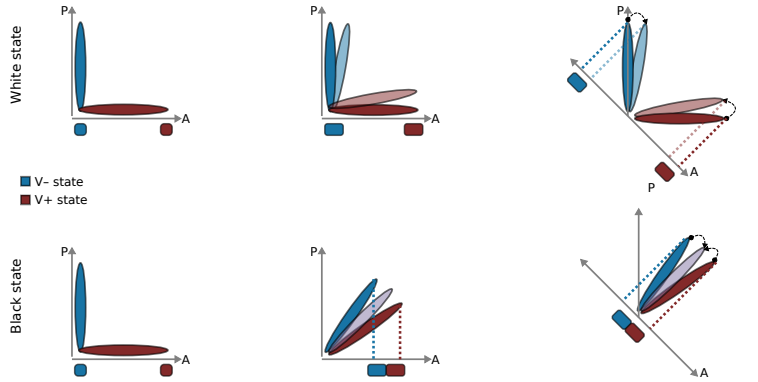

(a) Original FLCoS. (b) FLCoS without alignment layer. (c) FLCoS with analyzer at 135°

Figure 2.8: Transformation of the polarization domain. The P-axis reflects the angle of the polarizer, and the A-axis the angle of the analyzer. (a) With the alignment layer, the black and white displays only project two intensity levels: bright and dark. (b) Without the alignment layer, the white display remains relatively close to the original polarization states, but the black display shifts its brightness towards a cluster centered around 45°. (c) Phase modulation creates new projections, the black display becomes relatively dark, while the two clusters of the white display render medium-brightness.

SETUP

Since the microdisplay is contained in one package, we release the alignment layer from the FLCoS by mechanically releasing the pressure of the package[5]. Afterward, we test the same setups of our prior experiment: flashlight & photodiode to capture the reflected patterns, and ambient light & camera to capture the success rate.

RESULTS

Figure 2.6b shows the results for the reflected patterns. Without the alignment layer, the white display has a clearer alternating pattern between high and low, and the black display is mainly low. This setup still renders gray and negative images (Figure 2.7b). Thus, the success rate improves minimally to 34.0 %±6.9 %. In the next section, we show that a particular type of *phase modulation* provides a final solution to creating a screen-to-camera link with ambient light.

2.3.5. PHASE MODULATION: REMOVING "NEGATIVE" AND "GRAY IMAGES"

The main limitation of the previous steps is the presence of gray and negative images. Adding *phase modulation* [51] will remove these issues. In essence, the alignment layer forces the FLCoS to have only two possible polarization states: parallel or orthogonal to the analyzer (Figure 2.8a). Thus, all pixels –black and white– are limited to using a combination of bright and dark polarizations to render their desired state. The removal of the alignment layer *releases* a wider range of polarization states (Figure 2.8b) because they are no longer forced to be in either of the two states. For a white pixel, the polarization state presents two clusters, one cluster is close to the parallel orientation of the analyzer (bright) and the other cluster is close to the orthogonal orientation (dark). For

[5]The process was repeatedly applied to several FLCoS with similar results.

a black pixel, there is a single cluster, approximately at 45° from the analyzer (medium brightness). If we rotate the analyzer to an angle of 135° (Figure 2.8c), the black cluster becomes orthogonal to the analyzer, rendering a darker tone, and the two white clusters get projected to *similar* magnitude values, rendering brighter tones.

Note that this phase modulation method would not work if we do not release the alignment layer. With a 135° analyzer, the white and black states in Figure 2.8a would project to the same medium-brightness levels, making them indistinguishable from each other.

SETUP

To evaluate our joint solution, releasement of the alignment layer, and phase modulation, we test the same setups with the photodiode and camera, but with the analyzer at an angle of 135° w.r.t. the polarizer.

RESULTS

Figure 2.6c shows the reflection of the pulses, and we can notice that, in spite of the 50% duty cycle, we are able to provide different intensities for the white and black states across the entire time. For a white screen, the illuminance provides a medium-to-high brightness, and for a black screen, the illuminance switches between two low-brightness states. Figure 2.7c shows that changing the angle eliminates the *negative* and *gray images*, which boosts the QR success rate to 91.2 %±3.5 %, as illustrated in Figure 2.7f.

2.3.6. TRADE-OFF OF ELIMINATING "NEGATIVE" AND "GRAY IMAGES"

The main side-effect of the transformation of the polarization domain is the reduction of contrast between bright and dark states. Table 2.2 shows the contrast for all the setups in this section. Despite the low contrast of the SunBox setup, the QR success rate improves to 91.2 %, similar to the original microdisplay. In the next section, we present some techniques to deal with low-contrast images and variable light intensities.

2.4. ATTAINING RELIABLE LINKS

The prior section describes the optical design required to use FLCoS with ambient light. The images, however, can still appear distorted due to the variable and noisy nature of ambient light. In this section, we present the methods used to overcome those limitations in order to provide reliable links.

Unless stated otherwise, the following libraries are used in the development of the smartphone App: *OpenCV* for signal processing, *ZXing* for QR decoding, and *Backblaze's JavaReedSolomon*[6] for error correction.

2.4.1. DETECTING THE REGION-OF-INTEREST (ROI)

In the experiments done so far, the detection of the region of interest was a manual process. To ease this requirement, we implement an automatic detection process. The detection takes advantage of the reflective nature of the FLCoS, which is surrounded by

[6] Source: https://github.com/Backblaze/JavaReedSolomon

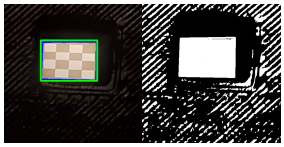

(a) Find contours using binarization.

(b) Equalization.

(c) Normalization.

Figure 2.9: Frame processing. Figure (a) shows a sample frame [left] and its binarized version [right]. The ROI is captured by a green contour. Figures (b) and (c) are the signal processing methods used to enhance the images within the ROI.

Table 2.2: Image contrast for different setups.

Feature	RGB LED	Ambient Light	
		Cross-polarizers	SunBox
Contrast	40 ± 5 %	17 ± 3 %	11 ± 1 %
White*	170 ± 27	163 ± 9	156 ± 6
Black*	0	27 ± 16	49 ± 5

* Intensity values range between 0 and 255.

a dark and opaque surface. Therefore, the camera sees the FLCoS as a high-brightness area over a dark background and performs the following three steps to detect the ROI:

- *Binarization:* the `adaptiveThreshold` function renders a black and white image (Figure 2.9a).
- *Rectangle detection*: the `findContours` function detects all shapes, and the `approxPolyDP` function approximates the shapes to the closest polygon.
- *Rectangle selection:* we filter rectangles by ratio and size. The aspect ratio of the FLCoS is 4:3, and we filter out rectangles larger than 2% and smaller than 20% of the entire screen.

The identified region is then sent to the QR library. The ROI method reduces the computation time and increases the QR success rate. Handling the entire frame takes ~205 ms and has a 65 % success rate, whereas handling only the ROI takes ~140 ms and has a 100 % success rate. This ROI method is used in the remainder of the paper.

2.4.2. ENHANCING THE IMAGE QUALITY FOR DAWN AND DUSK

Thus far, the system has been tested under constant and direct ambient light (~500 lx). However, we need to consider diffuse conditions with low light, such as those present during dusk and dawn or in low-lit indoor scenarios. We implement a simple toolchain to increase the contrast under those conditions. The tool chain uses equalization (`equalizeHist`) and normalization (`normalization`), as depicted in Figure 2.9b and Figure 2.9c.

These signal-processing methods have a minor effect under normal ambient light conditions. For example, with the setup used in section 2.3, the success rate increments scarcely from 91.2 % to 92.5 %, but the contribution of the methods is more noticeable in challenging setups. To assess this effect, we attenuate the light reaching the FLCoS. Using this low-lit setup, the signal processing stage increases the success rate from 70 % to 85 %.

2.4.3. CREATING A RELIABLE SIMPLEX LINK

SunBox implements a simplex channel with no feedback nor re-transmission of lost frames. Thus, to obtain a reliable link, SunBox requires the use of Forward-Error-Correction methods (FEC).

A well-known FEC method is Reed-Solomon codes (RS-FEC), also used internally by QR codes to recover from errors. The basic principle is to add extra bytes (e) to the original data, so the link can recover from $\frac{e}{2}$ errors at any *unknown location* or from e erasures at *known locations*. SunBox implements RS-FEC using the first byte of each QR as a numbering sequence, thus the receiver knows the location of the missing QRs, and can recover from missing frames. We can assume that the decoded QRs are correct due to their internal RS-FEC and parity checks.

To provide an example of how to choose the parameters for RS-FEC, we use the statistical distribution of the success rate for an experiment considering 15 FPS at the transmitter and 30 FPS at the receiver. Figure 2.10a and Figure 2.10e depict the *pdf* and *cdf*, which follow a Gaussian distribution. Gaussians concentrate ~97% of their probability mass between $\mu \pm 2\sigma$. Hence, for this setup, designing a RS-FEC that can recover from 15 % of erasures ($\mu - 2\sigma = 85\,\%$) implies that 97% of the messages will be reliably delivered.

RS-FEC increases reliability but adds overhead. To distinguish the goodput of our system (in section 2.6), it is important to quantify the amount of overhead. Denoting N as the total number of QR codes in the message and B as the number of bytes in each QR code, the total amount of information is $N \times B$. But out of the N QR codes, only K carry data ($N-K$ carry redundancy), and each QR code has a sequence number to detect erasures (1 byte). Hence, the amount of application-level data is reduced to $K \times (B-1)$, and the overhead ratio is given by:

$$O = \frac{(N-K) \times B + K}{N \times B} \tag{2.1}$$

In spite of this overhead, the strong advantage of RS is that the receiver only needs to get K out of N codes to successfully decode the message. It does not matter which K codes are received, it can be any combination. There are other erasure correction methods, such as rateless codes, which can adapt the data rate to the channel conditions. Those types of codes can be evaluated in future studies.

2.4.4. REDUCING THE TRANSMISSION DELAY

Many screen-to-camera systems follow the Nyquist sampling theorem, where the camera's frame rate is set to twice the screen's [33, 34, 52]. This approach introduces an overhead since many frames are sampled twice. Due to this reason, some studies increase the frame rate at the transmitter. For example, Zhang et al. set the transmission rate to 29.9 FPS for a camera rate of 30 FPS [53], reducing in this manner the transmission delay to half compared to a camera transmitting at 15 FPS. We follow this latter approach to trade off a few packet losses for a reduction in delay. For SunBox, a few extra losses are not an issue because we have RS-FEC to overcome erasures.

To obtain the optimal transmission rate, we first estimate the number of error-correction packets ($N-K$) required for different screen rates, from 15 FPS to 30 FPS, in steps of 5 FPS. In all these experiments, the rate of the camera is kept at 30 FPS. The statistical distributions of these results are presented in Figure 2.10, where the threshold for a success rate of ~97 % is set to $\mu - 2\sigma$ for all cases. Based on the determined thresholds ($\mu - 2\sigma$) and assuming $K = 54$ QR codes (application-level data), Table 2.3 estimates

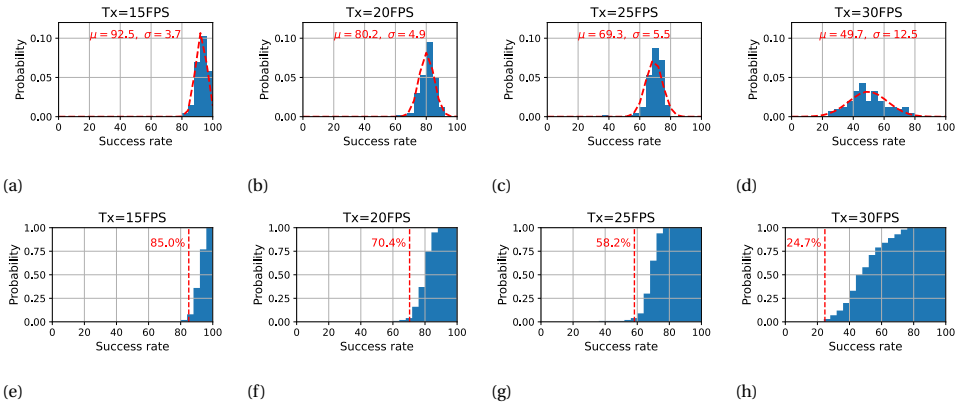

Figure 2.10: Figures (a) to (d): pdf of the success rate for 100 messages at different speeds (each message sends 100 QR codes). Figures (e) to (h): cdf with thresholds at $\mu - 2 \times \sigma$ to define the RS-FEC parameters.

Table 2.3: Parameters for a system with $K = 54$ and a success rate of 97%

FPS	$\mu - 2\sigma$	N (frames)	Overhead	Duration (s)
15	85%	64	20.6 %	4.26
20	70%	77	34.0 %	3.85
25	58%	93	45.3 %	3.72
30	25%	216	89.1 %	7.20

the total number of QR codes required by RS-FEC ($N = \frac{K}{\mu - 2\sigma}$, which includes data and redundancy); the overhead ratio (Equation 2.1); and the time required to receive the N frames at the given FPS (N/FPS). From that table, we can observe that, even though all the alternatives transmit K codes of data, the rates at 20 FPS and 25 FPS provide the shortest transmission delays. In section 2.6, we perform a more thorough evaluation and show that 20 FPS is the optimal transmission rate for various lighting conditions.

2.5. SYSTEM IMPLEMENTATION

On the basis of the previous experiments and observations, we now present a prototype for SunBox.

2.5.1. TRANSMITTER

The main components of the transmitter are presented in Figure 2.11a. The steps to generate the video with the sequence of QR codes are as follows. First, a processor (in our case, a laptop or a Raspberry Pi Zero) generates the sequence of QR codes and adds the necessary numbering and error correction bytes. The complete information is arranged in a 2D array, as presented in Figure 2.11b. Each row includes a numbering byte and payload bytes. The payload represents either data or RS-FEC redundancy. This sequence is then converted to a video stream. Some processors (laptop) need a video converter,

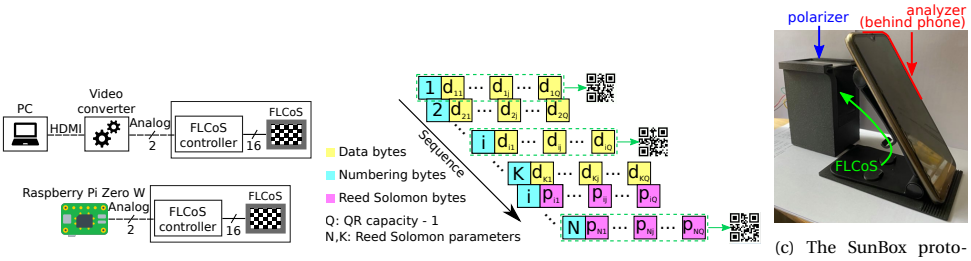

(a) Transmitter components. (b) Byte array to generate QR sequence. (c) The SunBox prototype

Figure 2.11: The transmission system. In (b) yellow are the original data bytes, magenta the RS bytes and cyan the numbering bytes. Each row produces a QR.

others (Raspberry Pi Zero) do not. The video converter adapts the signal to the format required by the FLCoS microdisplay. Finally, the FLCoS controller generates the signals to modulate each pixel of the matrix.

To assemble everything, we fabricate a small 3D-printed container and attach a phone holder, as shown in Figure 2.11c. The polarizer is placed on top of the container, and the FLCoS is inside the container. The encoded light is backscattered towards the smartphone. The analyzer is fixed within SunBox at an angle of 135° w.r.t the polarizer. The user's smartphone does not require any extra components for the system to work. The user simply has to push a button so the transmitter can start sending the video (continuously in a loop), and then, places the phone on top of the holder and starts the App to get the backscattered data.

2.5.2. RECEIVER

The receiver is a simple commercial smartphone. The main goals of our Android App design are to reduce the processing time and use of memory to allow SunBox to be used with any type of smartphone, including low-end devices. To accomplish these goals, our App performs four main tasks: camera configuration, ROI detection, frame capturing, QR decoding, and message recovering, as shown in Figure 2.12a.

Camera configuration. The first step is to configure the smartphone camera. By default, the App sets the zoom to its maximum value and the EV parameter to its lowest. The resolution is also a key parameter because it determines the quality of the image and the amount of memory used for processing. The App determines the best resolution automatically, based on the real-time capabilities of the phone, as described in the next section.

ROI detection. Following the method outlined in subsection 2.4.1, the program detects the FLCoS on the screen and, once detected, surrounds the FLCoS area with a rectangle in the UI and enables the capturing button.

Frame capturing. After the ROI is detected, the camera starts processing the frames in real-time. This step implements an extra optimization to reduce the delay. That optimization is explained next.

QR decoding. In this step, we enhance the image quality and decode the QR codes by applying the methods outlined in subsection 2.4.2. Three threads are run in parallel,

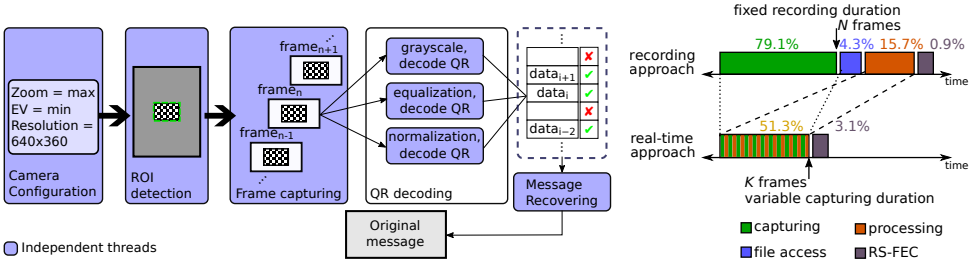

(a) Design outline of the Android App

(b) Real-time approach

Figure 2.12: Description of the Android App. Note that for the recording approach in (b) the capture ends when N QR codes are received and for the real-time the capture stops earlier, when K QR codes are received.

each corresponding to an image processing method: *grayscale, equalization* and *normalization*. Each of these methods tries to decode a QR code. If any of the threads returns successfully, it kills the other threads, saves the data of the QR code into a queue, and marks the sequence number as 'present'. Otherwise, the QR code is marked as 'missing'.

Message recovery. In the last step, the *Reed Solomon* algorithm uses the QR-data queue and the 'present/missing' marks to recover the message. The *Backblaze* RS-FEC processing time depends on the capabilities of the phones and the length of the message. In our experiments, we select the RS-FEC engine with N between 64 and 128, so low-end phones can run the algorithm.

The *frame capturing* process exploits the real-time features of Android using the *Camera2 API*. In general, a camera can capture a sequence of frames in real-time or record a video, Figure 2.12b compares both approaches. Given that most phones can operate in real-time at 30 FPS, we take the following steps:

- *Capturing.* Read a frame from the camera buffer instead of the internal storage (no *file access* stage).
- *Processing.* A frame's processing is done during the capturing of the next frame using multiple threads.
- *Decoding.* The final RS-FEC decoding process starts when K QRs are received, instead of waiting for all N.

To quantify the time saved, we implement both the recording and the real-time processing methods in Android. The run-time for the recording app is ~5.73 s and for the real-time app ~3.12 s. Figure 2.12b decomposes the amount of time taken by the individual steps of both approaches. A further improvement for the *capturing* stage would be to use the real-time feature at higher FPS (some phones are capable of operating at real-time with 60 FPS, c.f Table 2.5). However, we notice an image distortion when applying a zoom at that speed, rendering unreadable QR codes.

2.6. EVALUATION

In this section, we assess the SunBox system under different conditions using the setup presented in Figure 2.11c. Even though the FLCoS is inside a 3D case, any system using visible light modulation should check that there are no flickering effects. Given that the (backscattered) modulation is based on polarization, which is invisible to the human visual system, SunBox has no noticeable flickering effect. We asked five individuals to report if they noticed any flicker or disturbances while transmitting. All reported seeing a constant reflection from the FLCoS but without any flickering.

2.6.1. GENERAL SETUP AND METRICS

We assess SunBox under different conditions. Unless stated otherwise, the default settings are:

Message. The information sent by SunBox consists of a sequence of QR codes implementing RS(N,54): 54 QR codes for data and N total QR codes. After pushing a button in the transmitter, the video message is sent in a loop, thus the capture can start at any time.

Distance. The 3D casing provides a stable ~10 cm distance between the smartphone and the FLCoS transmitter. During capture, the phone is on the holder, not in the user's hands.

Camera. The phone is a Xiaomi Redmi 5A. The App sets automatically the resolution to 640 × 360, the zoom to the maximum value (8x), and the exposure value to the minimum (-2).

Light source. A desk lamp providing ~500 lx, which is the typical illumination in an office environment.

GOODPUT

Using the real-time approach, the app calculates the total time (t_{total}) from the start of the capture until the whole message is decoded. Denoting B as the number of bytes in a QR code, and recalling that $K = 54$, we define the goodput G based on an RS(N,K) as:

$$G = \frac{K \times (B-1) \times 8}{t_{total}} [bps] \tag{2.2}$$

MESSAGE SUCCESS RATE

Because the QR sequence is displayed in a loop, if the receiver fails to receive enough QR codes in the first loop, it keeps capturing frames until it completes the necessary number of QR codes to run the RS-FEC algorithm. We consider a message to be successfully delivered if it is received within one iteration of the loop. Because the transmission rate (f_{Tx}) and the reception rate (f_{Rx}) do not match, the number of transmitted frames (N) is different from the number of received frames (N_{Rx}). The number of received frames is defined as:

$$N_{Rx} = N \times \frac{f_{Rx}}{f_{Tx}}. \tag{2.3}$$

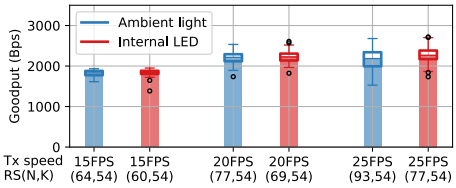

Figure 2.13: Increasing the transmitter speed. The number of data QR codes $K = 54$ is the same for all transmission rates.

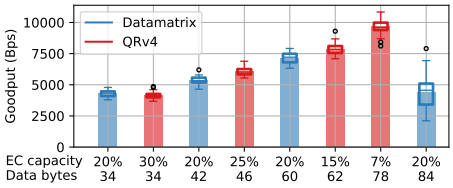

Figure 2.14: Goodput performance for different error-correction rates for QR version 4 and different Datamatrices capacities.

The App has a progress bar that displays the number of unique frames received. We consider a message to be successfully delivered if the number of received frames is less than N_{Rx}.

2.6.2. IDENTIFYING THE OPTIMAL TRANSMISSION RATE

In subsection 2.4.4, we provide a preliminary analysis of the benefits of increasing the transmission speed beyond the Nyquist rule. Now, we test the system to identify the best transmission speed considering all the methods in section 2.4 and section 2.5. Figure 2.13 presents these results and shows that a transmission speed of 20 FPS, using an RS(77,54), has the highest goodput with low variance. Therefore, we set the system to use these parameters: $N = 77$, $K = 54$, and, we use Equation 2.3 to determine if a message is received successfully during the first loop (the number of received frames must be less than $N_{Rx} = 116$).

To showcase the strength of our approach, we compare the goodput of SunBox, which uses ambient light, against the goodput of the original FLCoS projector, which uses embedded LEDs. The results are presented in Figure 2.13. First, we determine the optimal RS parameters for the original system (because the use of the RGB LED requires less redundancy in the RS parameters). Then, we perform the experiments at different speeds. The results show no significant effect over the goodput, with the extra advantage that, removing the embedded LEDs reduces the power consumption (as described in subsection 2.6.9).

2.6.3. ANALYZING THE EFFECT OF ZOOM AND DIFFERENT CODE DENSITIES

After selecting the suitable speed, we evaluate the effect of the camera's zoom and the code density. The prior experiments use the maximum zoom provided by the Xiaomi phone (8x) and the lowest code density (QR v1). Our aim is to study the correlation between the applied zoom, the data density of the QR code, and the camera resolution. The evaluation considers three zoom levels (4x, 6x, and 8x) and four QR codes with capacities of 17, 32, 53, and 78 bytes, corresponding to versions 1, 2, 3, and 4, respectively. Additionally, if the success rate is lower than 90%, we increase the resolution of the camera from 640×360 to 960×720.

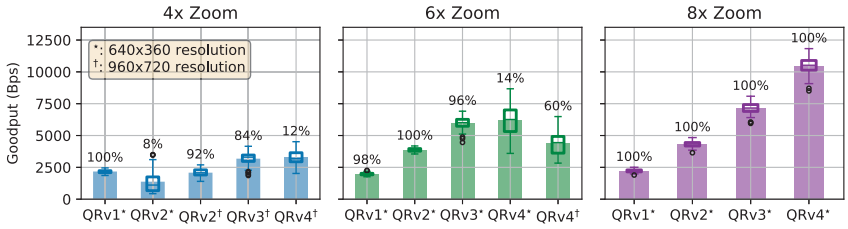

Figure 2.15: Camera zoom effect on performance for different QR densities. For denser codes, we increase the resolution of the image. At the top of each bar is the message success rate.

The results, in Figure 2.15, show two main results. First, even for the most basic phones in the market (30 FPS with 4x zoom, c.f. Table 2.5), SunBox provides a baseline performance above 2 kbps. Second, while basic phones (with a limited 4x zoom) would not benefit from increasing the code density and/or camera resolution, the majority of phones in the market would. Most medium-end phones provide an 8x zoom, which allows using dense codes (v4) to increase the goodput above 10 kbps, without the need to increase the camera resolution.

2.6.4. SELECTING THE BEST 2D CODES

As mentioned in subsection 2.2.5, two of the most widely used 2D codes are QR and Datamatrices. In this subsection, we identify the best code for SunBox. The main difference between QRs and Datamatrices is that QRs allow adjusting their error-correction rate, but Datamatrices do not. For example, QR version 4 provides four error-correction rates (7%, 15%, 25%, and 30%), while Datamatrices have a fixed rate of 20%. The higher the error-correction rate, the stronger the resilience of the message, but the lower the goodput.

Figure 2.14 compares QRs and Datamatrices containing a similar number of data bytes. Both codes provide a similar goodput when the error-correction rates of QRs are above 15%, but QRs significantly outperform Datamatrices with the lowest error-correction rate (7%). This occurs because, to maintain the 20% correction rate, the density required by Datamatrices is so high that the smartphone camera can no longer decode the messages reliably. Due to this insight, in the following sections, we keep the QR error-correction rate to the lowest value.

2.6.5. ANALYZING THE EFFECT OF LIGHT INTENSITY AND RADIATION PATTERNS

While artificial light is usually constant, we also evaluate the relationship between light intensity and SunBox's performance. Similar to subsection 2.6.3, our goal is to assess the resilience of the different code densities under various light conditions.

To control the light intensity, we add a dimmer to the setup. The results in Figure 2.17a show that SunBox is able to work even at very low light intensities. To put these results in context, it is important to note that 200 lx is the illumination required in a non-working environment (e.g. aisle), and 500 lx is the illumination required in a

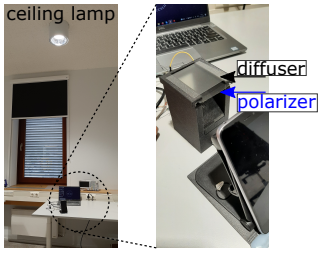

(a) Setup using the ceiling lamp and the diffusing film.

(b) FLCoS reflection without the diffusing film.

(c) FLCoS reflection with the diffusing film.

Figure 2.16: Experiments in an office space (~500 lx) using a diffuser film for locations with strong light intensities. The image in (c) is clear enough to trigger the transmission.

working setup (e.g. desk). QR version 4 starts failing only at 100 lx, versions 2 and 3 start failing with 50 lx, and version 1 continues to work even at 50 lx.

Intensity is not the only important parameter in lighting, the type of radiation (diffused or directed) is relevant as well. We find two main cases: rooms designed with (warm) *diffused* lights, such as living rooms; and rooms with (cold) *directed* lights, such as office spaces. SunBox operates without any modifications with warm diffuse lights, but with cold directed lights there are locations where the light is too intense. The issue and modification are depicted in Figure 2.16. Depending on the relative location between SunBox and the direct light source, in this case a ceiling light, the FLCoS may receive an intense beam that saturates the camera's sensor. To cope with this effect, a simple diffusing film can be placed over the polarizer, as shown in Figure 2.16a. This film distributes the focused light across the surface of the FLCoS, and its effect is demonstrated in Figure 2.16b and Figure 2.16c.

As shown in this section, SunBox is able to work with different types of *indoor ambient light*. However, as presented in subsection 2.6.8, we will see that natural sunlight presents other challenges.

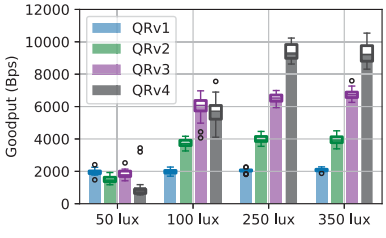

(a) Goodput for different artificial light intensities.

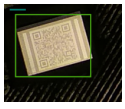

(b) ROI at 15°

(c) ROI at 30°

Table 2.4: Holding the phone by hand.

	Goodput	Success rate
QRv1	~2.0 kbps	90 %
QRv2	~3.6 kbps	75 %
QRv3	~4.9 kbps	50 %
QRv4	~5.3 kbps	10 %

Figure 2.17: Results under different external conditions.

Table 2.5: Features of the phones used during the experiments.

Phone model	Year	Max. zoom	Resolution used	RAM	Size (mm)	Camera position	Camera Speed
Samsung Galaxy A50	2019	4x	1280 × 720	4 GB	158.5 x 74.7	Right	30 FPS
Xioami Redmi 5A	2017	8x	640 × 360	2 GB	140.4 x 70.1	Right	30 FPS
Morotorla Moto G6	2018	8x	640 × 360	3 GB	153.8 x 72.3	Center	30 FPS 60 FPS
Smartisan DE106	2018	8x	1280 × 764	8 GB	153.3 x 74.5	Right	30 FPS

2.6.6. DIFFERENT PHONE ORIENTATIONS

In this section, we assess the performance of the system related to changes in the phone's position. We first change the phone's rotation, which makes the FLCoS appear inclined w.r.t. the camera. We use the QR version 4 and rotate the Xiaomi Redmi 5A phone 15° and 30°. The effect of the rotation, in Figure 2.17b and Figure 2.17c, is a larger ROI which causes a penalty in the goodput because the phone processes more pixels. Without rotation, SunBox provides more than 10 kbps, with a 15° rotation ~9.5 kbps, and with 30° ~9.0 kbps. These issues could be fixed with a more elaborated ROI detection method.

Another important requirement for the current version of SunBox is to use the phone holder. That is, the user has to place the phone on the 3D structure, instead of holding it with the hands. To show the importance of this requirement, we hold the phone in front of the analyzer, placing the wrists over the table where SunBox is located. We send information using QRs from version 1 to 4, and we notice that the success rate decreases for all densities, as presented in Table 2.4, being version 1 the most resilient to the user's handshaking. Overcoming this effect would require utilizing signal processing techniques that compensate for motion dynamics in smartphones [27].

2.6.7. PORTABILITY WITH DIFFERENT PHONE MODELS

Thus far, we have tested a single low-end phone (Xiaomi, 2017). To demonstrate the adaptability of SunBox, we test three other smartphones: a Samsung Galaxy A50, a Motorola Moto G6, and a Smartisan DE106. These phones are all low-end to mid-end phones launched a few years ago. Table 2.5 shows the features of each phone.

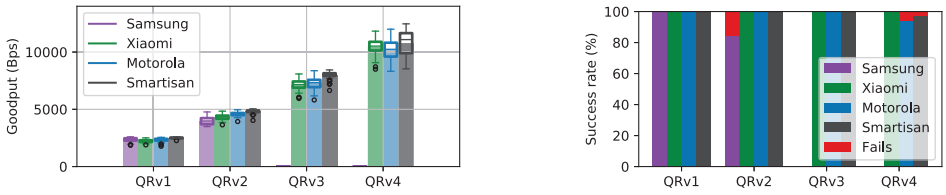

(a) Goodput of the system.

(b) Success rate of the system.

Figure 2.18: Goodput and success rate for different QR versions and different smartphones with (artificial) ambient light.

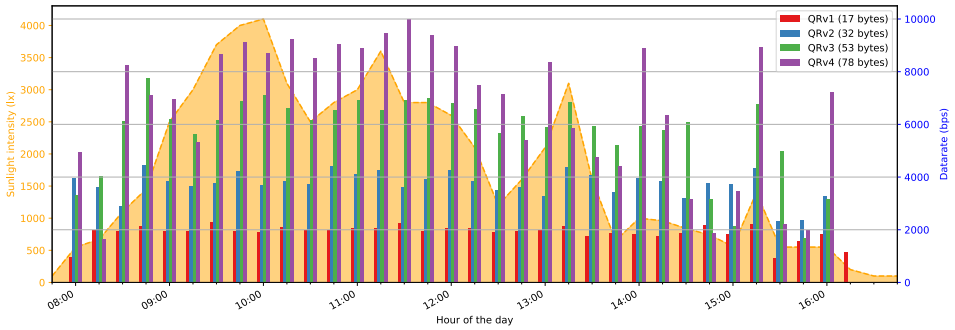

Figure 2.19: SunBox performance using sunlight. Note: at 15:00, a light rain started.

The Samsung Galaxy A50 features a camera with a maximum zoom of 4x, thus, the App increases the resolution to 1280×720. The results in Figure 2.18 validate the relevance of the camera's zoom: even with the higher resolution, the Samsung phone is only able to work with the QRv1 and QRv2, the latter with a smaller success rate. With the denser versions QRv3 and QRv4, the Samsung phone is unable to receive any QR. The Motorola Moto G6 and the Xiaomi Redmi 5A have similar performance, working efficiently with all the QR code densities. For QRv4, the Motorola Moto G6 shows a slight increase in goodput variance and a slight decrease in the success rate. The Smartisan DE106 has more RAM, which allows faster image processing, providing a slightly higher goodput. However, the camera resolution has a big influence on the exposure value (EV), requiring a resolution of 1280×768 to work reliably. Overall, SunBox is able to operate reliably with different types of phones.

2.6.8. NATURAL LIGHT

A critical difference between artificial and natural light is that the intensity and direction of natural light change over time. There is a significant difference between a clear day (tens of thousands of lux with light coming from mostly one direction) and a cloudy day (a few thousand lux with light coming from all directions). Furthermore, the geographical location (latitude) also impacts the amount of sunlight. We test SunBox during a challenging day in terms of sunlight: an overcast day during winter in the Northern Hemisphere, with some rain hours. We find that even on this challenging day, the system can successfully deliver messages from dawn to dusk. Similar to the experiments done in previous subsections, we test various code densities.

The setup of this experiment consists of placing the SunBox close to a large window and using the smartphone Xiaomi Redmi 5A as the receiver. The indoor light is turned off, so we are communicating only with sunlight. During an entire day, we send four messages every fifteen minutes, one corresponding to each QR version. Figure 2.19 and Table 2.6 show the results. The yellow background reflects the amount of sunlight (at 15:00, a light rain started), and the vertical bars capture the goodput with different data densities. We can observe that for sunlight intensities higher than 550 lx approximately, which occurs between 8:15 and 15:15 in a winter day (7h00m period), SunBox obtains

Table 2.6: Message success rate with sunlight. The right column shows the period when the success rate was steady at 100%

QR Version	Bytes per QR	Message success rate	Range of 100% message success rate	Total Time
QRv1	17 bytes	100.0%	08:15 to 15:15	7h00m
QRv2	32 bytes	100.0%	08:15 to 15:15	7h00m
QRv3	53 bytes	89.7%	08:30 to 14:30	6h00m
QRv4	78 bytes	51.7%	09:30 to 12:00	2h30m

an almost constant goodput for QRv1 and QRv2, 2 kbps, and 4 kbps respectively, with a 100% message success rate. For QRv3, the goodput is around 6 kbps but the 100% message success rate occurs between 8:30 and 14:30 (6h00m). This stable period starts with an intensity higher than 1100 lx but ends with an intensity of 800 lx. QRv4 has a 100% stable message success rate between 9:30 to 12:00 (3h00m) when the light intensity is over 2500 lx.

The key advantage of sunlight is that SunBox can be placed anywhere outdoors (we tested a few other outdoor locations with similar results), but we noticed an interesting phenomenon. At times, the goodput does not increase or decrease monotonically with the intensity of light. For example, during the period between 8:30 to 9:30, the sunlight intensity increases, but the goodput remains the same or even decreases. On the other hand, during the time 14:00 to 15:15, the goodput is high despite the low light intensity. Furthermore, SunBox only operates when the sunlight intensity is above a few hundred lux, while 50 lx were sufficient indoors. The reason for these phenomena is that, as stated before, not only the intensity of the ambient light matters but also its radiation pattern, which can change depending on the cloud conditions.

Overall, the results show that low-density codes, QRv1 and QRv2, are robust, attaining a 100% success rate for a long duration during a cloudy day (6h45m). The success rate of denser codes, on the other hand, tends to follow the intensity and radiation pattern of the ambient light. During summer or close to the equatorial line, SunBox would provide significantly better performance.

2.6.9. A STANDALONE SYSTEM RUNNING AN URBAN APPLICATION

Thus far, the experiments for SunBox have been performed using a laptop to provide the video input and power, and the payload has been text (a tale by Edgar Allan Poe, “The Black Cat"). In this section, we design a standalone system and develop a simple application based on Google Maps.

STANDALONE SYSTEM

To demonstrate the potential of SunBox, we combine a few components to create a self-contained embedded system, as shown in Figure 2.20a:

- *Single board computer:* Raspberry Pi Zero W, which can produce the input signal required by the FLCoS without the need of a video converter. Cost: 10€, Power (consumption): 400 mW, low-power mode.

- *Battery and DC/DC booster:* A LP785060 lithium-ion polymer battery and an Adafruit Powerboost 1000C. In combination, they output 5 V to feed the board. Cost: 20€, Power (provided): up to 5 W.
- *Solar panel:* SLMD262K 10L from IXYS (220 mm x 126 mm x 2.1 mm) to charge the battery. Cost: 65€, Power (provided): up to 5 W, depending on illuminance.

Overall, the total cost is below 200€, and the solar cell provides enough power to run the system.

POWER ANALYSIS OF MICRODISPLAY.

An important feature of using ambient light is the reduction in power consumption. To quantify the energy savings, we analyze the power consumption of the microdisplay.

The LCOS720 micro-projector has 4 different power supplies: VCC (supply for FLCoS panel), VIO (supply for I/O serial interface), DAVCC (supply for the embedded lights and their driver), and VCCX (supply for panel / EEPROM for LED calibration). In SunBox, we no longer need the DAVCC power supply, since the embedded lights are removed and the system communicates with ambient light. VCCX is used for color calibration of the embedded lights and is not needed either. We hypothesize VIO to be involved only in the start-up phase to configure the registers of the device, and it is not involved in the operation of the FLCoS. The nominal consumption of the entire micro-projector is 180 mW. However, considering only the VCC supply, which supports the operation of the FLCoS, the power consumption of the FLCoS core panel is 110 mW. Thus, if we could design a microdisplay for ambient light, the power consumption could be reduced by up to 40%.

AN URBAN APPLICATION.

With SunBox as an embedded system, several transmitters could be deployed across a town for travelers to get coordinates for touristic places nearby. The user would not need to rely on any type of radio signal, she would only need to put the phone on the SunBox holder and get information for restaurants, events, museums, etc.

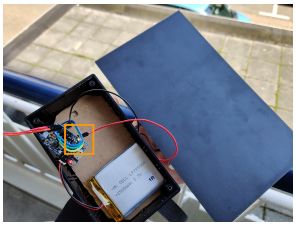

(a) Standalone system, powered by a solar cell.

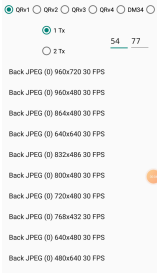

(b) Selection screen.

(c) ROI and data transmission.

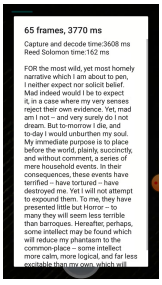

(d) Text output.

(e) Map output.

Figure 2.20: SunBox standalone components (a) and App view. (b) Select different QR versions and camera resolutions. (c) The progress bar location is top-left. (d) Simple text output: fragment of *The black cat* by Edgar Allan Poe. (d) Markers on the map with transmitted coordinates.

We develop a simple app based on Google Maps for this purpose, the screenshots of all the stages are presented in Figure 2.20:

1) We have a GUI to select the type of QR code, the values of N and K for RS-FEC, and to detect automatically all the possible configurations based on the real-time capabilities of the phone. This part does not need to be presented to the user. It is solely used to facilitate the evaluation of the different parameters.

2) The user starts the App, places the phone on the holder and the ROI is selected automatically. After the ROI is found, the user can push a button to start reading the video.

3) A green progress bar on the top left of the screen shows the number of received QR codes. When the App receives K unique QR codes, it stops and runs the RS-FEC algorithm to decode the message.

4) Initially we send only plain text. But sending geographical coordinates is simple too. The longitude and latitude contain 8-bytes each. Thus, even the least dense QR (version 1) can carry the coordinates for one location. The transmitter knows its location and sends coordinates for nearby places. The coordinates are then presented as markers in a map view using the GoogleMap SDK.

2.7. RELATED WORK

2.7.1. LIQUID CRYSTAL TO PHOTO-DIODE

The first group of studies related to our work is systems that use LCs to modulate light and photo-diodes (PDs) at the receiver. For our purposes, we divide them into two groups: single-pixel and multi-pixel.

SINGLE-PIXEL

These studies have a single LC surface at the transmitter and a single PD at the receiver. Due to the slow switching speed of the LC, their throughput is relatively low, around one kbps. Some of these studies require flashlights or lightbulbs to operate, such as *RetroVLC* [12] and *PassiveVLC* [13], while others can work with sunlight, like *LuxLink* [42] and *ChromaLux* [54].

MULTI-PIXEL

To overcome the limited speed of single-pixel approaches, systems like *RetroTurbo* [14] and *RetroI2V* [15] use multiple LC surfaces at the transmitter and/or multiple PDs at the receiver, together with more sophisticated modulation schemes. These MIMO systems can reach speeds up to 8 kbps. However, they require transmitters with big surface areas and powerful artificial light sources that consume between 3 W and 30 W.

A common aspect of all the above systems (single- and multi-pixel) is that they use big *nematic* LCs, with surfaces of several tens of cm^2, and photodiodes, which are significantly faster receivers than cameras. SunBox uses a microdisplay with *smectic* LCs, which have different optical features. And, in spite of using low-end smartphones with slow cameras (30 FPS), we can exploit any type of ambient light (artificial or natural) to achieve speeds between 2 kbps to 10 kbps.

2.7.2. CAMERA AS A RECEIVER

Other VLC systems exploit cameras as receivers instead of photodiodes. Cameras are slower but they have two appealing features: they are widely deployed in smartphones, and they have a 2D array of photo-sensors, which gives the advantage of spatial diversity. The key difference among these studies is the type of transmitter they use, and we identify three main groups.

LED TO CAMERA

These systems leverage the rolling shutter effect of cameras and require LEDs switching at kHz to transmit information. *Luxapose*[36] was one of the first methods to exploit this approach to transmit 8 symbols for indoor positioning. A more recent study proposes a more complex transmitter, using several LEDs to exploit the color and space dimensions, so the rolling shutter effect can still be exploited to achieve more than 100 kbps[30].

LED&LC TO CAMERA

Systems like POLI [55] combine RGB LEDs and LCs to transmit information exploiting the color dimension and achieving speeds ~500 bps. All the aforementioned systems (LED and LED&LC) need *active* control of the light source, which is something that SunBox does not require.

LC TO CAMERA

PIXEL [17] is the only study we found using ambient light and LCs to convey information, but the transmission is limited to 14 bps. Following a similar direction, systems such as *PolarTag* [56] do not modulate light *actively*, but they use a static 2D pattern, similar to a QR code, to change ambient light polarization and transmit static information. Like these LC-to-camera systems, we do not have active control over the light source, but by using a dynamic screen-like device, we can obtain speeds comparable to systems that modulate LEDs.

2.7.3. SCREEN TO CAMERA

Several studies have leveraged screen-to-camera communication to achieve multi-pixel data transmission. Studies such as *ChromaCode* [35] and *Pixnet* [32] exploit standard displays to achieve data rates above 700 kbps and 12 Mbps, respectively, and their range can reach the order of meters. *COBRA* [52] and *RD Codes* [57] develop custom 2D color barcodes to attain data transmissions greater than 100 kbps at short ranges. *Softlight* [33] adds the concept of rateless codes for different channel conditions, *Uber-in-Light* [58] uses color channels and MFSK for high throughput and reliability, and *SBVLC*[34] implements a *"fast QR filtering"* for consecutive QR codes. All of these approaches make use of active screens on smartphones, except for *Uber-in-Light* which makes use of a traditional screen. Compared to our approach, we only use ambient light as the carrier of the system and use a microdisplay for secure short-range communication. Furthermore, our system works under sunlight, which reduces the performance of most screens or demands more power to increase the screen light intensity.

Table 2.7: Different VLC systems

	Type	Source	Data rate	Power Tx	Range	Receiver	Outdoors
CVLC[30]	Active	3 RGB LED	>100 kbps	250 mW*	40 cm	Camera with lens	No‡
Passive-VLC[13]	Passive	LED Flashlight	1 kbps	400 µW + 3 W†	1 m	Photo-diode	Yes
PIXEL[17]	Passive	Ambient Light	14 bps	1 mW	10 m	Camera	No‡
LuxLink[42]	Passive	Ambient Light	80 bps	30 mW	4.5 m to 65 m	Photo-transistor	Yes
Chromalux[54]	Passive	Ambient Light	1 kbps	27.3 mW	1 m to 50 m	Color sensor	Yes
RetroTurbo[14]	Passive	LED lamp	8 kbps	0.8 mW + 8 W†	7.5 m	Photo-diode	No‡
SunBox	Passive	Ambient Light	10 kbps	110 mW	10 cm	Camera	Yes

* Estimated value as no power consumption is reported. † Corresponds to the power of the LED used.
‡ No reported outdoor experiment.

2.7.4. REFLECTIVE DISPLAYS

Overall, our work can be seen as an advancement at the intersection of the three areas mentioned above: *LCs* as transmitters, *cameras* as receivers, and *screens* as 2D surfaces with higher data densities. Our main motivation to merge these areas comes from reflective display technology [39], which exploits sunlight to backscatter images. Most of these reflective displays, however, are based on nematic LCs, making them slow, and are rather big. These two properties make them better suited for billboards. To create a secure and reliable link, we select a tiny microdisplay, which has the backscattering property but is not intended to work with ambient light due to the use of smectic LCs. In principle, our approach could be extended to larger screens for long-range broadcast channel applications instead of short-range personal channels.

2.8. DISCUSSION

SunBox is a novel platform that leverages ambient light, sunlight or artificial, to create a short-range wireless link. In this section, we discuss our system's limitations and possible improvements.

Hybrid systems. SunBox works from sunrise to sunset fueled by the light coming from the sun, as shown by our results in subsection 2.6.8. This limitation encourages designing a hybrid system that works during low-sunlight conditions. One possible system could place an LED light bulb on top of SunBox, which a rechargeable battery can power up. Once the system detects dim light conditions, it activates the artificial light to illuminate the surface of SunBox. A second alternative is to merge SunBox with another short-range wireless solution, like NFC, to cope with conditions when natural light is too low for the system to work, provided that the phone implements such a solution.

Effect of motion. Our system uses a smartphone holder to fix the position of the phone. However, we also tested SunBox holding the phone by hand and noticed a reduction in its performance. There are two consequences of adding motion to the system. First, the system detects the ROI at the beginning of the transmission process. Thus, if the motion leaves the reflective surface out of the ROI, the link is broken. Second, if

motion is minor and the surface is still inside the detected ROI, noise is added to the system, as pixel intensity can change due to motion. Potential solutions include adding a ROI-tracking mechanism and a more sophisticated image processing to account for the motion-related noise.

2.9. CONCLUSIONS

We propose a reliable short-range wireless system that exploits ambient light using a COTS microdisplay as a transmitter and a smartphone as the receiver. To the best of our knowledge, this work is the first to modulate ambient light using a screen-based on smectic LCs. SunBox obtains between 2 kbps and 10 kbps with a low-end phone (30 FPS) operating indoors, with standard lighting, and outdoors, during a cloudy day.

3

Sol-Fi: Enabling Joint Illumination and Communication in Enclosed Areas with Sunlight

In Chapter 2, the scenario considered is to create a short-range wireless link using a backscattering principle in an already illuminated environment. This chapter considers the totally opposite scenario: an enclosed area, such as a room without windows or a basement. Due to the advances in VLC, artificial light bulbs can provide illumination and wireless communication simultaneously. Artificial lighting, however, has some drawbacks compared to using daylight in enclosed spaces. First, using sunlight consumes less power. Second, the use of natural light improves the health and comfort of the occupants.

We propose a system, dubbed Sol-Fi, to provide joint illumination and communication in enclosed spaces using sunlight. Our system relies on two main components: commercial sunlight collectors and a novel transmitter to modulate ambient light. The sunlight collectors utilize optical fibers to guide natural light from open to enclosed spaces, and our transmitter modulates the incoming light providing two novel features. First, to analyze the pros and cons of the optical devices used in the literature for ambient light communication, Sol-Fi examines the properties of Liquid Crystals (LCs) and Digital Micro Mirror Devices (DMDs). Second, to investigate the trade-off between single- and multi-band communication, Sol-Fi proposes an optical design that can modulate the entire spectrum or divide it into different (individually modulated) bands. Second, to investigate the trade-off between single- and multi-band communication, Sol-Fi proposes an optical design that can modulate the entire spectrum or divide it into different (individually modulated) bands. Our evaluation shows that, depending on the number of bands (single or dual) and the type of modulator (LC or DMD), Sol-Fi provides a data rate between 0.8 to 80 kbps, a range between 0.5 to 5 m, and a field-of-view between 30° *to* 60°.

3.1. INTRODUCTION

This chapter aims to create a new type of light bulb, one that provides joint illumination and communication with sunlight. This new light bulb builds upon two main concepts: Li-Fi and sunlight collectors.

Li-Fi. The most popular application of VLC: is a technology that can transform light bulbs into wireless transmitters through the fast modulation of light intensity [59]. These systems use fast-switching and high-power LEDs to render illumination and wireless communication.

Sunlight collectors. Natural illumination is fundamental for humans and several studies report that the type of light affects our physiological [60] and mental well-being. Regarding the latter, rooms without windows lack natural light and visual stimuli [61], with consequences such as increased risks of depressive disorders [62] and reduced performance in workers [63] and students [64]. To quantify this situation, a wide study considering 3600 employees from eight countries, mainly in Europe, found that 42% of workers have no natural light [63]. The benefits of sunlight have motivated innovative *daylighting systems* that bring natural light to enclosed areas. These systems are classified as *passive* and *active*. Passive systems, known as sun tunnels, place a concave lens on a roof and use tubes to guide sunlight indoors. This approach is simple and not so expensive but does not provide much sunlight. *Active systems* have the opposite trade-off, they use a set of lenses to track the sun and optical fibers to guide natural light. Active systems, known as *sunlight collectors*, are more costly, but provide massive amounts of light at further distances [65], enabling the creation of 'natural' light bulbs. In this way, people enjoy the full benefits of natural illumination, even in the absence of windows.

Motivation. Inspired by the area of VLC and its application on *LiFi*, we focus on the following research question: *if a sunlight collector is already installed to bring natural light indoors, can we embed data inside sunlight to create a natural light bulb that provides illumination and communication?*

Such a communication system could provide three advantages: (i) a free, safe, and healthy spectrum, (ii) reduced power consumption, and (iii) reduced economic costs. Regarding the spectral benefits, the broad spectrum of daylight ensures a good quality of color rendering for the human eye and positively affects our body and mind in terms of physical, physiological, and psychological aspects [66, 67, 68]. To emulate a light source with a spectrum similar to sunlight, more than one type of LED is required. Regarding power consumption, daylight systems offer the advantage of avoiding the *double energy conversion* required by solar panels to power LEDs [69]. For example, converting sunlight to energy using solar cells provides at best a 40% lumen-to-watt conversion [70], and converting energy to light with LEDs provides a 10-30% watt-to-lumen conversion. Finally, regarding cost, research in the area of daylight systems suggests that redirecting sunlight is about 25 times more cost-effective than using solar panels to power LEDs [71]. Moreover, the energy that is not converted to light is usually dissipated as heat, which increases the cooling costs of buildings [72, 68].

Challenges. Modulating ambient light is a complex process studied in the area of Passive-VLC. Contrary to artificial light (LEDs), which are diodes modulated *directly at high speeds*, natural light bulbs are purely optical and require external modulators. This fundamental difference raises two challenges to design Sol-Fi.

Challenge 1: Limited optical modulators. Passive-VLC does not have modulators purposely designed for wireless communication, researchers are re-purposing optical devices originally designed for image projection. Currently, the state-of-the-art (SoA) relies on two types of modulators: liquid crystals (LCs) and digital-micro-mirror devices (DMDs). LCs are easy to modulate but have a slow bandwidth, and DMDs have the opposite trade-off. The design of transceivers with these optical devices is complex and no work has analyzed thoroughly their trade-offs.

Challenge 2: Single-band modulation. A salient feature of visible light is its broad spectrum. Active-VLC (e.g. LiFi) exploits this broader spectrum to attain high-data-rate links. However, most Passive-VLC transmitters modulate the *entire* visible light spectrum as a single band without exploiting multiple narrower bands to increase the data rate [13, 54, 18, 42, 17, 14, 12, 73]. Multi-band modulation with sunlight is an open challenge in Passive-VLC and it is important to tackle it, otherwise, a key spectral advantage of natural light will remain unexploited.

Contributions. To provide natural light and communication, Sol-Fi makes the following contributions.

Contribution 1: Device analysis [section 3.2]. We propose a system that integrates novel Passive-VLC methods with sunlight collectors. Our design removes the need of reflective surfaces to guide natural light and analyzes the pros and cons of the two modulators used in the SoA (LCs and DMDs).

Contribution 2: Optical design [section 3.3]. We combine optical and embedded systems to build a natural light bulb that modulates information. The design considers both modulators (LCs and DMDs) and utilizes Frequency Shift Keying (FSK) to compare their performance *under the same setup.*

Contribution 3: Multi-band modulation [section 3.4]. Contrary to other passive platforms, we propose the first method to modulate two independent bands. Our approach follows a careful optical design to divide the wide spectrum of sunlight into two narrower bands in order to increase the data rate. We implement a basic multi-band prototype and test it in two scenarios: a controlled environment using constant light, and under the changing conditions of natural sunlight.

Our evaluation shows that depending on the number of bands and the type of modulator used (LC or DMD), Sol-Fi can modulate the healthy spectrum of sunlight attaining links with a data rate between 0.8 kbps and 80 kbps, a range between 0.5 m to 5 m, and a FoV between 30° to 60°.

3.2. ANALYZING PASSIVE MODULATORS

The main idea of Sol-Fi is to combine commercial sunlight collectors with a novel framework for passive modulation, as shown in Figure 3.1a. If sunlight collectors are already present in a building, our framework shows that data could be added to the system. In this section, we introduce the sunlight collector used in our work and analyze the different types of modulators available in the SoA.

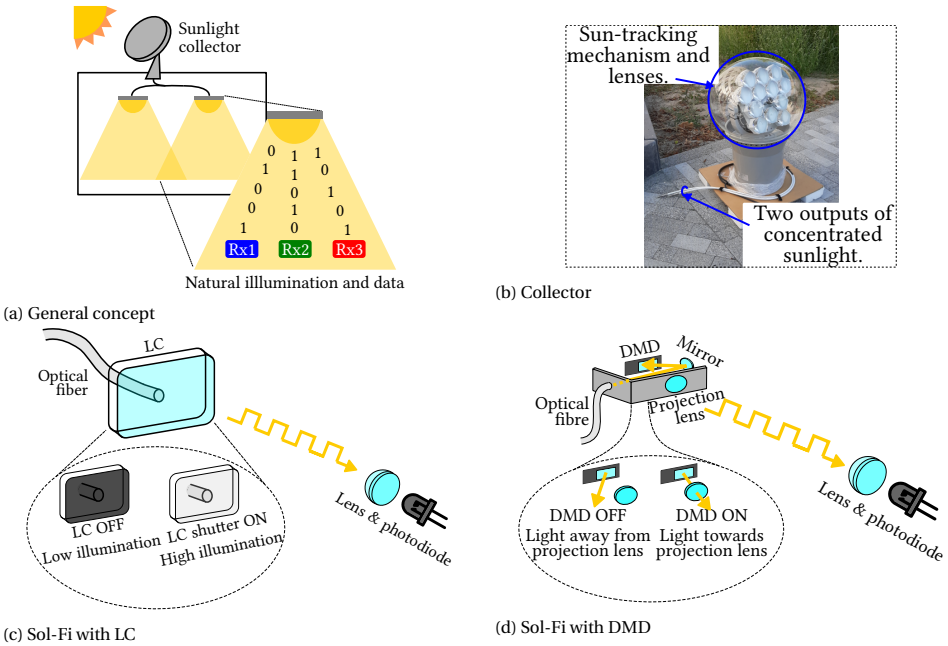

Figure 3.1: Sol-Fi concept and components. With LCs (c), the light is either blocked or let pass through. With DMDs (d), the light is either directed towards the intended direction or towards a different one.

3.2.1. SUNLIGHT COLLECTORS

Sunlight collectors are a subclass of a broader type of solution, called *active daylight systems* [74]. These systems use a mechanism to track the sun's position in order to gather and concentrate the largest amount of sunlight. Among the various daylight systems in the market, the sunlight collector has three main features that make it suitable for our prototype implementation: mobility (it can be carried to different places), flexibility (light is guided by optical fibers, which can be bent), and a small output area, which eases the modulation process. Two types of collectors are provided by Parans [75] and Himawari [76], both designed to be placed over roofs. Our implementation uses the latter (Figure 3.1b) because it is lighter and easier to move. The main shortcoming of the sunlight collector is its price (around €5000) due to its optical components and the complexity of the sun-tracking mechanism. This particular system provides optical fibers for two natural light bulbs.

Although research studies suggest that daylight systems can save more than 60 % of

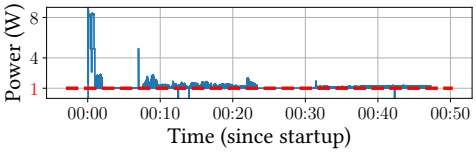

Figure 3.2: Sunlight collector's power consumption.

energy consumption [68], it is important to empirically measure the sunlight collector's power consumption. Figure 3.2 shows the power consumption of the collector we use during one hour. At the startup, which occurs once a day, the power goes up to ~8 W and after that, it oscillates between 1 W to 2 W to track the sun. The realignment occurs every two seconds, which are the peak values around 2 W, and then reduces to around 1 W. For this amount of power, the collector provides an average luminous flux of 4500 lumens. This large amount of flux is attained because sunlight's illumination ranges from a few klux at sunrise and sunset to more than 100 klux at midday. To obtain the same amount of lumen, LEDs would require a power between 35-40 W.

Regarding communication, *natural and artificial light systems can complement each other using hybrid systems*. For example, natural light systems are better suited for environments that are predominantly occupied during the day, such as classrooms, libraries, and laboratories that have limited or no access to windows. However, similar to *hybrid* daylighting systems [68], which combine artificial and natural light bulbs, our approach can leverage active-VLC (LiFi with standard LEDs), during the night or periods of low sunlight intensity. In our Discussion section (section 3.7), we concisely review hybrid systems.

3.2.2. MODULATOR REQUIREMENTS

There are two aspects that make the modulation of natural light challenging. *First*, while optical fiber systems offer a wide range of components for fast switching, attaining data rates of Pbps [77], they are designed for light that is polarized, monochromatic (around 1550 nm) and coherent. Sunlight is unpolarized, broadband and non-coherent, thus, preventing the use of these fast-switching optical devices. *Second*, the inherent limitations of LCs and DMDs. Due to the lack of modulators for ambient light, all the advancement in Passive-VLC relies on devices originally designed for displays (LCs) and projectors (DMDs). These devices pose various trade-offs that need to be analyzed. Before describing the unique features of LCs and DMDs, let us introduce six requirements that an *ideal modulator* for Sol-Fi should have.

1. **Low attenuation.** The modulator should not decrease the luminous flux delivered by the sunlight collector. The efficiency should be close to one.

2. **Large area.** The larger the area, the more flux that can be modulated. An ideal modulator should have an area compared to an artificial light fixture (several cm^2).

3. **Fast switching.** Passive modulators have an intrinsic (slow) mechanical component. The faster the mechanical switching, the faster the link.

4. **No flickering.** Contrary to radio waves, light waves can be seen by people. Thus, all communication systems based on light must be flicker-free.

5. **Low power.** Passive modulators are low power, but the lower the power consumption, the more cells that can be used to increase the transmitter's area (R2).

6. **Low cost.** Similar to the low power case (R5), the lower the cost, the more devices that can be used to increase the transmitter's area.

Requirements R1 and R2 improve the range and coverage of the link. Requirement R3 increases the data rate and requirement R4 is needed to pass the IEEE standard for safe VLC transmissions. Requirements R5 and R6 facilitate the design of bigger transmitters, improving in that manner R2.

3.2.3. PASSIVE MODULATORS

To modulate ambient light, all Passive-VLC systems in the literature use either LCs [17, 13, 15] or DMDs [78, 18]. The operating principles of both devices are shown in Figure 3.1, and the relation between their features and the requirements for our ideal modulator is summarized in Table 3.1.

LC shutters are transmissive surfaces that either block or let light pass through, based on a driving voltage. Except for a couple of studies, Passive-VLC has relied almost exclusively on this modulator. Considering Sol-Fi's requirements, the main advantages are their large surface area (R2, several cm^2), low power consumption (R5, sub-milliwatt), and low cost (R6, a few dollars per cell). There are, however, a few shortcomings. First, the attenuation is high due to the use of polarizers (R1), which cut 50% of the luminance. Second, the switching speed is slow (R3), reaching only a few hundred Hz. These low switching speeds lead to single-cell data rates that attain at most 1 kbps [13, 15]. Third, the slow speed leads to a higher probability of observing flickering (R4).

DMDs are reflective surfaces consisting of micro-mirrors that switch between two angles. By default, DMDs have a slow refresh rate (60 Hz), but a recent study proposed a new controller that can modulate low-end DMDs at hundreds of kHz [18]. The advantages of DMDs are *(i)* their low attenuation, since they reflect more than 97% of light (R1); *(ii)* their high switching frequency (R3), which is over 30 times faster compared to LC shutters; and *(iii)* the reduced risk of flickering due to the high switching frequency (R4). However, DMDs have several disadvantages too. The most important is its reduced area (R2), which is two orders of magnitude smaller than LCs, reaching only a few mm^2. Other disadvantages are the higher power consumption (R5, tens of milliwatts) and cost (R6, a few tens of dollars per DMD).

3.2.4. TRADE-OFF ANALYSIS

As shown in Table 3.1, no modulator satisfies all requirements. R4 (no-flicker) is satisfied by both devices because we use FSK to modulate signals, as described later. Thus, the trade-off analysis has to focus between requirements R1 (attenuation) and R3 (data rate), which favor DMDs; and requirements R2 (area), R5 (power) and R6 (cost), which favor LCs.

DMDs have the advantage of providing a switching speed that is 30 times higher than LCs' (R3), but comparing R1 (attenuation) versus R2/5/6 (area, power, and cost) requires more analysis. The (de)modulation of FSK signals in passive systems consumes tens of mW [42]. Hence, the benefit of the sub-mW operation of LCs is not in reducing the system's *overall* power consumption, but in enabling a bigger transmitter's area with negligible extra power. Similarly, the benefit of the LCs' low cost is its ability to increase the transmitter's area rather than on reducing the total cost of the platform. All in all, we have a trade-off between low attenuation (R1) and bigger areas (R2/5/6). To analyze this trade-off, we quantify the optical performance of a single LC cell versus a single DMD

	R1	R2	R3	R4	R5	R6
LC	~50%	cm^2	100's bps	can flicker	sub mW	few $
DMD	~100%	mm^2	10's kbps	no flicker	10's mW	10's $

Table 3.1: Comparison between LCs and DMDs

cell. Considering an illuminance $\mathscr{I}$ (in lux), and denoting A and a as the areas of an LC and DMD, respectively, the luminance provided by the LC is $\mathscr{L}_L = \mathscr{I}A/2$ (divided by 2 due to the polarizers), and the one provided by the DMD is $\mathscr{L}_D = \mathscr{I}a$. However, considering that the area of the DMD is two orders of magnitude smaller, the luminance provided by the LC is, approximately, fifty times higher than the one provided by the DMD ($\mathscr{L}_L/\mathscr{L}_D \approx 50$). To match the LC's luminance, an optical system would need to concentrate more luminous flux on the DMD.

Contribution 1: Our analysis of LCs and DMDs clarifies their fundamental trade-offs. Overall, we are left with one modulator (LC) that can provide 50 times more luminous flux, enabling a longer range and wider coverage; and another modulator (DMD) that can provide 30 times faster switching speed, enabling higher data rates. *Due to this disparate trade-off, we cannot select only one modulator, and thus, Sol-Fi considers different optical designs to evaluate both modulators.*

3.3. SINGLE-BAND LINK

To evaluate the illumination and communication capabilities of Sol-Fi, we consider three metrics: FoV, range and data rate. These metrics are evaluated on two optical designs, one for LCs and the other for DMDs. This section first describes the transmitters and receiver, and then, presents their evaluation.

3.3.1. LC MODULATOR

The simplest implementation of Sol-Fi is to place the optical fiber coming out of the sunlight collector behind an LC shutter, as shown in Figure 3.1c. Compared to other sunlight links based on LCs, the advantage of using the sunlight collector is that the optical fibers provide a wider field of view with the same direction throughout the day. The SoA relies on reflective surfaces to direct sunlight toward the LC. Those reflective surfaces are not realigned through the day, and when they are aligned with the sun, usually radiate parallel rays that form FoVs close to 0°. Below, we present the nominal (theoretical) values of our design and later we evaluate them in a real setup.

- **Switching speed.** The modulator's switching speed is defined as the sum of the rise and fall times. We use an LC shutter with a switching speed of 160 Hz.
- **FoV.** LCs do not change the direction of light passing through. Hence, the FoV is determined by the aperture of the optical fiber, which in our case has an FoV of ±30°.
- **Loss.** Since LC shutters utilize polarizers, the optical power is reduced by half. In theory, this attenuation reduces the range by a factor of $\sqrt{2}$.

Hardware implementation. We build a 3D holder to place the fiber behind the LC and the LC is controlled by an Arduino-Due. This implementation is shown in Figure 3.9a.

3.3.2. DMD MODULATOR

Contrary to LCs, which are not designed for a specific light pattern (diffused or directional), DMDs are designed to receive directional light (parallel rays). When used for Passive-VLC, DMDs have the advantage of low attenuation (R1), but the fact that the area is small (R2) and the impinging rays are parallel, leads to a reflected beam with an almost 0° FoV.

To broaden the FoV of our DMD-transmitter, we build upon the principles used in (mini)projectors. Modern projection technology uses LEDs, filters, mirrors, lenses and DMDs. These components perform two tasks. First, they guide the light emitted by the LEDs into the DMD. Second, they cast the image reflected by the DMD into the intended projection area. For Sol-Fi, we disassemble a commercial mini-projector and modify it in two main ways. First, we remove the original controller and DMD, which are designed for video rendition, and connect a controller and DMD designed for Passive-VLC. The contribution of Sol-Fi is not on the DMD controller, we use methods that have been already reported in the SoA [18]. Second, we remove the LED lights and filters, and modify the casing to place our optical fiber as the light source. With these modifications, shown in Figure 3.1d, our DMD-transmitter is able to (i) receive sunlight, instead of LED light, and (ii) project a wide FoV, similar to a lamp, instead of a narrow beam. Considering these factors, the features of this design are:

- **Switching Speed.** DMDs modified for Passive-VLC operate at switching speeds of hundreds of kHz, several orders of magnitude higher than LCs.
- **FoV.** Since we follow the mini-projector guidelines, the FoV should be similar to the one stated in the datasheet of the original mini-projector, which is $\pm 32.8°$ [79].
- **Loss.** The DMD reflects most of the light, but the system faces losses because the coupling between the optical fiber and the DMD is suboptimal compared to the coupling between the original LED and DMD. Next, we describe the measures taken to minimize optical losses.

Hardware implementation. To reduce the losses, it is important to use a projector where the diameter of the original LED is similar to the optical fiber's diameter. For this reason, we select the DLPM2000EVM mini-projector from Texas Instruments and an Eska® 3mm-diameter plastic optical fiber (POF). A 3D support is built to place the fiber close to the internal mirror and DMD of our custom projector. For the controller and DMD, we use an FPGA to modulate the DLP2000 DMD. This DMD has two tilt angles, $12°$ and $-12°$, and a rotation axis of $45°$.

3.3.3. RECEIVER

Photodiodes (PDs) and cameras are widely used as receivers in Active- and Passive-VLC. Our receiver uses a PD due to its fast response and low power consumption compared to a camera. The receiver is the same for both modulators and places a TEPT4400 phototransistor on a board that includes a single-stage amplifier with variable gain. Following

(a) LCD (b) DMD

Figure 3.3: Measured MFSK symbols. The blue and green signals are measured at 20 cm and 160 cm, respectively.

the customary principle of adding a lens to increase the received light intensity, our design uses a 9.5 mm plano-convex (PCX) lens with an anti-reflective coating on top of the PD. This increases the range of the system without compromising the lightweight property (and mobility) of the receiver.

3.3.4. MODULATION

The contribution of our work is *not* on the modulation approach. We follow the guidelines presented in prior studies for LCs and DMDs. FSK is chosen because it prevents flickering in slow LC modulators (R4). Our Mary-FSK (MFSK) approach is the same for both transmitters (LCs and DMDs). The only difference is the base frequencies chosen for each.

Considering the switching speeds of each modulator and the bandwidth of the receiver, we use four base frequencies for the LC[1] (M=4, 2 bits per symbol): 400 Hz, 800 Hz, 1.2 kHz, 1.6 kHz; and higher frequencies for the DMD: 20 kHz, 40 kHz, 60 kHz, 80 kHz, as shown in Figure 3.3. These schemes lead to a data rate of 800 bps for the LC and 40 kbps for the DMD. Both data rates fall between the ranges reported for other single-cell transmitters: 0.1 to 1.0 kbps for LCs [42, 17, 13], and 4 to 80 kbps for DMDs [78, 18]. The transmissions use the following sequence: `IDLE`, `STX` (Start Transmission), `DATA PACKET`, `ETX` (End Transmission), and `ETB` (End of Transmission Block). And with both modulators, the transmitters send the message `"Hello world!"` continuously. The receiver sends the data to a laptop, where an FFT is used to decode the data.

3.3.5. EVALUATION

The evaluation has two components, illumination (optical loss and FoV) and communication (BER). Given that sunlight is variable, *we use an artificial light source to have a controlled setup for this section and the next one. In section 3.5, we evaluate the system with sunlight.* To mimic the optical input provided by sunlight collectors, we connect one end of an optical fiber to a flashlight, and the other end to our transmitters.

To resemble an enclosed space, the evaluations of this section and the next one are done in a dark room. For each transmitter, we measure the illuminance (lx) and bit-error-rate (BER) every 20 cm along two lines. One line goes through the middle of the FoV (bisector) and the other through one of the edges of the FoV (due to symmetry, the other edge has the same result). The results for illumination are presented in Figure 3.4

[1] Note that with FSK, we can modulate the carrier at higher frequencies than the switching speed (160 Hz) because we do not need square waves, triangular waves are sufficient.

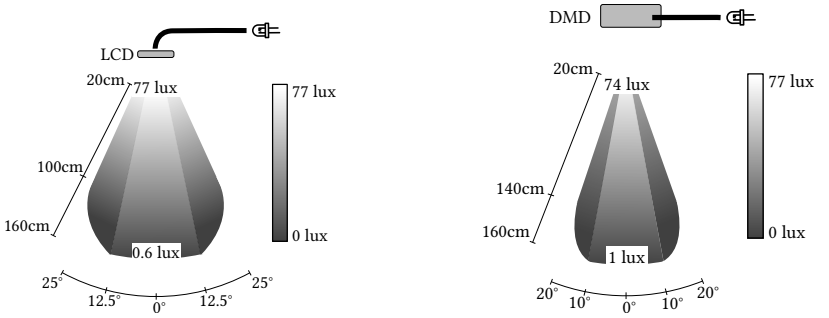

(a) LCD (b) DMD

Figure 3.4: Controlled illumination for single-band.

and for communication in Figure 3.5.

OPTICAL LOSSES

Given that we are not interested only in illumination, but also in communication, we borrow the concept of *close-in measurements* from wireless communication to analyze optical losses. We set a luxmeter at a distance of 20 cm from the output of the optical fiber and evaluate two setups, one connecting the fiber to the LCD-transmitter and the other connecting it to the DMD-transmitter. With these measurements, we find a loss of 66 % for the LCD-transmitter (higher than the expected theoretical loss of 50 %); and a loss of 70 % for the DMD-transmitter. This evaluation shows that –in spite of the lower attenuation of the DMD (R1, 97% reflectivity)– both transmitters lead to similar losses. *The losses of the LC, however, are fundamental due to the use of polarizers, while the DMD losses can be reduced significantly with a better optical coupling between the fiber and the DMD (to reach the* 97 % *efficiency), as discussed later.*

FIELD-OF-VIEW.

Figure 3.4 shows that the FoV of the LC design is similar to the aperture of the optical fiber, 30° versus 25°, which is expected since the LC is agnostic to the radiation pattern. But the FoV of the DMD-transmitter is narrower, 30° versus 20°. This is likely due to the suboptimal coupling of the optical fiber with the mirrors, lens, and DMD.

COMMUNICATION

To assess the reliability of the link, we measure the BER along the bisector and one of the edges of the FoV. As Figure 3.5 shows, both transmitters provide perfect links along the bisector up to 160 cm. But along the edges, the link becomes unreliable after 100 cm for the LC-transmitter and after 140 cm for the DMD-transmitter. Having shorter edge links is not unusual because many radiation patterns are stronger along the bisector and weaker at the edges (called Lambertian patterns). The reason for the longer range along the edge of the DMD-transmitter is the optical design. Projector optics aim at casting light in a more homogeneous manner across all angles.

It is important to note that the highly reliable links in this section are obtained even for low light conditions (below 80 lx). These lux values are clearly too low to provide adequate illumination, but these are controlled tests done with artificial light to benchmark

both modulators under the same conditions. With sunlight, which is stronger, we will see that the illumination increases significantly.

Contribution 2: Our results show that it is possible to connect optical fibers with passive modulators, which will enable using the output of sunlight collectors. Furthermore, as we will discuss in the related work section, our optical designs overcome the most important limitation in current Passive-VLC studies in the SoA: the fact that the FoV of SoA platforms is close to 0° when working with natural light.

3.4. DUAL-BAND LINK

The prior section uses a single-band link, that is, the entire spectrum is modulated at once. To increase the data rate, it would be valuable to divide the spectrum into multiple channels. A well-known method for exploiting the spectrum in communications systems is to divide the available bandwidth into narrower bands. These OFDM approaches are widely used in Active-VLC. Passive-VLC, on the other hand, has no control over the light source, and hence, the challenge is greater. *To the best of our knowledge, there is no passive communication platform that attempts wavelength division with natural light.*

To tackle this challenge, we apply the general principle of wavelength division multiplexing (WDM). Applying this principle to Passive-VLC, however, requires considering some important differences. First, in optical fiber systems, WDM is an efficient technique because either the laser light is already divided in narrow bands or *in-fiber* filters allow band division within the fiber, thus reducing loss. Sol-Fi, on the other hand, requires an efficient filtering approach to divide natural light into narrower bands. Second, the light transmitted in optical fiber systems is not exposed to users. This means that the fibers' output can emit any spectrum. Sol-Fi, on the other hand, needs to guarantee that the (re)combined bands produce a white spectrum that is suitable for illumination.

3.4.1. SUNLIGHT (DE)MULTIPLEXING

Our prototype divides the spectrum into two bands. With facilities able to build purpose-designed filters for communication (and not only for human vision) the approach can be generalized to obtain more bands.

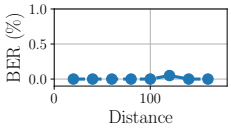

(a) LC, center of FoV

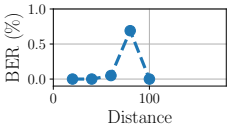

(b) LC, edge of FoV

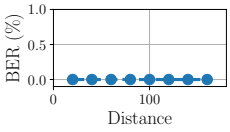

(c) DMD, center of FoV

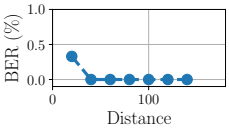

(d) DMD, edge of FoV

Figure 3.5: BER for controlled single-band setups.

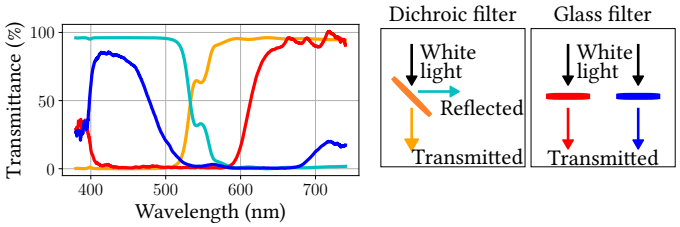

Figure 3.6: Spectral response of dichroic filters used at the transmitter (turquoise and orange) and glass filters used at the receiver (blue and red).

MULTIPLEXER

The goal of the multiplexer is to divide the spectrum into *complementary* bands, whose (re)combination delivers white light suitable for illumination. Among the various types of off-the-shelf filters, the *Dichroic filter* has a response that satisfies this need. Figure 3.6 depicts the response of a dichroic filter that splits the spectrum into two complementary bands: one band is transmitted (orange) and the other band is reflected (turquoise).

An important property of dichroic filters is that by changing the light's angle of incidence (AoI), we can fine-tune the cut-off wavelength. Our implementation uses a red color dichroic filter from Thorlabs[2]. We select this filter because at an AoI of 45° the cut-off wavelength is 550 nm, close to the middle of the light spectrum. These dichroic filters are used for both modulators, LCs and DMDs. Given that the sunlight spectrum changes during the day, such as in sunsets with more red components, the system would require a tunable filter to split the spectrum into balanced bands.

DEMULTIPLEXER

The receiver for the dual-band designs requires two photodiodes, each having an optical filter in front. However, contrary to dichroic filters, whose response depends on the angle of incidence, the receivers need to be angle-independent so users can be located at any position within the transmitters' FoV.

A suitable filter for the receiver's requirements is the glass-colored filter, which is angle-independent, but the trade-off is that it has a narrower spectral response, which leads to some energy loss. One filter should be close to the blue band, and the other close to the red band, leaving the green band free to avoid cross-talk. We implement our receivers with commodity glass filters, with a response depicted in Figure 3.6. Similar to the case of dichroic filters, tunable filters would be required for different sunlight conditions, to match the filters in the multiplexer.

3.4.2. TRANSMITTERS AND RECEIVER

Given that both dual-band designs (LC and DMD) use the same filters, we first analyze their common characteristics regarding speed, FoV, and loss; and then, we provide the differences regarding the implementation.

- **Data rate**. Since we use two channels, the speed is double of the single-band design, leading to 1.6 kbps for the Dual-LC transmitter and 80 kbps for the Dual-DMD transmitter.

[2]Dichroic Filters: https://www.thorlabs.com/newgrouppage9.cfm?objectgroup_id=986

- **FoV**. In the dual-band design, the transmitter radiates two beams, each with a different color, as shown in Figure 3.7. With a proper optical design, the coverage of both beams would overlap precisely, recombining into white light and leading to the same FoV as for the single-band design. In our prototype, however, the coverage does not overlap precisely because of the big size of the dichroic filters (25.4 mm diameter), leading to three regions: a white cone in the middle, where both bands overlap and generate white light, and orange and turquoise stripes at the sides of the cone. Due to this effect, the FoV of the overlapping white cone is narrower than the FoV of the single band.

- **Loss**. A general principle of multi-band designs is to trade off a higher data rate for a shorter range. Since the energy of the entire spectrum is divided into sub-bands, the signals travel shorter distances. This trade-off applies to all wireless systems.

LC TRANSMITTER.
The Dual-LC transmitter is depicted at the top of Figure 3.7a. Recalling that the sunlight collector has two optical outputs, our emulated setup has two flashlights each connected to one fiber. The fibers' outputs are orthogonal to each other and launched towards two dichroic filters oriented at an angle of 45°. This design allows rendering one spectrum with the *transmission* of the dichroic filter (orange) and the other with the *reflection* (turquoise). The output of each dichroic filter is modulated independently by an LC shutter but given that both optical outputs point in the same direction, they recombine into white light.

DMD TRANSMITTER.
The Dual-DMD transmitter is depicted at the top of Figure 3.7c. Given that the size of the dichroic filter is bigger than the optical enclosure of the mini-projector, instead of placing the filter before the modulator (as with the LCs), we place the filters after the DMD modulates the signal. The hardware setup duplicates the single-band design, we use two optical enclosures (mini-projectors) each with a DMD that is independently modulated.

RECEIVER.
The receiver is the same for both designs and it duplicates the setup of the single-band receiver: two phototransistor boards, each with a glass filter in front.

3.4.3. SPECTRAL ANALYSIS

To gain a deep understanding of Sol-Fi, we need to analyze the transformations of the spectrum at various points throughout the illumination process, as shown in Figure 3.7.

Step 1: Light source. The spectrum of the light source, point ① in Figure 3.7, helps determine the width of the bands to balance the division of luminous flux. In our dual-band design, we use 550 nm as the spectral boundary. Note that for the sunlight spectrum (Figure 3.10), the spectral boundary should be slightly above the 600 nm mark. But given that the spectrum of the sun changes throughout the day, cooler (bluer) in the morning and warmer (more yellow) in the afternoon, we leave the boundary at 550 nm, at the risk of having one band stronger than the other.

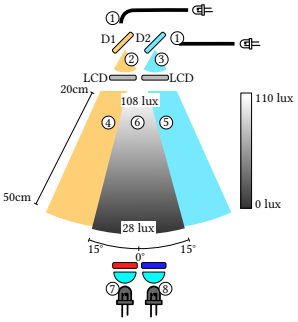

(a) Illumination for Dual-LC.

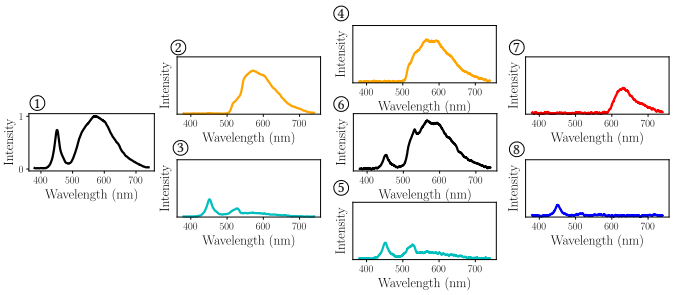

(b) Spectral analysis for Dual-LCD modulator.

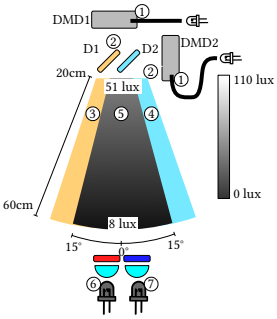

(c) Illumination for Dual-DMD.

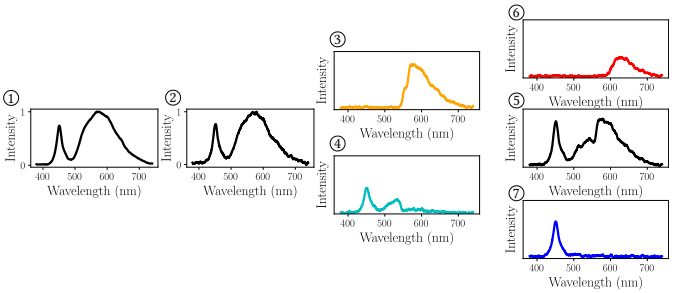

(d) Spectral analysis for Dual-DMD modulator.

Figure 3.7: Illumination and spectral analysis for the dual-band setups.

Step 2: Modulator. The modulator should, in principle, cause only attenuation but no spectral distortion. The DMD does not cause any distortion, since there are no spectral changes between points (1) to (2) in Figure 3.7d; but the LC causes some distortions, which can be particularly noticed at points (3) and (5) in Figure 3.7b. This occurs because the LC is not really a shutter that blocks light, but rather a device that transforms the color of the incoming light via internal polarization changes [17]. Thus, the LC transforms the incoming spectrum into a different tone of white, but these tones are still perceived as white color by the human eye.

Step 3: Dichroic Filter. It is important to consider if *all* rays reach the filter in parallel, else each ray –arriving at a different angle– will be mapped to a different spectrum. Given that the FoV of the optical fiber (30°) is bigger than the FoV of the mini-projector (20°), the rays coming out of the fiber reach the dichroic's surface with a wider range of angles. Due to this reason, the bands of the DMD-transmitter (points (3) to (4) in Figure 3.7d) have less overlap (cross-talk) than the LC-transmitter bands (points (2) to (3) in Figure 3.7b).

Step 4: Recombined white light. The light coming from the dichroic filters will recombine. Some of the original spectra will be lost, but the remaining spectrum should still fall within the range associated with white light for the human eye. For the LC (point (6) in Figure 3.7b), the illumination attains a warmer tone (because some of the blue energy is lost), while for the DMD (point (5) in Figure 3.7d), the illumination does not change much compared to the original source.

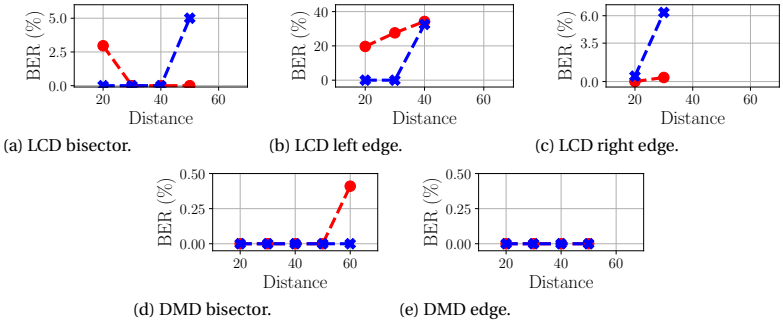

Figure 3.8: BER for dual-band setups in a controlled environment. The color represents each channel.

Step 5: Glass filter. The glass filters have a narrower response than the dichroic filters, which helps to limit cross-talk. It is important to note that the spectra of the LC bands are a bit noisier than those of the DMD bands. This noisier behavior explains why LC links perform slightly worse than DMD links in the controlled scenarios (Figures 3.5 and 3.8), in particular for the blue channel (Figure 3.8).

Overall, our spectral analysis shows that the DMD is a better modulator because it sharply divides the communication bands, adds less noise, and provides illumination that is close to the original source. However, in our sunlight evaluation, we will see that the bigger area of the LC (R2) provides an important advantage due to the amount of luminous flux it modulates.

3.4.4. EVALUATION

Similar to subsection 3.3.5, we assess the illumination and communication of the dual-band systems inside a dark room. The bands send different data: one sends `"Hello world!"` and the other `"Bye, aliens!"`, at the same rate. Thus, we have two channels with a joint data rate of 1.6 kbps and 80 kbps, for the LC and DMD setups, respectively.

OPTICAL LOSSES

Following the same 'close-in measurements' method as for the single band, we place the luxmeter at a distance of 20 cm from the optical fiber's output, and in between, we measure the responses of the dichroic filter. Our design obtains an almost perfect division of the spectrum, 53.6 % of the energy goes to the orange band and 51.6 % to the turquoise band (the sum is greater than 100 % due to the overlap in the middle). The efficient division of the bands, however, is not maintained in the communication channel due to the mismatch between the filters at the transmitter and receiver. Based on the spectral responses in Figure 3.6, we estimate a loss of 52 % for the turquoise/blue channel and a loss of 24 % for the orange/red channel, but it is important to consider that the final loss depends on the spectrum of the light source, which is variable for sunlight.

FIELD OF VIEW.

Contrary to the single-band case, the FoV has three regions: orange stripe, white cone and turquoise strip. Given that the overlap of the two bands is not precise, the FoV of the white cone is reduced to ±15°, with the LC setup showing wider stripes at the edges

because it has a wider FoV than the DMD setup. *This non-overlapping issue is not a fundamental problem, a more elaborated optical design could obtain a precise overlap delivering the same FoV as the single-band case*: ±25° for LCs and ±20° for DMDs.

It is important to note that, compared to the single-band case, the dichroic filters change the illumination intensity. In the single-band case, both designs provide an intensity close to 75 lx at 20 cm, but in the dual-band case, the LCs provide 110 lx (Figure 3.7a) while the DMDs provide 51 lx (Figure 3.7c). In theory, the illuminance for both setups should be similar but they are not due to the different angles of incidence arriving at the dichroic surface, as explained in Step 3 in subsection 3.4.3. In the LC case, the wide aperture of the optical fibers causes heterogeneous angles of incidence, which lead to a spectral leakage that increases the overlap between the two bands. In the DMD case, the angle of incidence is more homogeneous due to the optical design of the projector, but this good filtering performance removes some energy around the 550 nm band compared to the single-band case.

COMMUNICATION

Since the symmetry along the bisector is lost due to the different color bands, we measure the BER in three lines: the bisector and two lines at ±15° edges. For this evaluation, the receiver is placed at different ranges, in steps of 10 cm. The results are presented in Figure 3.8.

Overall, the LC setup does not have a good performance with the controlled scenario. The bisector and edge lines have locations where the BER is above 1 %, with the left edge having BERs that are above 20 %. This occurs due to uneven illumination and spectrum. But with sunlight, we will observe that the overlap gets better at longer ranges, providing reliable links with both bands. The DMD setup has a stronger performance, with a BER <1 % for all the positions and directions, due to the better filtering process and more even illumination and spectrum (compared to the LC setup). Thus, for the DMD setup, we only assess one edge.

Contribution 3: Until now all Passive-VLC studies have modulated ambient light as a single band. Our work is the first to provide a basic multi-band communication with sunlight. Overall, the DMD continues to appear as a device with better properties, leading to more reliable links.

3.5. SUNLIGHT EVALUATION

Sunlight is inherently variable. During our experiments, it ranged from a few thousand lx to values above 100 klx, depending on how clear or cloudy the day is. The luminance gathered by the Himawari collector is delivered through two optical bundles (6 fibers per bundle) with an angular aperture of 58°. The sunlight spectrum can include strong IR (infrared), which radiates heat. Sunlight collectors can mitigate excessive heat with IR filters and cooling systems [80]. However, to reduce the design complexity, our implementation places the transmitters at a distance of 2 cm from the fiber's output. This distance allows heat to dissipate, at the cost of reducing the captured light.

Before proceeding, it is important to put ranges and illuminance in context. A communication range of 1.6 m from a ceiling is valid for user spaces[3], and desk lamps have a

[3] Construction standards suggest a ceiling height of 2.75 m (where light bulbs hang), and working desks (sitting

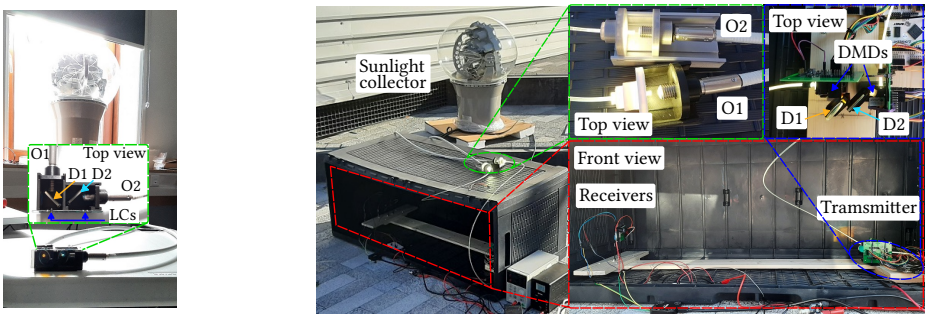

(a) LC setup.

(b) DMD setup.

Figure 3.9: Setups for both modulators using the sunlight collector.
D: dichroic filter, O: output of collector.

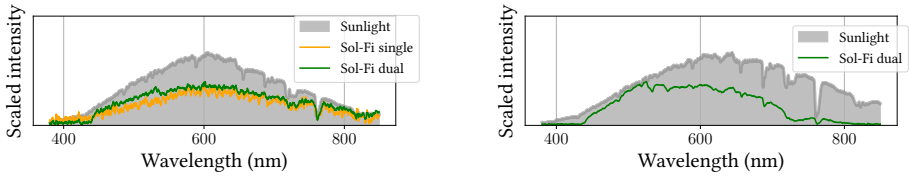

(a) LC-Sol-Fi

(b) DMD-Sol-Fi

Figure 3.10: Measured spectra.

range that is half of that or less. Regarding illuminance conditions[4], a cozy (low-light) living room receives around 60 lx and a working desk around 360 lx. Table 3.2 summarizes the results of all setups regarding illumination, range, FoV and data rate.

3.5.1. SOL-FI WITH LCS: EXPLOITING LARGE AREAS

This experiment is performed in a *dark room:* the sunlight collector is located next to a window, while the other blinds are closed, c.f. Figure 3.9a. Note that this setup introduces undesirable noise because the room is not completely dark, but we will see that in spite of these non-ideal conditions, the system provides reliable links.

SINGLE CHANNEL

For the single-channel setup, the two collector outputs are placed behind one LC shutter. The intensity of sunlight is so high that, in spite of the 66 % attenuation of the LCs, the illuminance at a 1 m distance is above 1000 lx (more than enough for any human task), and at a 5 m distance around 100 lx (sufficient for a living room or hallway). Due to this high intensity, the links are perfect at all locations and the spectrum still captures all the bands required for a healthy and comfortable natural illumination, as depicted in Figure 3.10a. To test the setup under more stringent conditions, we remove the lens from the receiver, which reduces the SNR. The results of this configuration are presented

or standing) are placed between 0.8-1.2 m

[4] Luminance (in Lumen, lm) and Illuminance (in Lux, lx) are different metrics: 1 Lumen = 1 Lux × $1m^2$

	Single band		
Modulator	**LC**		**DMD**
Data rate	800 bps		40 kbps
Range	Up to 5 m		Up to 1.5 m
Angle in the FoV	0°	25°	0°
Illumination†	100 lx	80 lx	100 lx
Channel	White	White	White
BER†	0.02 %	0.24 %	0.0 %

	Dual band							
Modulator	**LC**						**DMD**	
Data rate	2 × 800 bps						2 × 40 kbps	
Range	Up to 3 m						Up to 0.8 m	
Angle in the FoV	+30°		0°		-30°		0°	
Illumination†	100 lx to 200 lx						30 lx	
Channel	Red	Blue	Red	Blue	Red	Blue	Red	Blue
BER†	0.02 %	1.65 %	0.0 %	0.06 %	0.0 %	0.0 %	0.04 %	0.0 %

Table 3.2: Results for all setups using sunlight. 100 lx is comparable to the light in a hallway. †: At the max. range.

in Table 3.2 for the maximum range of our lab (5 m). Even in this case, the BER remains below 1 % for an FoV of ± 25°.

DUAL CHANNEL

For the dual setup, the collector outputs (O1 and O2) are first aimed at their corresponding dichroic filters (D1 and D2), and the bands are modulated independently by the LCs, as shown in the top view box of Figure 3.9a. For the daylight conditions present during the experiment, the illumination at a communication range of 3 m ranges from 100 lx to 200 lx over the FoV. Table 3.2 presents the results, where we can see that except for the red channel at +30°, all the other links attain a BER below 1 %. Furthermore, the recombined spectrum is similar to the original (single-band) sunlight, providing all the health benefits (Figure 3.10a) plus an almost perfect color illumination at the bisector (Figure 3.11b).

3.5.2. SOL-FI WITH DMDS: LEVERAGING SPEED

A major advantage of the big LC area is that it can capture all the luminance radiated by the collector's output. Each output has six optical fibers put together into a sealed enclosure with a 1.2 cm diameter. Given that the LC's area has several cm^2, all the luminance radiated by the bundle passes through the LC. For our purposes, an *ideal DMD design would insert the fibers coming from the collector directly into the DMD*, but this is not possible because we cannot disassemble the fibers coming out of the sunlight collector without damaging them.

To overcome this issue, we place our 3 mm fiber at a distance of 2 cm from the bundle[5], as shown in one of the top views of Figure 3.9b (O1 & O2). The losses of this coupling can be overcome with a professional design. However, despite this loss, we will see that

[5]The distance of 2 cm is based on the fiber properties: glass fibers (bundle) can tolerate heat, but we use plastic fibers that are easy to handle but do not resist heat.

sunlight is so strong, that the DMD setup provides an illuminance similar to a desk lamp. Compared to the LC setup, the DMD design is more complex and delicate. For this reason, we build a *portable dark enclosure*, using a black box as shown in Figure 3.9b. In these experiments, due to the physical constraints of the black box, we only measure the bisector.

SINGLE CHANNEL.

Different from the LC, the DMD area does not allow pointing both collector's outputs into a single DMD. Thus, the setup takes only one of the collector's outputs and launches the light into the fiber connected to the DMD. Note that using a single output implies that in this case, we have half the luminous flux received in the LC case with a single-band. To place the receiver inside the box, we use a wood plank where the receiver is placed every 10 cm from a range of 0.7 m up to 1.5 m. The BER was zero for all the locations and the illuminance ranges from approximately 600 lx to 100 lx, providing sufficient light for a working space. Table 3.2 shows the results for the longest range.

DUAL CHANNEL

For the dual channel, each collector bundle is coupled to the input fiber of the respective DMDs and then launched toward the dichroic filters. Considering that the signal strength of this setup is lower (because we use two bands instead of one), we test distances from 40 cm to 80 cm, in steps of 10 cm. The BER of both channels is 0.0 % at all points, and the illuminance ranges from around 100 lx at 40 cm to 30 lx at 80 cm. The latter is presented in Table 3.2. Regarding the recombined spectrum, most of the sunlight visible spectrum is present, with a reduced IR spectrum (Figure 3.10b) due to the heat dissipation of our optical coupling. Despite this loss, the color temperature is not affected significantly, as presented in Figure 3.11c. Losing some of the IR spectra simply makes the light cooler (less energy in the yellow and orange bands).

Important trade-off between single and bual bands. Table 3.2 shows that the dual band designs double the data rate but reduce the range. This is a standard trade-off in wireless systems because single channels maintain all the energy in one band, while multi-channel systems divide that energy.

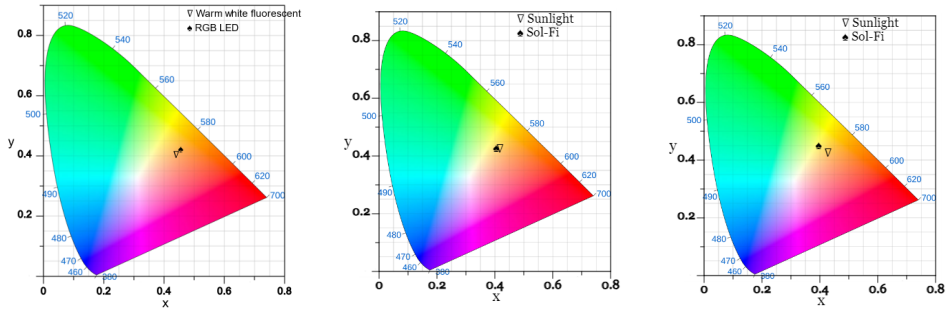

(a) Artificial light (b) LCD dual (c) DMD dual

Figure 3.11: Color quality of Sol-Fi for the dual band

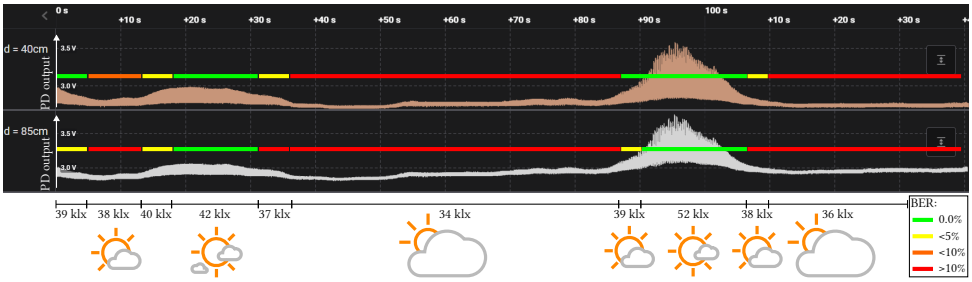

(a) Signal strength and BER (green/orange/red bars) of two PDs during cloudy conditions

(b) Cloud conditions

Figure 3.12: Sol-Fi's performance under variable sunlight conditions (30-40 klx with clouds).

3.5.3. VARIABLE SUNLIGHT CONDITIONS

All previous results are obtained during clear days. A thorough evaluation requires cloudy periods with reduced sunlight intensity and diffused radiation. To anonymously describe our meteorological conditions, we provide as a reference New York City, which has a similar latitude to our location. At that latitude, sunlight ranges from a few thousand klx at sunrise and sunset up to values beyond 150 klx at noon. This radiation pattern holds for most of the year with some variance due to the different seasons [81].

We test Sol-Fi with clear (direct sunlight) and cloudy skies (diffused sunlight) using the single-channel DMD setup at two distances, 40 cm and 85 cm. Figure 3.12 shows the results, where the link oscillates between operational (green) and failure (red) depending on the cloudiness level. We noticed that the link's performance decreased during cloudy periods with diffused light intensities around 30 klux or lower.

Another effect of sunlight fluctuation is the variation of the unmodulated light intensity at the receiver. For the setup using LCs and sunlight, there was unmodulated light (noise) coming from the window and reaching the receiver but the system kept working. Moreover, there are two possible solutions to filter unmodulated/ambient light. First, the light can be filtered during the demodulation process as DC bias. Second, the receivers can restrict their FoV to partially block ambient light and increase the SNR [82].

3.6. RELATED WORK

Passive-VLC with LCs. In the SoA, Passive-VLC systems have widely adopted LCs as optical transmitters. These systems can be divided into two categories: when the light source and receiver are *co-located* (*reflective* systems), or in *different locations* (*transmissive* systems). In the first category, the LCs require *artificial lights* and retro-reflectors to modulate light back in the direction of the light source [12, 15, 14, 13]. In the second one, the LCs are used alone as a modulator, while another part of the system redirects light

towards the receiver [42, 54, 83]. The version of Sol-Fi using LCs is similar to the latter group, but it has two main differences compared to all the reflective and transmissive systems cited above.

The *first difference* is only operational. All the above systems have narrow beams (limited FoV), either due to the inherent behavior of retro-reflectors or the small parallel beams radiated in transmissive systems. Thanks to the default properties of sunlight collectors, Sol-Fi's FoV is wide and constant throughout the day. The *second difference* is more fundamental. No study has provided WDM with sunlight. The majority of studies do not modify the spectrum in any way [12, 15, 14, 13, 42], and only two studies modify the spectrum but do *not* create independent channels [54, 83]. ChromaLux isolates a *single color channel* to obtain a faster-switching response of the LC [54], and SpectraLux 'distorts' the entire LC spectrum to transmit different colors [83], encoding multiple bits per color. Neither of these studies creates independent parallel channels inside the spectrum.

DMDs & (Passive)VLC. Even though commercial DMDs are developed primarily for video projection, they have also been used in applications such as spatial modulation, microscopy, and data center interconnection [84, 85]. Some studies have also explored the use of DMDs in VLC, specifically for localization [86, 78, 87]. In those systems, a dedicated light source (LED or laser) is required, and in addition, a limited range and data rate are demonstrated due to the slow switching times of the off-the-shelf controllers. Another study developed a custom controller and demonstrated that DMDs can be used for Passive-VLC, attaining data rates up to 80 kbps [18], with a *narrow beam*. Our system attains half this data rate (40 kbps) for the single-band case due to the optical losses at the interface with the sunlight collector, which limits the signal strength. Reducing these optical losses for the DMD-Sol-Fi setup would improve the data rate. However, aside from adding a dual-band feature, our system also largely improves the FoV compared to the SoA.

Sunlight communications. A few recent studies have also identified the benefits of using sunlight for indoor wireless communication. These are valuable designs, but *they do not provide real implementations, mainly simulations.*

In [88, 16], a *smart window* is embedded with a special dual-cell crystal shutter (DLS). The connectivity in this setup relies on the relative position of the window and the sun, while Sol-Fi's reliance on sunlight collectors provides a stable direction (link) throughout the day. Additionally, the number of DLS goes up to 70 for a single channel. In Sol-Fi, the number of LCs goes up to the number of channels. Another study, LiFiTube [89] explores the use of a tubular light guide (TLG), which could be seen as pipes that guide sunlight, but their efficiency is lower compared to the sunlight collector, which tracks the sun. Additionally, the TLG's output size is large, which requires LiFiTube to use 28 LCs for modulating a single channel.

The fact that the above studies do not provide real implementations highlights the difficulty of combining complex optical systems with Passive-VLC. Sol-Fi's basic prototypes are the first to implement a natural light bulb that also provides communication by using not only LCs and implementing a single channel like the studies above but also using DMDs and dual-channel capabilities.

Multi-band systems with Active-VLC. The use of multiple bands is also explored in Active-VLC (LiFi). While the higher speed achieved by Active-VLC is orders of magnitude larger than the speed achieved by Passive-VLC, including Sol-Fi (tens of kbps vs. hundreds of Gbps), this is mainly due to the fact that Active-VLC systems can modulate LEDs at high speeds, but not because they use numerous channels. In one study [90], the system uses an RGB LED to provide illumination up to 3 m while providing 50 Gbps per channel, achieving a total of 300 Gbps with six channels: three color channels (red, green and blue) multiplied by two polarization directions. Other theoretical studies propose using more channels: up to 12 channels for short distances [91], and up to 20 channels for room illumination [92], but they rely on simulations. These studies show that achieving multiple channels with different spectra (more than three) is not simple even with artificial light (LEDs). Sol-Fi is a first attempt to get multi-band transmissions with natural light.

3.7. DISCUSSION

Sol-Fi is the first attempt to provide a natural light bulb with communication capabilities, but the power consumption and optical losses are still high, and its performance depends on environmental conditions. To describe the first two drawbacks, Table 3.3 shows the power required to provide an indoor area with illumination and connectivity using various methods.

Hybrid systems. As stated in section 3.2, Sol-Fi is a diurnal technology that would require interacting with other wireless systems. Considering a room that requires illumination and communication, Table 3.3 shows that WiFi and *LiFi [94] can provide Mbps, but the costs of illumination and wireless connectivity would be above 10 W (8 W for illumination plus 1.4-6 W for wireless connectivity)*. The sunlight collector can provide more illumination using less power, but there are 3 key challenges. The first two are to increase the data rate and reduce the optical losses (as discussed later in this section). The last one is to integrate this passive VLC with an active VLC system so the illumination and data rate can be kept constant during the day and night. If these issues are tackled, future wireless systems could provide the best combination of energy efficiency and robustness by designing a hybrid system that exploits natural light during the day (like Sol-Fi), artificial light during the night (mostly LiFi, since the cost of adding communi-

Setup	Light		Wireless		Speed
	Lum. Flux	Power	Control	Modulator	
WiFi	~800 lm	~8 W	~6 W [93]		Mbps
LiFi[94]	~800 lm	~8 W	~1.4 W		Mbps
Collector	4.5 klm	< 2 W	-	-	-
LC-Sol-Fi	1-2 klm	<2 W	30 mW	µW	<1.6 kbps
			2 mW⋆	µW⋆	
DMD-Sol-Fi	10-130 lm	<2 W	1.3 W	193 mW	<80 kbps
			2 mW⋆	45 mW⋆	

Table 3.3: Sol-Fi and other wireless technologies, assuming an enclosed area.
⋆ The estimated low-power setup.

cation on top of illumination is not high), and radio systems to provide coverage in areas and times where light is not robust.

Optical losses & light quality. Table 3.3 shows that an 8 W LED provides a room with 800 lm (recall that lumen is not the same lux). In our experiments, the sunlight collector gave almost 6x more luminance (4.5 klm) consuming 4x less power (<2 W). However, even though DMDs have high reflectivity (97%), the luminance of our DMD-transmitter reduces to 10-130 lm. There are three main reasons for this loss. The first two are the optical couplings between the collectors' outputs and our fibers, and between our fibers and the DMD. These losses can be overcome by designing a custom collector with fibers that can be plugged directly into the DMD with the appropriate lenses. The third loss is due to the dichroic filters, which are also responsible for light division and further free-space recombination. An optical design that captures the transmitted and reflected components could overcome the losses. Moreover, a more elaborated solution is the use use of *in-fiber* filters in combination with optical fiber circulators. This system would keep the light-division system inside the fiber, thus reducing losses and resulting in two fibers with complementary spectra. After independent modulation, a fiber coupler recombines both bands into one fiber, with a better color distribution. This implementation would require combining cutting-edge *industrial* methods from sunlight collectors, optical fibers and projector technologies.

Power consumption. One advantage of Passive-VLC is its low power consumption compared to WiFi or LiFi, which require several watts. However, our DMD transmitter still uses too much power, more than 1 W, due to the precise timing required to modulate the *video controller*. We generate those signals with the Artix-7 FPGA board, which is not optimized for low power but for fast prototyping. Looking at the datasheet of the Apollo4 Plus (Ambiq) [95], working at 1.9 V and 40 MHz, we estimate that a DMD-transmitter could consume around 200 mW (controller+DMD), but this alternative requires a careful PCB design and interrupt handling. A further potential reduction is to design a custom DMD without the video projection overhead. We use the DMD as a single pixel modulating at max 80 kHz (all micromirrors move synchronously), we do not need to modulate each pixel at 40 MHz. The DMD data sheet indicates that bypassing the video control could reduce the power consumption to 45 mW. Such a design could only be done by a DMD manufacturer, but we estimate that a simpler slower controller with a 'single-pixel' DMD would consume around 50 mW.

Line of sight (LoS). Non LoS (NLoS) VLC is based on light reflections. In those cases, factors such as the SNR, the number of reflections and the surface reflectivity affect the link quality [96, 97]. Sol-Fi was not tested under NLoS, but the performance would reduce (similar to what would happen to any other VLC system).

3.8. CONCLUSIONS

This work proposes a novel framework to design the first natural light fixtures that provide all the health benefits of sunlight plus wireless communication. Our framework proposes a thorough analysis of different modulators, providing a wide FoV channel with multi-band capabilities. Our results show that even with sub-optimal off-the-shelf components, sunlight could provide illumination and communication through a new generation of low-power passive transmitters.

4

Edge-Light: Exploiting Luminescent Solar Concentrators for Ambient Light Communication

*While Passive VLC systems exploit ambient light, most have a fundamental constraint: the link can **only** follow the propagation direction of ambient light. In the previous chapters, we explored different methods to counteract this effect. In Chapter 2, SunBox relies on a reflective surface to backscatter ambient light, while, in Chapter 3, a mechanical system keeps track of the sun and concentrates its light for the Sol-Fi system. This chapter explores a different scenario: a swarm of ground robots that want to communicate with sunlight. This robot-to-robot communication requires the redirection of sunlight sideways - parallel to the ground - regardless of the sun's position. To allow 'lateral communication' with ambient light, we propose using Luminescent Solar Concentrators (LSCs). These optical components receive ambient light on their surface and re-direct part of the spectra towards their edges.*

The work presented in this chapter has three main contributions First, we benchmark various optical properties of LSC to assess their performance for ambient light communication. Second, we combine LSC with liquid crystal (LC) shutters to form lateral links with ambient light. Third, we test our links indoors and outdoors with artificial and natural ambient light. As a sample application, we enhance two robots with our LSC links and show that they can exchange simple commands and coordinate tasks by communicating only with sunlight.

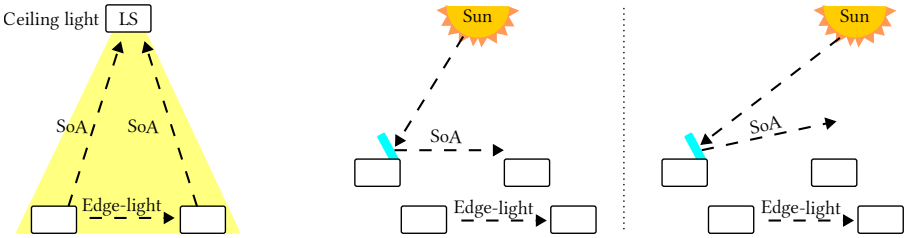

(a) Indoor backscattering Passive VLC. (b) Sunlight Passive VLC.

Figure 4.1: Different scenarios comparing Edge-Light to SoA.

4.1. INTRODUCTION

As mentioned in Chapter 1, VLC can complement radio wireless communications by exploiting visible light and it can be divided into two subdomains: Active VLC and *Passive VLC*. Among the advantages of Active VLC are the data rate, which achieves several hundred Mbps (or even Gbps [98]), and the direction of light, which is controlled by the orientation of the LED. In contrast, *Passive VLC*'s main advantage is the low energy consumption: less than one micro-joule per bit [13], while active VLC with similar ranges consumes 30× more energy per bit [99]. However, the performance of *Passive VLC* is limited to a few Kbps in speed and most of the transmitters use liquid crystal (LC) shutters to control the intensity of ambient light [54, 17, 83, 42, 13, 12, 15, 100, 14], which limits the link to follow the same direction.

Challenge: link rigidity. Passive VLC is a promising technology for low-end embedded applications but has shortcomings. One of those limitations is the inability to modify the link's direction. Contrary to radio systems, whose antenna arrays can determine the beam direction, passive VLC has *no control* over the light source. This lack of control implies that the communication direction is fixed: the link can *only* follow the same propagation direction of ambient light. Consider the scenario in Figure 4.1a, where objects in different areas report information to the light source using existing backscattering methods [13, 12]. With current techniques, the objects cannot communicate directly with each other. Placing mirrors on the side could enable lateral communication, but if the objects move the reflection angles change and the links break (Figure 4.1b). The mirrors would need to be mechanically aligned, increasing the complexity and energy cost of the system. This misalignment issue would be even more critical in scenarios with mobile robots.

Contribution: lateral communication. To expand the link design space of passive VLC, we propose using Luminescent Solar Concentrators (LSC). These optical materials absorb a specific band of light and convert it to a different band (color). LSC also feature wave-guiding properties, the converted band is emitted towards the edges. A typical application of LSC is energy harvesting in windows. The LSC receives sunlight over its surface and redirects part of the spectrum towards the edges (window frame) where solar panels harvest energy arriving from the converted band [101].

A key advantage of LSC is that, independently of the incidence angle of ambient light, it *always* directs spectral energy towards the edge, no mechanical alignment is required.

In this work, we analyze the optical properties of LSC and design a novel link to achieve lateral communication with ambient light. Overall, our study, named Edge-Light, provides the following contributions.

Contribution 1: LSC analysis [section 4.2]. Two central properties of any wireless link are its range and field-of-view (FoV). LSC materials have a limited optical conversion efficiency, around ~5 %[1] or higher for research-based LSC [102, 103]. Due to this low efficiency, the expected strength of the LSC's emitted light is limited. We thoroughly analyze different commercial LSCs to identify the one that provides the best coverage in terms of range and field-of-view.

Contribution 2: wireless link design and evaluation [section 4.3]. LSC redirect light but does not modulate it. To build a transmitter, we pair LSC with liquid crystal (LC) shutters and implement frequency-based modulation to cope with the variable intensity of ambient light. To build a receiver, we consider the fact that LSC absorbs white light but emits color light. Thus, we analyze two sensing approaches: color sensors and photodiodes plus color filters. Our final receiver includes various optical components to increase the link's SNR. We perform a thorough evaluation of Edge-Light under artificial ceiling lighting and natural sunlight.

Contribution 3: sample application in robot-to-robot communication [section 4.4]. We build different prototypes of Edge-Light on top of robots and design a protocol for them to exchange three different commands. Our evaluation shows that robots can reliably send these commands (rotate, move forward, stop) for ranges up to one meter. As a sample application, we show a scenario where a single robot cannot move a box, but two robots coordinate and move the box communicating their commands only with sunlight.

4.2. LUMINISCENT SOLAR CONCENTRATOR

In essence, an LSC receives light spectra on its surface and emits a different spectrum while guiding it to its edges. To describe the LSC operation we need to define three bands: *incoming, absorbing* and *emitted*. Figure 4.2 shows how these bands interact with each other. First, the incoming band is received over the LSC surface. In our case, the incoming band is white ambient light. Second, internally the LSC transfers spectral energy from an *absorbing band* to an *emitted band*. In Figure 4.2, the LSC absorbs energy from the blue band and transfers it to the emitted green band. The incoming light does not need to be white and the emitted light can be of different colors. Furthermore, independently of the angle of incidence of ambient light, the LSC always emits light towards the edge. This is an important property to maintain a lateral link when the light source or object moves.

These absorption and emission features stem from the physical structure and properties of two materials constituting an LSC: a host and a dopant. The *host* is, in essence, a waveguide, and its main function is to trap the emitted light by total internal reflection (TIR), guiding this light to its edges. The *dopant* is added to the host and it defines the absorption and emission properties of the LSC. At a molecular level, the dopant absorbs

[1] We measure the *peak intensity* in the absorption band and *peak intensity* in the emission band of one COTS LSC.

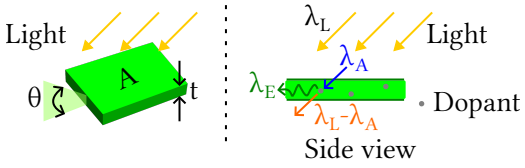

Figure 4.2: LSC overview. Area: (A), thickness (t) and field of view (FoV, θ). Dopants molecules absorbe photons (λ_A) in the absorption band and emits photons (λ_E) in the emission band.

Manufacturer	Colours	Thickness (mm)
Alt®	Green, Orange	3 mm
Pyrasied©	Blue, Green, Red	8 mm

Table 4.1: LSC materials

photons from a specific wavelength and then emits a photon in a different wavelength.

The research community has explored various types of materials to manufacture LSC while tuning and improving its response. There are different types of hosts that implement different types of TIR, such as refraction-based [104, 105] or photonic crystal [106, 107]; and different types of dopants, such as organic luminophores or quantum dots (QD) [108, 101], to control not only the LSC's absorption and emission spectra but also its response time. Delving into the details of the various types of LSC is not in the scope of this research, but as this material is a core component of our system, we analyze in this section the properties of commercial of-the-shelve (COTS) LSC. We purchase an assortment of LSCs from Alt® and Pyrasied©, presented in Table 4.1, and analyze their performance. For these LSCs, the host is acrylic (Polymethylmethacrylate, PMMA) and the dopants are fluorescent dyes.

From a wireless communication perspective, we are interested in analyzing three main LSC parameters. First, the spectral response of the emission band, since color bands represent independent channels in optical communication. Second, the signal-to-noise ratio (SNR) of the emission band, because it determines the link quality. Third, the response time of the dopant, to guarantee that no delays are introduced in the modulation process.

4.2.1. SPECTRAL RESPONSE

The spectral response of the LSC is defined by the absorption band and the emission band.

Considering that LSCs have different spectral responses, the research questions we need to answer are: *What LSCs are better suited for passive communication? Which emission bands provide the stronger signals? Which emission bands could be combined to provide multiple input channels?* To answer these questions, we provide a thorough analysis of the absorption and emission bands of the four different colors of LSC[2]. However, since most COTS LSCs are sold without information regarding their spectral response, we must empirically determine it.

[2] Blue, Green and Red from Pyrasied©. Orange from Alt®

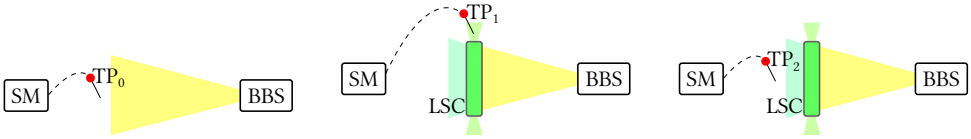

(a) Light emitted by the BBS. (b) Light emitted laterally by LSC. (c) Light passing through the LSC.

Figure 4.3: Setup to measure the LSC spectrum. SM: spectrometer, BBS: broadband source. TP: test point.

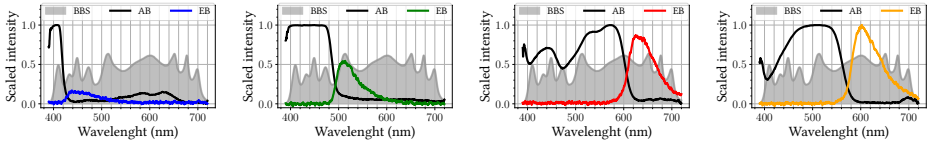

(a) Blue LSC (b) Green LSC (c) Red LSC (d) Orange LSC

Figure 4.4: Spectral response of the LSCs. BBS: broadband light source, AB: Absorption band, EB: Emission band.

Setup. To measure the light spectra of the LSCs, we use a spectrometer and a broadband light source (BBS). The first step is to get the spectrum of the BBS as a reference, which is the test point 0 (TP_0 in Figure 4.3a). Second, to measure the emission band, we illuminate each LSC with the BBS and place the spectrometer on the edge of the LSC (TP_1 in Figure 4.3b). Finally, as it is not possible to measure the absorption band directly, we next place the spectrometer behind the LSC to determine the spectrum that passes through it (TP_2 in Figure 4.3c) and estimate the absorption band using Equation 4.1, where S represents a scaling function to normalize the output from 0 to 1.

$$AB = S(TP_0 - TP_2) \tag{4.1}$$

Results. Figure 4.4 shows the measured and estimated spectra for each LSC. The shaded gray curves capture the *incoming band* spectrum from the BBS, which provides similar intensities for all bands in the visible spectrum. The black curves represent the estimated *absorption bands*, which are normalized.

The measured *emission band* is presented as a colored line corresponding to each LSC and normalized based on the highest spectral peak of all emission bands (orange in our case). The results show that the red and orange LSCs provide stronger intensities, while the blue LSC provides a weak emission. This occurs because the optical energy within the absorption band is transferred to the emission band. Since the red and orange LSCs have broad absorption bands (black curves), they provide more energy to their emission bands compared to the blue LSC, which has a narrow absorption band.

The red and orange LSCs, however, have overlapping bands, which would cause interference if they are used simultaneously in a network. The green and red LSCs, on the other hand, could provide independent channels. Due to this reason, we consider the green and red LSCs in our evaluation.

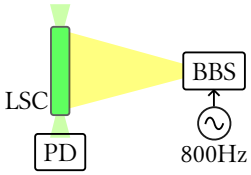

Figure 4.5: LSC SNR and response time measurement setup. PD: photodiode.

Dimensions (cm×cm)	Thickness (mm)	SNR (db)
4 × 4	3	1.89
9.6 × 7.6	3	3.48
9.6 × 7.6	8	3.72

Table 4.2: SNR for different sizes of green-emitting LSCs

4.2.2. SIGNAL-TO-NOISE RATIO

In the prior subsection, we analyzed the effect of the *dopant*. We measured the strength of the emission band, which is dictated by the chemical properties of the dopant. In this subsection, we analyze the effect of the *host*. In particular, the impact that the host's size has on link quality.

Intuitively, a bigger LSC should emit more energy. As shown in Figure 4.2, a larger area (A_i) would allow capturing more light, and a bigger volume ($A_i \times t_i$) means that more dopants could interact with the incoming light in the absorption band. Therefore, the light emitted by a larger and thicker LSC is expected to be stronger than a smaller and thinner one.

To demonstrate the effect of the LSC's size on the signal strength, we select similar LSC materials but with different areas and thicknesses. Using the setup in Figure 4.5 and a set of LSC with emission band in the green spectrum, we illuminate the LSC sample with a light source that is oscillating at a frequency of 800 Hz. We place the setup in a dark room and a photodiode (PD), located at 10 cm from the LSC sample, captures the signal emitted by the edge of the LSC. We compute the SNR by calculating the power spectral density (PSD), based on the Fast Fourier Transform (FFT), and comparing the signal's spectral power vs. the noise spectral power. The results in Table 4.2 show that the area plays a dominant role in increasing the SNR, but the thickness does not. Thus, in our implementation, we try to maximize the area of our transmitter.

4.2.3. RESPONSE TIME

In the prior section, we saw that a bigger host increases the SNR, but the host is also a waveguide: it steers the emitted light to the LSC edges. And, an important parameter of a waveguide is its response time, which depends on its material and dimensions. In general terms, a thicker waveguide has a slower response time. However, for an LSC an extra factor, related to the dopants, affects the response time.

LSCs have been found to have fast responses (in the order of MHz) [101]. The primary reason for this is related to a dopant parameter called *fluorescent lifetime* which can be as short as nanoseconds [109, 110]. This parameter is related to the speed of

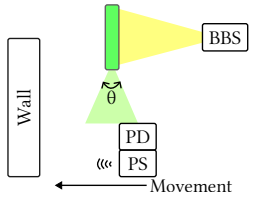

Figure 4.6: Setup for measuring LSC output FoV. PS: proximity sensor.

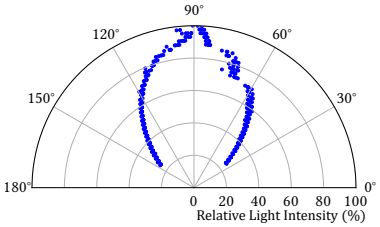

(a) 3 mm green-emitting LSC sample.

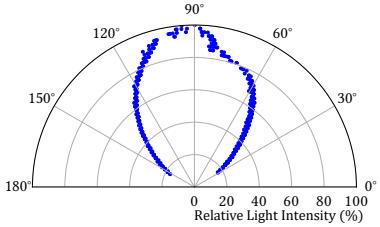

(b) 8 mm green-emitting LSC sample.

Figure 4.7: FoV for two LSC samples of the same material but different widths. Distance between PD and LSC is 36 mm.

the dopants reacting to the incoming photons in the absorption band, it means that a higher speed will increase the response of the LSC. In the next section, we propose using liquid crystal shutters as light modulators, and their switching speeds are an order of magnitude slower than the response time of the LSC. Thus, the response time of LSCs is significantly higher than needed for our platform, making LCSs a suitable choice for our purposes.

4.3. WIRELESS LINK DESIGN

Our aim is to create a wireless link using the LSC based on the properties we analysed previously: its ability to absorb light in a wide angle of incidence and re-emit it in a different direction (to its edges); and its ability to absorb and emit specific optical bands of the light spectrum. In this section, we present first the design of the transmitter and next the design of the receiver.

4.3.1. TRANSMITTER

In this section, we first characterize the field-of-view, then we propose a method to increase the signal strength, and conclude with the description of the modulation.

ESTIMATING THE FIELD OF VIEW

An important parameter in wireless communication is the field of view FoV of the transmitter, which is the angle θ in Figure 4.2. Since the LSC is a waveguide, the field of view (also called numerical aperture), depends on the refractive index of the waveguide material. The host material is PMMA (acrylic), the same material as plastic optical fibres (POF), thus it is expected they have a similar FoV of ±30°.

Dimensions (cm×cm)	Thickness (mm)	$SNR_{old} \rightarrow SNR_{new}$
4 × 4	3	1.89 dB → 2.40 dB
9.6 × 7.6	3	3.48 dB → 3.73 dB
9.6 × 7.6	8	3.72 dB → 4.03 dB

Table 4.3: Boost in SNR by the use of a retro-reflective surface.

We use the setup in Figure 4.6 to measure the FoV of two green-emitting LSC samples with different widths, 8 mm and 3 mm. The setup uses an ultrasound proximity sensor (PS) attached to the PD to measure the distance relative to a reference point[3]. The results presented in Figure 4.7, normalized to the maximum intensity, show that the FoV is the same as optical fibers, ±30° and the width has little effect on the coverage.

INCREASING THE SIGNAL STRENGTH

The working principle of the LSC is stochastic: there is a probability (P_A) that a photon in the absorption band triggers a photon in the emission band. A direct way to increase this interaction is to add a reflector under the LSC, thus the photons that are not absorbed by the LSC are forced to pass through it one more time, increasing the chances for them to interact with the dopants and emit more light in the emission band. To test this principle, we place the three LSC samples of different dimensions over a retro-reflective (RR) surface and use the setup on Figure 4.5 to measure the increase in signal strength. The results in Table 4.3 show an increase of 0.3 dB. Since the RR surface does not add much overhead, it is thin and light, we use this tape for the remainder of the paper. A mirror could be used instead of the RR tape, but mirrors are heavier and more brittle.

MODULATION WITH LIQUID CRYSTALS (LCS)

LSC redirects light but does not modulate it. To modulate information, we build on top of the area of ambient light backscattering [13, 12], which uses liquid crystal (LC) shutters to control light intensity. An LC's working principle is based on polarisation changes controlled by voltage: it blocks light when its pins are driven by a voltage above a threshold (dark state), and it allows light to pass through when its pins are driven by a voltage below a threshold (transparent state). LCs are efficient devices that consume sub-microwatt power, but they have a slow switching speed, which limits the data rate. In our sample application, we send simple commands between robots, and hence, the data rate is not a major disadvantage.

Our final transmitter design, presented in Figure 4.8, consists of three layers, from top to bottom: an LC, an LSC and an RR tape. For the modulation method, we use Frequency Shift Keying (FSK) due to its resilience to ambient light noise [42]. To generate pseudo-sinusoidal carriers, a micro-controller (Arduino Due) drives the LC input voltage at different speeds between 0 V and 3.3 V to oscillate between the blocking and transparent states.

The commands for our application are encoded as symbols in different carrier frequencies. We use a total of three commands (symbol frequencies) as shown in Table 4.4

[3]The FoV of the PD is larger than the LSC

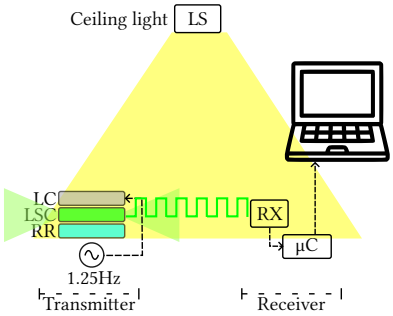

Figure 4.8: Setup for testing the receivers under a controlled scenario. μC: microcontroller.

Symbol	Frequency (Tx)	FFT Frequency (Rx)
S_1	5.0 Hz	5.0 Hz
S_2	6.67 Hz	6.25 Hz
S_3	10.0 Hz	10.0 Hz

Table 4.4: Frequencies for each symbol, based on a 25 ms timer.

in the *'Frequency (TX)'* column. The column *'FFT Frequency (Rx)'* is used at the receiver side and is explained in the next section. In subsection 4.3.3, we delve into more details about these symbol's frequency selection.

4.3.2. RECEIVER

The receiver design considers two main points, reducing the noise level (increasing the SNR) and selecting the best photosensor to decode the color channels. Depending on the system, SNR levels require a minimum for successful operation. LoRa requires a minimum of 0 dB but the SNR can be as low as −20 dB depending on the *spread factor* [111]. For a good WiFi connection, the lowest SNR is 25 dB. For our system, we determine an empirical threshold for the SNR of ~5 dB for the link to work with a high success rate, from our results in section 4.4.

NOISE REDUCTION

In free-space optical communication, it is not only important to assess the FoV of the transmitter, which impacts coverage, but also the FoV of the receiver because it affects the SNR. Ideally, the receiver's FoV should focus *only* on the edge of the LSC because that is the only surface that transmits the signal (S). The space above and below the edge consists of ambient light noise (N). At short ranges, the receiver's FoV covers mainly the LSC edge (high SNR), but as the range increases, the LSC's edge covers only a small part of the receiver's FoV (low SNR).

To cope with ambient noise, a common practice in optical systems is adding a lens in front of the photosensor to focus on the transmitter area. Since the LSC emits the modulated signal on its edge, which has a width in the order of mm, and the strongest light is emitted at the middle point of its width, reducing the FoV allows increasing the

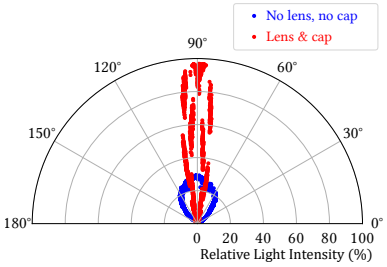

Figure 4.9: Effect of the lens on the receiver: FoV reduction and range increase. Distance between PD and LSC is 76 mm.

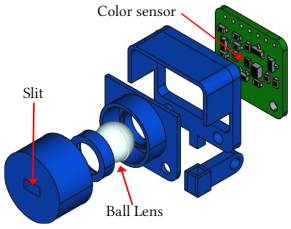

Figure 4.10: Final receiver physical design, including a lens, covers and a small slit.

Type	Sensor	Supplier	Angular range[1]	Response time
Light sensor	DFR0026[2]	DFRobot	±45°	15 µs
Phototransistor	TEPT4400	Vishay	±30°	~15 µs
Color sensor	TCS34725	Adafruit	±55°	Variable

Table 4.5: Types of devices used in the receiver design.
1: Angle of half sensitivity.
2: Based on the PT550 phototransistor.

signal strength. To keep a lightweight implementation we select a small 9 mm ball lens[4] surrounded by a cap to limit the amount of ambient light further reaching the surface of the optical sensor.

Figure 4.10 shows the final design of the receiver which we manufacture using a 3D-printing process. This design enhances the SNR, and thus, the range of our link as depicted in Figure 4.9, where the signal strength is increased by a factor greater than 3×.

SENSOR SELECTION

For the receiver, we consider the three sensors presented in Table 4.5: one ambient light sensor, a phototransistor (PT) with tunable gain, and a colour sensor (CS). Color sensors are slow and provide a programmable gain and response time. The response time is determined by the *integration time*, which is the exposure period of the sensor to control its sensitivity. The color sensor has a trade-off: a large integration time renders a higher sensitivity at the cost of increasing the reading time. To attain the fastest possible link, we use the two fastest integration times available for the color sensor, which are 2.4 ms and 24 ms. Moreover, the color sensor features 4 channels: a *clear channel*, which works similar to a photodiode measuring the intensity based on the whole spectrum, and 3 RGB color channels, which measure the intensity of the spectrum corresponding to red, green or blue colors.

The selection criteria for the sensor is the performance under ambient light conditions, using the setup in Figure 4.8 with the transmitter sending a constant pulse at

[4] Ball lens: 9 mm, K9 glass, Back focal length: ~2 mm

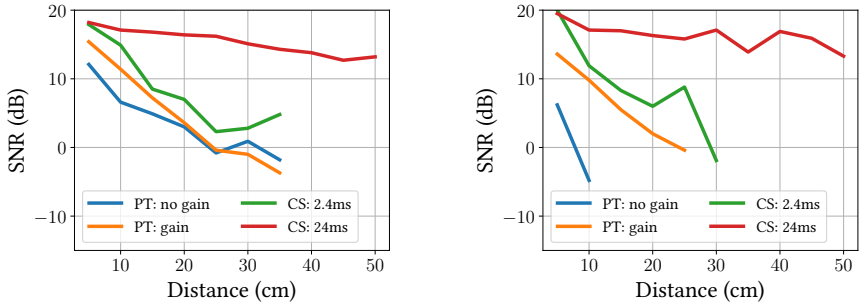

(a) Receivers with no color filter.

(b) Receivers with color filter.

Figure 4.11: SNR for different receivers using the same transmitter.

1.25 Hz (as in Figure 4.5). Using the SNR as a metric, and testing for different distances, we analyze three configurations:

- Bare ambient light sensor.
- PT, varying gain according to range.
- CS, reading the *clear channel*.

The results in Figure 4.11a show that the color sensor at the slowest speed outperforms the other sensors, which is an expected result since the higher exposure time to light allows a stronger signal at the cost of a slower sampling rate. A slow sampling rate is, in general, a shortcoming, but in our design it is not because the LC modulators are slow to begin with.

Color filtering dimension. Due to the intrinsic ability of the LSC to absorb and emit different spectrum bands, a further step into the receiver design is assessing its ability to discern different colors. This ability could enable multiple channels to work simultaneously with little interference. To test color filtering, we modify the setup for each sensor:

- Ambient light sensor with a green glass filter.
- PT with a green glass filter.
- CS, reading the green channel.

Using these setups, we note a degradation of all receivers except for the color sensor with a 24 ms sampling rate, as shown in Figure 4.11b. Given that the color sensor with a sampling rate of 24 ms provides the best SNR with three color channels, we use that photosensor in our system.

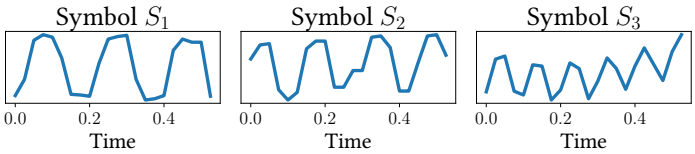

Figure 4.12: Samples of the received symbols S_1, S_2 and S_3, corresponding to 5 Hz, 6.67 Hz, and 10 Hz, respectively.

DEMODULATION.

To decode the information, we use the Fast Fourier Transform (FFT) implementation on the Arduino libraries (*arduinoFFT*[5]). The demodulation considers the following parameters:

- Sampling frequency (f_S): 40 Hz.
- Number of samples (N_S): 32.

The first parameter (f_S) is determined by the color sensor sampling rate. The second parameter (N_S) is set to 32[6]. Both parameters set the resolution of the FFT, which defines the column *"FFT Frequency (Rx)"* of Table 4.4 as the best match to the transmitted frequencies. Overall, our transmitter and receiver designs allow us to build a novel short-range wireless communication system, outlined in the next section.

To successfully decode a symbol (instruction) from the received signal, the demodulation process analyzes the frequencies of interest: 5 Hz, 6.25 Hz and 10 Hz, and selects the one with the highest power. However, using the highest spectral energy as the only criterion for decoding a symbol could lead to errors due to ambient light noise. Therefore, we set two conditions for a symbol to be successfully decoded. First, we set a minimum threshold for the spectral power of the highest frequency. Second, the power ratio between the highest and the second highest symbol frequencies needs to be higher than a threshold. Both thresholds are found empirically during experimentation. Figure 4.12 shows samples of the three symbols received by the CS.

4.3.3. EDGE-LIGHT: A FULL-DUPLEX TRANSCEIVER

Based on the previous sections, we implement a full-duplex wireless link based on the transmitter and receiver designs, and Figure 4.13a shows a schematic description of the Edge-Light transceiver. The goal of this transceiver is to communicate wirelessly over a short distance using ambient light as the source of illumination for the LSC. Compared to all prior studies, *the key novelty of Edge-Light is that the communication is lateral to the propagation direction of ambient light.*

A 3D-printed structure holds the microcontroller, transmitter, and receiver. The transmitter includes three layers –LC, LSC, retro-reflector–, and radiates the modulated beam of light throughout the 360°. Additionally, since the aim is to use different types of ambient light with different intensities, the Arduino implements a calibration function to avoid saturation of the receiver's color sensor, sampling it and tuning its gain.

[5] arduinoFFT: https://github.com/kosme/arduinoFFT/tree/master
[6] N_S must be a power of two for the *ArduinoFFT* implementation.

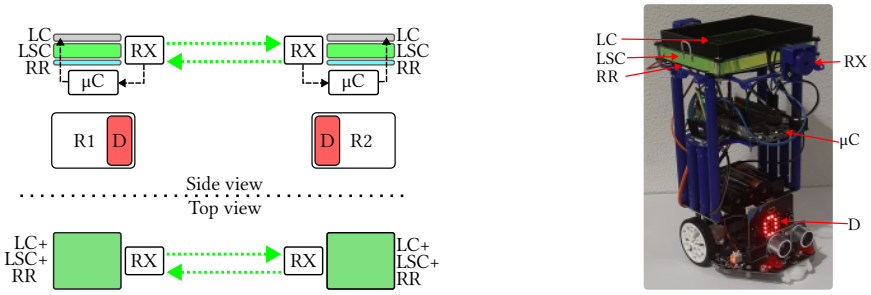

(a) Transeivers system diagram.

(b) Implementation.

Figure 4.13: Edge-Light implementation of a full-duplex link. R: robot, D: display.

To showcase our mobile Edge-Light implementation and ease its assessment, we use the *Maqueen PLUS v2*[7], which is a STEAM educational robot controlled by a *micro:bit*[8] microcontroller, and place an Edge-Light transceiver on top of the robot. Thus, the robot is able to send and receive commands from other robots.

The robot sends commands using the symbols' frequencies, switching to a different frequency to change the command. We set some conditions that limit these frequencies. First, the color sensor sampling interval must be higher than 24 ms. Second, to avoid using more than one timer, we set an interval of 25 ms (or 40 Hz) to both read the color sensor and change the state of the LC, which limits the highest frequency detected by the FFT to 10 Hz[9]. Furthermore, we discard frequencies below 2.5 Hz to avoid overlapping with slow changes in light intensity, which can be caused by motion (indoors) or variation in weather conditions (outdoors). These constraints combined with the selected FFT size (32 bits) render the frequencies in Table 4.4.

On the other hand, for the robot to receive a command, the transceiver is constantly trying to decode symbols from the color sensor and sends the result to the robot's controller via a serial port. We leverage the LED panel of the *micro:bit* as a visual aid to show the decoded symbol, so we can validate visually the link. We also use the wheels and engines to assess Edge-Light under motion, as presented in the next section.

4.4. EVALUATION

In this section, we evaluate the performance of Edge-Light under two conditions: standard indoor illumination and sunlight. Our setups include a static and mobile evaluation of the link.

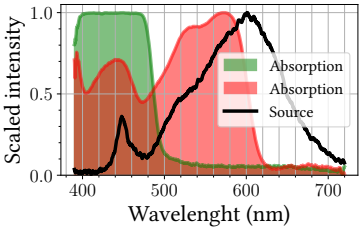

Figure 4.14: Spectrum of indoor ambient light. Overlaid are the absorption spectra of the green and red LSC.

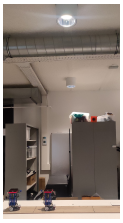

Figure 4.15: Setup for indoor experiments.

4

4.4.1. INDOORS: CONSTANT CEILING LIGHT

Indoor environments with human presence usually require around 500 lx of illumination. We test Edge-Light in a working environment using a ceiling light that provides around 450 lx[10].

Lighting is provided by different types of bulbs. Depending on the architectural design, light bulbs provide different radiation patterns and spectra. The radiation patterns do not affect significantly the operation of the LSC, because LSCs are agnostic to the incidence angle of ambient light. The light spectrum may have an impact depending on the technology used to generate white light, but the green and red bands are well within the visible light spectrum, and hence, Edge-Light works under different ambient light conditions, as it is shown later in an outdoor setup.

Given that the ambient light spectra play a role in the emitted band, as mentioned in section 4.2, the first step of our analysis is to measure the spectrum of the light source. Figure 4.14 shows this spectrum, which is a typical white light source, noting that its intensity is weak at lower wavelengths (towards the color blue) and stronger at higher wavelengths (towards the color red). Thus, we expect the performance of the red LSC to be better than the green LSC. To analyze the performance of the different emitted bands, the evaluation includes robots with different Edge-Light transmitters: one with a green LSC and one with a red LSC.

The distance between both robots is increased, starting from 15 cm, in steps of 15 cm. At each step, the robots are static and constantly sending one of the 3 symbols. To assess the link, we use the SNR of each symbol's frequency (Table 4.4) and the symbol success rate (SSR), the percentage of correctly decoded symbols.

RESULTS

Figure 4.16 present the results, which show a better performance of the red LSC compared to the green LSC, giving a greater SNR and SSR at all distances and for all symbols (frequencies). The results show that the SNR decays as the symbol frequency increases.

[7] Maqueen Plus: https://wiki.dfrobot.com/SKU_MBT0021-EN_Maqueen_Plus_STEAM_Programming_Educational_Robot

[8] micro:bit https://microbit.org/

[9] The FFT detects frequencies below 20 Hz. However, by using the same timer for modulation and demodulation, the highest is 10 Hz

[10] The light intensity is measured at the floor level of the room used in the experiments.

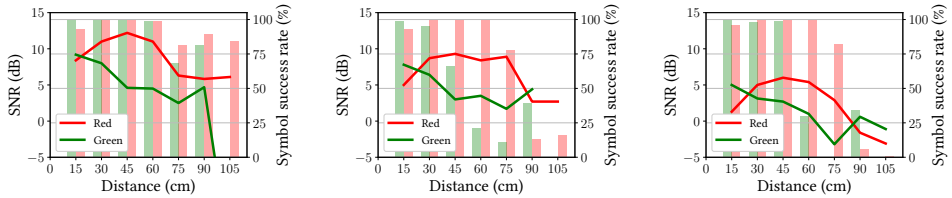

(a) Symbol S_1 (5.0 Hz) (b) Symbol S_2 (6.7 Hz) (c) Symbol S_3 (10.0 Hz)

Figure 4.16: SNR (lines) and SSR (bars) for indoor experiments at different distances with static transceivers, red and green LSC.

This occurs because as the switching frequency of the LC increases, the contrast between the dark and transparent states reduces. Another feature of the results is the low performance of the S_2 symbol, with a performance similar to the symbol with the fastest frequency, S_3. The reason for this phenomenon is the mismatch between the transmitted frequency and the frequency bin from the FFT, 6.7 Hz and 6.25 Hz, as described in Table 4.4. The mismatch reduces the link's performance at this particular frequency.

Overall, we note that, indoors, Edge-Light works better with the red LSC because its absorption band matches better with the illumination. Next, we test the system in a mobile setting. From the results, we notice that in the static case an SNR lower than 5 dB drastically reduces the link's performance.

4.4.2. VARIABLE INCIDENCE LIGHT: THE EFFECT OF MOTION

The previous test does not include motion. Under that setup, the intensity and incidence angle of ambient light is constant. In this section, we let the robots communicate while both move in line. The movement of the robots changes their relative position concerning the ceiling illumination, creating a "dynamic" lightning condition with changes in intensity and incidence angles.

The distance between the robots is set to 30 cm because based on the previous results that distance gives a reliable SSR for all symbols with both LSCs, green and red. We set the following conditions for the movement: a speed of ~6 cm/s for both robots and they move for ~25 s covering a distance of ~150 cm.

For the experiments, we placed the robots under the same ceiling light as before and gave both robots a trigger signal to start the motors. At all times, both robots transmit and decode information, transmitting only one symbol per experiment. Each experiment is repeated twice per symbol to get one hundred samples per symbol.

RESULTS

Mobility reduces the performance of Edge-Light, more specifically the SNR and the SSR of the green LSC. Figure 4.17 shows the SNR and SRR for both LSC transceivers. Next, we describe the reasons why mobility reduces the system's performance.

SNR under dynamic conditions. For the static conditions under indoor illumination, all parameters are fixed, including the intensity and incidence angle of light. Therefore, the signal is constant with a periodic oscillation at the transmitted frequency. However, under dynamic conditions, the signal becomes highly variable as shown in Fig-

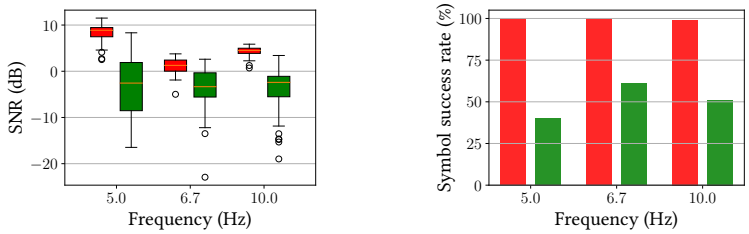

(a) SNR (b) SSR

Figure 4.17: SNR and SSR for indoor experiments with transceivers in motion.

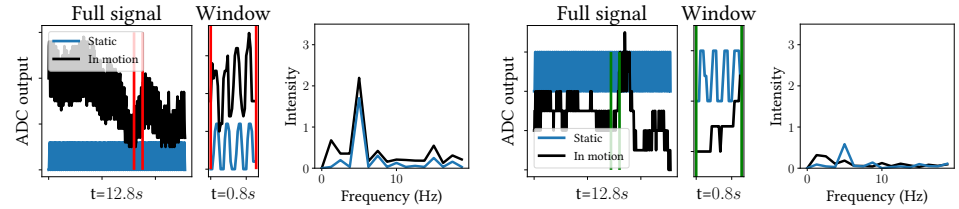

(a) Time domain (b) Frequency domain (c) Time domain (d) Frequency domain

Figure 4.18: Time and frequency signals comparison between the *static* and *in motion* cases for the symbol S_1 (5 Hz) for red-LSC Edge-Light (a, b) and green-LSC Edge-Light (c, d)

ure 4.18a. Due to this variability, the FFT leads to a noisy spectrum for the green LSC, as depicted in Figure 4.18b.

The mobility noise comes from two sources. First, moving towards/away from the light source creates changes in intensity. Second, the mechanical vibration caused by the robots' motion introduces small misalignments that lead to changes in intensity. Regardless of the added noise addition, the red LSC maintains a strong spectral response, as shown in Figure 4.18b.

4.4.3. OUTDOORS: VARIABLE SUNLIGHT INTENSITY

The main idea behind Edge-Light is to create a wireless link that leverages sunlight using LSCs. Therefore, our next experiments assess the system's performance during daylight.

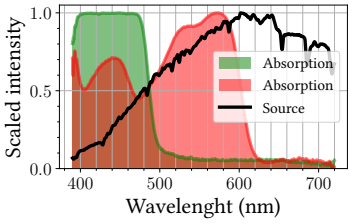

Figure 4.19: Sunlight spectrum during the outdoor experiments. Overlaid are the absorption spectra of the green and red LSC.

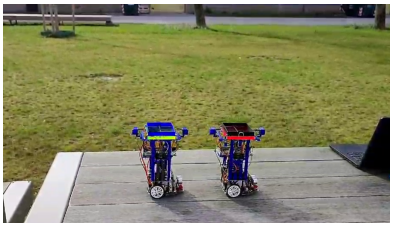

Figure 4.20: Outdoors experiment setup.

The experiments are performed between 11:00 and 14:00 the same day. During these periods we recorded sunlight intensities larger than 100 klx, 20 times stronger compared to the indoor experiments. Figure 4.20 depicts a sample deployment outdoors. Another important point is that the spectrum of sunlight differs from the spectrum of indoor lighting, as depicted in Figure 4.19. Compared to indoor light, sunlight is stronger in the absorption band of the green LSC but still matches better with the band of the red LSC.

Similar to the indoor experiments, each robot is placed at a fixed distance from the other, while they send and receive information simultaneously, without any relative motion between them. Due to the higher light intensity, the calibration function of the CS is important to avoid saturation.

RESULTS

The stronger sunlight intensity boosts the link's performance, as shown in Figure 4.22. More light reaches the LSC surface, boosting the edge light emission. The range is *almost* doubled, from 50 cm to 100 cm for the green LSC and from 75 cm to 150 cm for the red LSC.

While the range is boosted, sunlight also brings variability issues. This variability can be observed in the higher number of outliers present in the boxplot of the outdoor scenario (Figure 4.21) compared to the indoor one (Figure 4.17a). Sunlight variability can occur at a slow pace and high pace. At a slow pace, the changes in intensity are gradual and Edge-Light works well. However, at a high changing pace, we observed errors even at close ranges, as shown in Figure 4.22c, where the green LSC has a low SSR at 50 cm. During this part of the experiment, the intensity oscillated rapidly –a few times per second– due to a cloudy and windy part of the day where sunlight changed between 80 klx to 50 klx, affecting the decoding performance. Since the red LSC has a stronger signal strength, these variations did not affect the red LSC as much as the green LSC.

The outdoor Edge-Light's experiments show its ability to harness sunlight to create a new type of wireless link. In the next section, we take a step further and use Edge-Light as a communication system for robots.

4.5. ROBOT-TO-ROBOT COMMUNICATION

Thus far, the experiments presented rely only on one color sensor, which is facing the other robot directly. This setup limits the mobility of the robots, as they can only move in a straight line. Because the LSC transmitter is omnidirectional, we enhance the Edge-Light receiver by adding 3 extra color sensors at each side of the robot, thus adding the

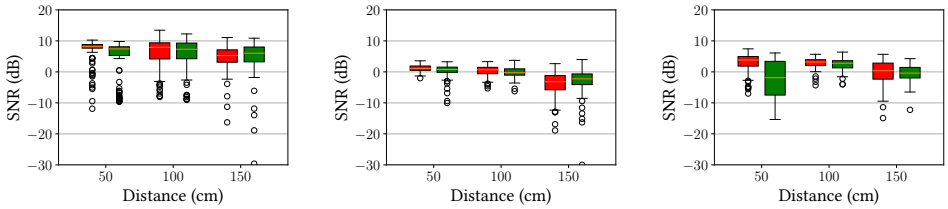

(a) Symbol S_1 (5.0 Hz) (b) Symbol S_2 (6.7 Hz) (c) Symbol S_3 (10.0 Hz)

Figure 4.21: SNR for outdoor experiments at different distances with stationary transceivers, red and green LSC.

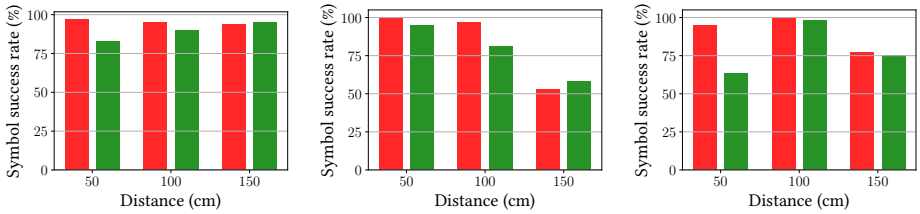

(a) Symbol S_1 (5.0 Hz). (b) Symbol S_2 (6.7 Hz). (c) Symbol S_3 (10.0 Hz).

Figure 4.22: SSR for outdoor experiments at different distances with stationary transceivers.

option for the robots to rotate and keep connected.

To attain robot cooperation, we program one robot as the *parent* and the other as the *child*. The robots exchange 3 symbols which translate into 3 instructions: IDLE, MOVE FORWARD, ROTATE 90°, and the logic for executing a task is the following:

1. The parent detects an IDLE message from the child.
2. The parent sends a MOVE FORWARD/ROTATE message to the child.
3. The child detects the MOVE FORWARD/ROTATE message, and sends the same instruction back to the parent, so both robots can start a coordinated movement. After a specific amount of time, the child executes the instruction.
4. The parent detects the instruction from the child, which acts as an acknowledgment, waits for a specific amount of time and executes the instruction.

In the next section, we use two robots and this set of instructions to carry out two basic tasks: coordinated movement of the two robots and simultaneously pushing a box. The box is too heavy to be pushed by one robot, but it can be pushed by two robots.

4.5.1. ENABLING ROBOTS' JOINT TASKS WITH EDGE-LIGHT

In this section, the robots use the 3 instructions (IDLE, MOVE FORWARD and ROTATE) to perform coordinated or collaborative tasks. Similar to the previous section, the robots are placed in different scenarios. Due to the better performance of the red LSC, the experiments are done with that configuration. Additionally, the robot on the right side of

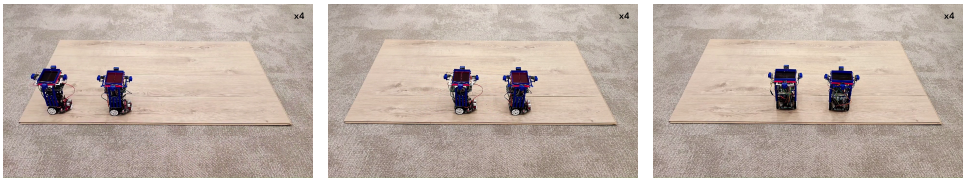

(a) Starting position. (b) MOVE FORWARD, IDLE. (c) ROTATE, IDLE.

Figure 4.23: Indoor coordinated task. **The video is attached to this submission.**

all figures in this section is set to be the parent. **These experiments are better appreciated in the videos attached to this submission.**

INDOOR SCENARIO: CEILING LIGHT.

Under a standard ceiling fixture, the robots perform one coordinated task and one collaborative task.

Coordinated task. In this experiment, the parent requests the child to move to a different point and then come back to the starting point. In the video, the oscillation of the LCs is visible while transmitting the messages. Figure 4.23 shows snapshots of the video. The exact instructions sent by the parent are:

1. MOVE FORWARD, IDLE
2. ROTATE, IDLE
3. ROTATE, IDLE
4. MOVE FORWARD, IDLE

Both calibrations are repeated for each task.

Collaborative task. Some robot tasks require cooperation. To showcase a sample scenario, we devised a setup where the goal is to push a carton box. First, the parent tries to push the box using the sequence:

1. MOVE FORWARD, IDLE
2. ROTATE, IDLE
3. MOVE FORWARD

However, the engines of one robot are not powerful enough to achieve the task, and after the final step of the task sequence, the box does not move and the robot gets stuck in front of the box (Figure 4.24c). In a second setup, the parent and child coordinate their moves to push the box successfully, Figure 4.25c.

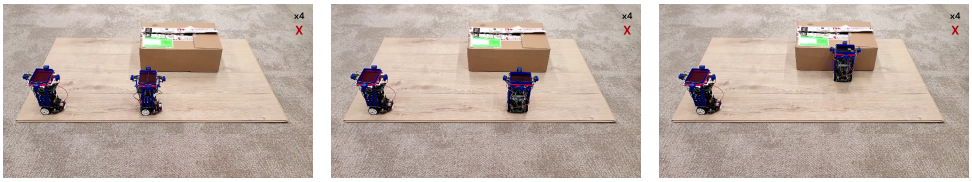

(a) Starting position. (b) ROTATE. (c) MOVE FORWARD.

Figure 4.24: Unsuccessful individual task. One robot fails to push the carton box. **Video is attached**

(a) Starting position. (b) ROTATE, IDLE. (c) MOVE FORWARD.

Figure 4.25: Successful collaborative task. Two robots push the carton box. **Video is attached**

OUTDOOR SCENARIO USING SUNLIGHT.

The communication between moving robots also works under sunlight.

Coordinated task The parent is programmed with the same instructions as the indoor coordinated task (MOVE FORWARD, IDLE, ROTATE, IDLE, ROTATE, IDLE, MOVE FORWARD, IDE). The result is a successful in-sync motion and rotation of the parent and the child, as depicted in Figure 4.26. Regardless of the type of illumination, indoors and constant or outdoors and variable, Edge-Light is able to establish an optical wireless connection between robots to perform joint tasks.

4.6. RELATED WORK

The analysis of the SoA focuses on visible light communication. VLC aims to complement, not replace, radio-frequency (RF) systems. RF is a mature technology with higher data rates and better power efficiency than VLC, such as BLE. Visible light communication is a young technology with ample room for improvement but exploits a free and empty spectrum.

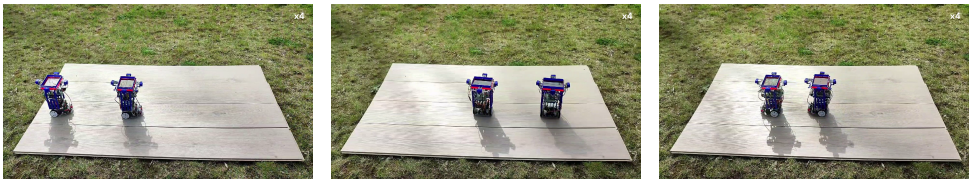

(a) Starting position. (b) ROTATE, IDLE. (c) MOVE FORWARD, IDLE.

Figure 4.26: Outdoor coordinated task. **Video is attached**.

4.6.1. ACTIVE VLC

The research community has explored the concept of VLC since 2000[112] and the advances in this field have encouraged the development of commercial VLC platforms. *LiFi*, the commercial implementation of VLC, renders a combination of illumination and VLC up to ~10 m, with some companies reportedly attaining data transmission speeds up to 1 Gbps[113], including devices such as dongles and access points to provide full internet connectivity to mobile devices.

The scientific community explores many variations of VLC achieving higher speeds. In one study, a VLC link of 300 Gbps is demonstrated by using elaborated optical methods, such as wavelength-division multiplexing (WMD) and orthogonal polarization channels[98]. On the other hand, lower-end systems which build upon more simple devices attain links of around 100 kbps[99].

Compared to our work, the implementation of Edge-Light requires a minimum amount of energy compared to (Active) VLC, because the latter requires power to generate light and embed information into it, while Edge-Light uses the LSC ability to repurpose light from the environment, such as sunlight.

4.6.2. PASSIVE VLC

Light is a ubiquitous source: during the day sunlight illuminates outdoor environments and, because humans need light to perform tasks, indoors or at night we use artificial lighting systems. This overall presence of light has inspired researchers to design and create *Passive VLC* systems that reuse ambient light, thus reducing the energy budget. The work in PassiveVLC[13] uses 0.12 µJ energy per bit, while in [99] this parameter is 30 times larger, 1 mJ.

Among the different passive VLC works, we identify 3 main categories. First, we have the *backscattering* passive VLC systems, which work by using a reflective material to guide back to its source while modulating the reflected light usually using an LC[13, 12, 14, 15]. Second, other systems focus on using LC as *transmissive surface* to modulate ambient light, which is redirected towards the LC using optical devices[42, 54]. Finally, the third category includes systems that implement a *reflective surface* that redirects the light towards the intended receiver[18].

Related to our work, Edge-Light takes inspiration from the backscattering systems because it also uses light that illuminates a surface. However, Edge-Light redirects light to its edges and not back to the source. Also, these backscattering systems do not work using sunlight. Compared to the LC systems, Edge-Light uses the same device to modulate the light reaching the surface of the LSC. The complexity of the third type of system is greater than the implementation of our system.

4.6.3. LSC APPLICATIONS

The ability of the LSC to absorb a band of light and emit a different band on its edges has been leveraged in several fields. We mention three of the most relevant

PHOTOVOLTAICS AND BUILDINGS

The main use of the LSC is in combination with PV cells[103, 102], which are attached to the emitting edges of the LSC to gather light. The size of the LSC panel influences its

performance and research in the performance and optimization of large LSC panels[114, 115]. These large LSC panels are used in buildings as part of windows[115, 116, 117, 118, 119] to capture part of the sunlight spectrum, re-emit light in a different optical band and concentrate it directly on the surface of the solar cells attached to the LSC edges. This application has also triggered the development of *smart windows*[120, 121], which adds the feature of controlling the window's opacity while it gathers and concentrates light.

HORTICULTURE

Plants use a specific part of the light spectrum for the photosynthesis process. Thus, small LSCs can be designed to absorb the bands not used by plants and placed on the top of a greenhouse. These LSCs re-emit light in the spectrum bands used for photosynthesis and concentrate it on their edges. This re-emitted light is captured by optical fibers attached to the LSC edges, and guided to plants located at a lower level in the greenhouse, bringing useful light to the deeper levels without using energy to power up devices. A trial of this concept resulted in a 7 % increase in the crop yield for tomatoes, using 24 cm^2 LSC panels and plastic optical fibers[122].

VLC

In optical wireless communications, LSC is an attractive solution as a receiver antenna due to its large FoV. Such an antenna receives light on its surface and emits light on its edges, where a PD is attached[123]. The malleability of acrylic-based LSC allows the creation of different shapes for the receivers, leveraging planar-parabolic shapes to increase the gain[124] or spherical shapes to manufacture almost omnidirectional receivers[125]. Moreover, the ability to absorb specific spectrum bands allows the implementation of a wavelength-selective receiver seamlessly by stacking two LSCs with complementary absorption bands, for instance, one green and one red. The top LSC absorbs only green light, and lets the other bands pass, while the bottom LSC absorbs the red light; creating a two-band receiver in the same area[126].

Compared to our work, we take a different approach to using the LSC as a VLC transmitter instead of a receiver.

4.7. DISCUSSION

This section presents some limitations of the current system and potential improvements at each stage.

Range between transceivers. The communication range for our current setup is limited to 50 cm indoors, and it almost doubles outdoors but remains below two meters. A way to increase the range is to add an optical component at the edge of the LSC to concentrate the beam into a narrower (longer) shape. A suitable device to achieve this goal is a collimation lens, which can redirect the light and make it horizontal and more focused towards the receiver. However, implementing this setup increases the alignment constraints between the transmitter and the receiver, which could reduce the system's mobility.

Link's speed. In the current configuration, the link's data rate is limited by the LC speed and the *integration time* of the CS. The LC speed is a physical limiting factor. How-

ever, the LC can operate at a *faster mode*, which reduces the contrast between states, thus reducing also the SNR. The previously discussed lens system could improve the SNR and make this *faster mode* readable. Regarding the CS, if the SNR is large enough, the *integration time* could be reduced to 2.4 ms or we can use a faster CS.

Increasing the number of robots. Edge-Light allows lateral communication between robots and our experiments show how two robots (one parent, one child) communicate using one of the four CS on each side. To increase the number of robots sharing commands simultaneously, we need to set the initial conditions of the parent's location, i.e., if the parent is between two children, the children should read the corresponding CS. The parent/child communication logic must be upgraded because the parent needs to handle receiving symbols from multiple CS, and the acknowledgment and waiting time to execute must be synchronized among more robots. The current hardware implementation of our robot-to-robot communication allows the parent to communicate with a maximum of four children simultaneously. Another possibility is to leverage the malleability of the LSC, which is basically an acrylic, to create transceivers with different shapes, like circular or hexagonal, and add more CSs. Such a setup could enable lateral communication in more directions, such as diagonal.

Different light sources. During our experiments, we used two different light sources: an indoor ceiling light and sunlight. Nonetheless, different artificial light sources have different spectra and refresh rates. Regarding the light source spectrum, a previous spectral analysis of the ambient light is necessary to select the appropriate LSC, which can be commercially available or custom-made in a research facility. The current implementation of Edge-Light uses frequencies below 10 Hz and the usual refresh rates of LED bulbs are higher than 100 Hz, thus we notice no impact in our current implementation. If the hardware allows increasing the transmitter and receiver's frequencies, they must avoid being close to the flickering rate of LED light bulbs.

FFT computation. The implementation of the FFT uses the *arduinoFFT* library with 32 samples per FFT window. With the current sampling period, 25 ms, we found that the number of samples is enough to decode the symbols, regardless of the mismatch for the third symbol, in less than one second. Increasing the number of samples leads to a finer frequency resolution at the cost of more time to capture the signal and compute the FFT.

Multiple transmitters, single receiver. One key feature of the LSC is that the material sets the output spectrum at the edges. In our implementation, we use red and green LSCs, with minimum overlap between the output spectra. Our receiver, based on a CS, is able to differentiate the spectrum by filtering the incoming light into three color channels. One open possibility is to combine multiple transmitters with different color outputs close to each other and in the range of a single receiver. In this way, a single CS can read its red and green channels independently and decode each channel, effectively doubling the speed of the link. However, a careful analysis of the spectra and a CS calibration should be implemented to reduce the effect of the spectrum overlap.

4.8. CONCLUSIONS

In this work, we propose a novel passive VLC transmitter which can work using ceiling lighting and, most significantly, sunlight. Our design is based on an LSC, a material with the capacity to absorb light from the top, redirect it and concentrate it later-

ally. The full transmitter design incorporates LCs to modulate the incoming light on top, thus modulating the light emitted from the edges. By combining it with an appropriate receiver, in this work a color sensor, we implement a transceiver for a full-duplex optical wireless link. Furthermore, we realize robot-to-robot communication using the Edge-Light transceiver, allowing robots to coordinate collaborative tasks using a sunlight-based wireless connection. Overall, our work demonstrates a new approach in LSC applications and the potential of our transceiver to create a low-power passive VLC link.

5

CONCLUSION

The demand for more bandwidth and *greener* solutions has encouraged the development of novel wireless technologies, one of them being *Passive VLC*, which can potentially reduce the energy required to provide wireless connectivity. Nonetheless, *Passive VLC* development, and thus its adoption is hindered mostly due to the low speeds of the modulators and the difficulties in aligning transmitters with the sun's position. Hence, we considered the following research question:

What new optical devices and methods can be implemented in Passive VLC to improve its performance?

This dissertation addressed two key limitations of sunlight-based *Passive VLC* systems: attainable data rate and dependency on the light source position. Each chapter presented a VLC system design that works with artificial ambient light and, most importantly, sunlight. Furthermore, along with each design, we demonstrated the feasibility of such systems by implementing prototypes and assessing their performance using the sun as the light source.

5.1. CONTRIBUTIONS

Our research approach for developing new *Passive VLC* platforms focused on the design at the system level, exploring the use of devices, techniques and materials from other optical domains and tailoring them to be used in VLC systems. Our work makes the following contributions to *Passive VLC* research:

Screen-to-camera communication for smartphones using sunlight. *Passive VLC* systems have focused mainly on using a single receiver, such as a photodiode or phototransistor, and not on cameras mainly due to their low sampling rate. In Chapter 2, we focused our efforts on developing a system that uses a smartphone camera as the receiver. Our system leverages a fast LC reflective array (tiny FLCoS screen) to backscatter sunlight to the smartphone's camera while embedding a sequence of 2D patterns, such as QR codes. The camera decodes these patterns after the light passes through a po-

larizer, creating a short-distance wireless link between the screen and the smartphone without any RF devices.

Furthermore, the **Sunbox** system works from sunrise to sunset, leveraging the ability of the camera to adapt to different light conditions caused by changing weather during the day. Overall, our system can reach speeds from 2 kbps to 10 kbps, faster than previous *Passive VLC* systems using cameras as receivers.

Combining natural illumination with *Passive VLC* and color-multiplexing. The need to reduce the high energy footprint of illumination has encouraged the development of systems that redirect sunlight indoors. These systems offer a unique opportunity to merge *Passive VLC* with illumination, an unexplored combination that we targeted with the **Sol-Fi** approach (Chapter 3). We combined the optical properties of a sunlight collector with two different modulators: LC and DMD, demonstrating the trade-off between reduced optical losses (LC) and high speed (DMD).

To push our system's boundaries, we developed a color multiplexing scheme or WDM, inspired by similar approaches of other optical systems. Our dual-band engine divides the collected sunlight into two optical bands with similar energy, modulates them independently, and recombines them into *white* sunlight, ready to provide illumination. With this approach, we duplicate the system's data rate. Furthermore, our design enables the first *Passive VLC* system with wavelength division multiplexing (WDM).

Use of novel materials to create new *Passive VLC* links. Our research involved exploring materials and techniques from other optical domains and applying them to new *Passive VLC* systems. In Chapter 4, we based our design on a luminescent solar concentrator (LSC), a material mainly used in photovoltaic technology. An LSC emits light on its edges when illuminated from the top. Based on this optical property, our insight was to use LCs to control the incoming light and emit it in modulated patterns at the edges. Our system's prototype, named **Edge-Light**, uses color sensors to decode the data and coordinate tasks between robots. A key property of Edge-Light is that it provides link connectivity independently of the sun's position.

5.2. LOOKING BACK

Passive VLC poses a thought-provoking research challenge: modulate an uncontrollable light source. In this thesis, we presented three system designs and implementations that address the research question by improving *Passive VLC* in terms of data rate and independence of the light source position. The studies presented in this work show a clear trade-off in *Passive VLC*: complexity against data rate. The Sol-Fi system (Chapter 3) is the fastest of this dissertation. At the same time, its multichannel implementation is the most complex optical setup of this thesis. Conversely, Edge-Light's implementation (Chapter 4) is the simplest, relying more on the material's optical properties, and rendering the slowest speed. SunBox (Chapter 2) sits between the trade-off: the implementation is fairly simple (although the complexity is transferred to the hardware: a camera and its driver) and achieves fast data rates.

Similar to traditional RF wireless systems, there is no *one-size-fits-all* solution for *Passive VLC*. This dissertation presented different *Passive VLC* systems fueled by natural and artificial ambient light for various scenarios: indoors and outdoors, and from

short-range systems using cameras, to decimeter-range platforms using color sensors and meter-range links combined with indoor illumination. Overall, the linking chain among all chapters is that the systems implement multiplexing to some extent. SunBox uses spatial multiplexing and Sol-Fi uses color-multiplexing to increase the transmission speed, while Edge-Light has the potential to create independent channels by using different LSC materials that emit different colors.

5.3. FUTURE WORK AND CHALLENGES

The research community continues to explore *Passive VLC* as a *greener* alternative to traditional wireless systems. This dissertation proposes novel platforms that push the boundaries of previous works. Nonetheless, *Passive VLC* systems still have a long way to reach the performance of more mature wireless technologies, like RF.

5.3.1. SCREEN-TO-CAMERA COMMUNICATION WITH SUNLIGHT

In Chapter 2, using a reflective surface, we present the SunBox system, the first passive screen-to-camera communication. The area of this surface is in the order of mm^2, less than 20 % of the active camera area. Therefore, one direct way to improve the data rate or range is to increase the surface area, and we identify two ways of devising this. First, using more than one reflective transmitter, that is having multiple inputs (MI). We obtained initial results for this principle in [127], where we use two tiny screens transmitting simultaneously to double the data rate and using two ROIs to decode each. However, we have only evaluated this design with LEDs and not with ambient light. Second, using a larger screen, which is explored in [128] with screen sizes of 48 cm by 27 cm and 144 cm by 80 cm. These bigger screens allow ranges up to 50 cm and 1.5 m, respectively, but at a lower data rate. There is still room for further research in the area of passive screen-to-camera communication. A direct approach not yet explored is to increase the screen and camera speed, which directly increases the data rate. Most commercial devices, both smartphone cameras and screens, are limited in speed or require special processes to attain higher refresh or capturing rates[1].

5.3.2. NATURAL ILLUMINATION AND PASSIVE VLC

The performance of the *natural VLC bulb* presented in Chapter 3 depends on the sunlight intensity. Thus, the system's performance reduces or stops working under the presence of clouds or at night. Therefore, there is potential to integrate Sol-Fi with traditional VLC (based on LEDs) to provide illumination and communication in low-sunlight conditions. Another area for improvement is to increase the number of channels. Currently, we have only two color channels. A more detailed analysis of optical filters could enable the addition of more channels to increase the system's data rate.

Sol-Fi demonstrated the combination of natural illumination and VLC using the sunlight collector as the daylighting system. There are, however, other types of daylighting systems, such as heliostats and solar tubes, that can also be investigated for applications with *Passive VLC*. In fact, one recent study provides some initial insights about the use of solar tubes with LCs [89]. One key difference among these daylighting systems compared

[1] Phones with high-speed cameras require root access to enable this feature for real-time processing.

to Sol-Fi is the light output size: Sol-Fi has a small output, in the order of centimeters, while the heliostat and solar tube output is in the order of meters. A smaller output eases the light modulation process. Another difference is in terms of power consumption, solar tube is a passive system, i.e. it consumes no power, while SunBox and the heliostat use power to track the sun's position. As a consequence, the optical output of these two latter is higher compared to the first one.

5.3.3. EXPLORATION OF OPTICAL MATERIALS AND METHODS

A common factor for all the works in this dissertation is the use of *new* optical devices and methods for *Passive VLC*. Nevertheless, other materials and methods from the optical domain also have the potential to improve *Passive VLC* systems. One such material is the polymer dispersed liquid crystal (PDLC), which is used to provide privacy with smart windows. A PDLC changes between transparent and light-scattering states, and the switching between these two states can be used to modulate light. However, it requires a complex driving signal and high power which can limit its application to *Passive VLC*. Another device that can be exploited is an event camera. This type of camera is expensive and requires more complex setups, but it can detect changes in pixel intensity faster than traditional cameras, enabling significantly higher data rates. Finally, the exploration of alternative LSC materials to the commercial ones used in Edge-Light is open. An example is LSC which emits in the near-infrared (NIR) to avoid the visible spectrum. However, the commercial availability of this LSC is limited.

The inspiration for this thesis stems from the gap between the field of wireless technology, specifically VLC, and the use of natural sources to create wireless links. Along each chapter, we aim to develop a system that uses new approaches to implement optical links and tries to improve these links, compared to previous works. Harnessing the optical power of a vast resource, the sun, to fuel VLC systems poses a tremendous challenge. The work presented in this thesis is a small step forward to *Passive VLC*, a more sustainable approach to wireless communication.

BIBLIOGRAPHY

[1] The World Bank. *Mobile cellular subscriptions*. https://data.worldbank.org/indicator/IT.CEL.SETS. Accessed: 15/06/2024. 2022.

[2] Ericsson. *Mobile subscriptions forecast*. https://www.ericsson.com/en/reports-and-papers/mobility-report/dataforecasts/mobile-subscriptions-outlook. Accessed: 15/06/2024. 2023.

[3] Statista. *IoT connections worldwide 2022-2033*. https://www.statista.com/statistics/1183457/iot-connected-devices-worldwide/. Accessed: 15/06/2024. 2024.

[4] IoT Analytics. *Number of connected IoT devices growing 16% to 16.7 billion globally*. https://iot-analytics.com/number-connected-iot-devices/. Accessed: 15/06/2024. 2023.

[5] International Energy Agency. *Data Centres and Data Transmission Networks*. https://www.iea.org/energy-system/buildings/data-centres-and-data-transmission-networks. Accessed: 15/06/2024. 2023.

[6] My NASA Data - NASA. *Electromagnetic Spectrum Diagram*. https://mynasadata.larc.nasa.gov/basic-page/electromagnetic-spectrum-diagram. Accessed: 15/06/2024. 202.

[7] British Broadcasting Corporation. *London 2012: Olympics to create 'record' wireless spectrum demand*. https://www.bbc.com/news/technology-16686471. Accessed: 15/06/2024. 2012.

[8] Federal Communications Commision. *Auction 107: 3.7 GHz Service*. https://www.fcc.gov/auction/107. Accessed: 15/06/2024. 2022.

[9] CompaniesMarketCap. *Largest airlines by market cap*. https://companiesmarketcap.com/airlines/largest-airlines-by-market-cap/. Accessed: 15/06/2024. 2024.

[10] National Telecommunications and Information Administration. *United States Frequency Allocation Chart*. https://www.ntia.gov/page/united-states-frequency-allocation-chart. Accessed: 15/06/2024. 2016.

[11] Y. Tanaka et al. "Indoor visible communication utilizing plural white LEDs as lighting". In: *12th IEEE International Symposium on Personal, Indoor and Mobile Radio Communications. PIMRC 2001. Proceedings (Cat. No.01TH8598)*. Vol. 2. 2001, F–F. DOI: 10.1109/PIMRC.2001.965300.

[12] Jiangtao Li et al. “Retro-VLC: Enabling Battery-free Duplex Visible Light Communication for Mobile and IoT Applications”. In: *Proceedings of the 16th International Workshop on Mobile Computing Systems and Applications*. HotMobile ’15. Santa Fe, New Mexico, USA: Association for Computing Machinery, 2015, pp. 21–26. ISBN: 9781450333917. DOI: 10.1145/2699343.2699354. URL: https://doi.org/10.1145/2699343.2699354.

[13] Xieyang Xu et al. “PassiveVLC: Enabling Practical Visible Light Backscatter Communication for Battery-free IoT Applications”. In: *Proceedings of the 23rd Annual International Conference on Mobile Computing and Networking*. MobiCom ’17. Snowbird, Utah, USA: Association for Computing Machinery, 2017, pp. 180–192. ISBN: 9781450349161. DOI: 10.1145/3117811.3117843. URL: https://doi.org/10.1145/3117811.3117843.

[14] Yue Wu et al. “Turboboosting Visible Light Backscatter Communication”. In: *Proceedings of the Annual Conference of the ACM Special Interest Group on Data Communication on the Applications, Technologies, Architectures, and Protocols for Computer Communication*. SIGCOMM ’20. Virtual Event, USA: Association for Computing Machinery, 2020, pp. 186–197. ISBN: 9781450379557. DOI: 10.1145/3387514.3406229. URL: https://doi.org/10.1145/3387514.3406229.

[15] Purui Wang et al. “Renovating road signs for infrastructure-to-vehicle networking: a visible light backscatter communication and networking approach”. In: *Proceedings of the 26th Annual International Conference on Mobile Computing and Networking*. MobiCom ’20. London, United Kingdom: Association for Computing Machinery, 2020. ISBN: 9781450370851. DOI: 10.1145/3372224.3380883. URL: https://doi.org/10.1145/3372224.3380883.

[16] Sahar Ammar et al. “Sun-Fi: Architecting Glass for Sunlight Data Transmission”. In: *IEEE Communications Magazine* 61.8 (2023), pp. 175–180. DOI: 10.1109/MCOM.002.2200603.

[17] Zhice Yang et al. “Wearables Can Afford: Light-weight Indoor Positioning with Visible Light”. In: *Proceedings of the 13th Annual International Conference on Mobile Systems, Applications, and Services*. MobiSys ’15. Florence, Italy: Association for Computing Machinery, 2015, pp. 317–330. ISBN: 9781450334945. DOI: 10.1145/2742647.2742648. URL: https://doi.org/10.1145/2742647.2742648.

[18] Talia Xu, Miguel Chávez Tapia, and Marco Zúñiga. “Exploiting Digital Micro-Mirror Devices for Ambient Light Communication”. In: *19th USENIX Symposium on Networked Systems Design and Implementation (NSDI 22)*. Renton, WA: USENIX Association, Apr. 2022, pp. 387–400. ISBN: 978-1-939133-27-4. URL: https://www.usenix.org/conference/nsdi22/presentation/xu-talia.

[19] 1826-1893 Guillemin Amédée Victor. *El mundo físico : gravedad, gravitación, luz, calor...* Ed. by Montaner y Simón. Barcelona : Montaner y Simón, 1882. URL: https://bvpb.mcu.es/es/consulta/registro.do?id=485530.

[20] Raphael Tuck & Sons. *"OILETTE" Postcard No. 9328*. https://www.tuckdbpostcards.org/. Accessed: 15/06/2024. 1907.

[21] Broadcast Electronics. *TV transmitters*. https://www.bdcast.com/products/tv-transmitters/. Accessed: 15/06/2024. 2023.

[22] Broadcast Electronics. *Radio transmitters*. https://www.bdcast.com/products/radio-transmitters/. Accessed: 15/06/2024. 2023.

[23] Sunwave Communications Co. *4G eNodeB*. https://en.sunwave.com/4G-eNodeB-pl3916350.html. Accessed: 15/06/2024. 2024.

[24] Phillips lighting. *Standard LED bulbs*. https://www.lighting.philips.com/prof/led-lamps-and-tubes/led-bulbs/standard-led-bulbs/LP_CF_6979538_EU/family. Accessed: 15/06/2024. 2024.

[25] Philips. *Autoverlichting | Koplampen | LED-lampen*. https://www.philips.nl/c-e/au/autoverlichting/koplampen/led-lampen.html. Accessed: 04/07/2024. 2024.

[26] Karan Ahuja et al. "LightAnchors: Appropriating Point Lights for Spatially-Anchored Augmented Reality Interfaces". In: *Proceedings of the 32nd Annual ACM Symposium on User Interface Software and Technology*. UIST '19. New Orleans, LA, USA: ACM, 2019, pp. 189–196. DOI: 10.1145/3332165.3347884. URL: https://doi.org/10.1145/3332165.3347884.

[27] Jackie (Junrui) Yang and James A. Landay. "InfoLED: Augmenting LED Indicator Lights for Device Positioning and Communication". In: *Proceedings of the 32nd Annual ACM Symposium on User Interface Software and Technology*. UIST '19. New Orleans, LA, USA: ACM, 2019, pp. 175–187. DOI: 10.1145/3332165.3347954. URL: https://doi.org/10.1145/3332165.3347954.

[28] Trong-Hop Do and Myungsik Yoo. "Two-Dimensional Coding for Optical Camera Communication using CMOS Sensors". In: *International Conference on Information and Communications 2017*. ICIC '17. Hanoi, Vietnam: IEEE, 2017, p. 314. DOI: 10.1109/ICIC42290.2017. URL: https://doi.org/10.1109/ICIC42290.2017.

[29] Yanbing Yang et al. "Pushing the Data Rate of Practical VLC via Combinatorial Light Emission". In: *IEEE Transactions on Mobile Computing* 20.5 (May 2021), pp. 1979–1992. ISSN: 1558-0660. DOI: 10.1109/TMC.2020.2971204.

[30] Liqiong Liu et al. "Beyond 100-kbit/s Transmission over Rolling Shutter Camera-based VLC Enabled by Color and Spatial Multiplexing". In: *Proceedings of the Optical Fiber Communication Conference (OFC) 2020*. OFC '20. San Diego, California, USA: Optica Publishing Group, 2020, M1J.4. DOI: 10.1364/OFC.2020.M1J.4. URL: http://opg.optica.org/abstract.cfm?URI=OFC-2020-M1J.4.

[31] Anran Wang et al. "InFrame++: Achieve Simultaneous Screen-Human Viewing and Hidden Screen-Camera Communication". In: *Proceedings of the 13th Annual International Conference on Mobile Systems, Applications, and Services*. MobiSys '15. Florence, Italy: ACM, 2015, pp. 181–195. DOI: 10.1145/2742647.2742652. URL: https://doi.org/10.1145/2742647.2742652.

[32] Samuel David Perli, Nabeel Ahmed, and Dina Katabi. “PixNet: Interference-Free Wireless Links Using LCD-Camera Pairs”. In: *Proceedings of the Sixteenth Annual International Conference on Mobile Computing and Networking*. MobiCom ’10. Chicago, Illinois, USA: ACM, 2010, pp. 137–148. DOI: 10.1145/1859995.1860012. URL: https://doi.org/10.1145/1859995.1860012.

[33] Wan Du, Jansen Christian Liando, and Mo Li. “Softlight: Adaptive visible light communication over screen-camera links”. In: *IEEE INFOCOM 2016-The 35th Annual IEEE International Conference on Computer Communications*. INFOCOM ’16. San Francisco, CA, USA: IEEE, 2016, pp. 1–9. DOI: 10.1109/INFOCOM.2016.7524510.

[34] Bingsheng Zhang et al. “SBVLC: Secure barcode-based visible light communication for smartphones”. In: *IEEE Transactions on Mobile Computing* 15.2 (Feb. 2015), pp. 432–446. DOI: 10.1109/TMC.2015.2413791. URL: https://doi.org/10.1109/TMC.2015.2413791.

[35] Kai Zhang et al. “ChromaCode: A Fully Imperceptible Screen-Camera Communication System”. In: *IEEE Transactions on Mobile Computing* 20.3 (Mar. 2021), pp. 861–876. ISSN: 1558-0660. DOI: 10.1109/TMC.2019.2956493. URL: https://doi.org/10.1109/TMC.2019.2956493.

[36] Ye-Sheng Kuo et al. “Luxapose: Indoor Positioning with Mobile Phones and Visible Light”. In: *Proceedings of the 20th Annual International Conference on Mobile Computing and Networking*. MobiCom ’14. Maui, Hawaii, USA: ACM, 2014, pp. 447–458. DOI: 10.1145/2639108.2639109. URL: https://doi.org/10.1145/2639108.2639109.

[37] Maury Wright. *Philips Lighting deploys LED-based indoor positioning in Carrefour hypermarket*. May 2015. URL: https://goo.gl/a0tGIj.

[38] Shuyu Shi et al. “Reading between Lines: High-Rate, Non-Intrusive Visual Codes within Regular Videos via ImplicitCode”. In: *Proceedings of the 2015 ACM International Joint Conference on Pervasive and Ubiquitous Computing*. UbiComp ’15. Osaka, Japan: ACM, 2015, pp. 157–168. DOI: 10.1145/2750858.2805824. URL: https://doi.org/10.1145/2750858.2805824.

[39] Samsung. *Reflective Display Technology*. Dec. 2017. URL: https://pid.samsungdisplay.com/en/learning-center/blog/reflective-display-technology.

[40] Weiwei Jiang et al. “Pulse: Low Bitrate Wireless Magnetic Communication for Smartphones”. In: *Proceedings of the 2014 ACM International Joint Conference on Pervasive and Ubiquitous Computing*. UbiComp ’14. Seattle, Washington: ACM, 2014, pp. 261–265. DOI: 10.1145/2632048.2632094. URL: https://doi.org/10.1145/2632048.2632094.

[41] Hao Pan et al. “MagneComm: Magnetometer-Based Near-Field Communication”. In: *Proceedings of the 23rd Annual International Conference on Mobile Computing and Networking*. MobiCom ’17. Snowbird, Utah, USA: ACM, 2017, pp. 167–179. DOI: 10.1145/3117811.3117824. URL: https://doi.org/10.1145/3117811.3117824.

[42] Rens Bloom, Marco Zúñiga Zamalloa, and Chaitra Pai. "LuxLink: Creating a Wireless Link from Ambient Light". In: *Proceedings of the 17th Conference on Embedded Networked Sensor Systems*. SenSys '19. New York, New York, USA: ACM, 2019, pp. 166–178. DOI: 10.1145/3356250.3360021. URL: https://doi.org/10.1145/3356250.3360021.

[43] Wenkai Liu et al. "Screen-Camera Communication System Based on Dynamic QR Code". In: *IOP Conference Series: Materials Science and Engineering* 790.1 (Mar. 2020). ISSN: 1757-899X. DOI: 10.1088/1757-899X/790/1/012012. URL: https://doi.org/10.1088/1757-899x/790/1/012012.

[44] Sung-Yoon Jung et al. "Complementary Color Barcode-Based Optical Camera Communications". In: *Wireless Communications and Mobile Computing* 2020.1 (Feb. 2020). ISSN: 1530-8669. DOI: 10.1155/2020/3898427. URL: https://doi.org/10.1155/2020/3898427.

[45] Control Electronic Co. Ltd. *0.2 inch FLCOS Micro Display Module for 720x540 HMD, Video Glasses*. Jan. 2020. URL: http://www.szcontrol.com/Index/pdetail/id/305.html.

[46] Basler AG. *Overlapping Image Acquisition*. Feb. 2021. URL: https://docs.baslerweb.com/overlapping-image-acquisition.

[47] Ryan Chylinski. *Time-lapse photography: A Complete Introduction to Shooting, Processing, and Rendering Time-lapse Movies with a DSLR Camera*. Cedar Wings Creative, 2012. ISBN: 9780985375706.

[48] Qi Guo et al. "Ferroelectric Liquid Crystals: Physics and Applications". In: *Crystals* 9.9 (2019). ISSN: 2073-4352. DOI: 10.3390/cryst9090470. URL: https://www.mdpi.com/2073-4352/9/9/470.

[49] David Doroski, Stephen H Perlmutter, and Garret Moddel. "Alignment layers for improved surface-stabilized ferroelectric liquid-crystal devices". In: *Appl. Opt.* 33.13 (1994), pp. 2608–2610. ISSN: 2155-3165. DOI: 10.1364/AO.33.002608. URL: http://opg.optica.org/ao/abstract.cfm?URI=ao-33-13-2608.

[50] J.C. Jones, M.J. Towler, and J.R. Hughes. "Fast, high-contrast ferroelectric liquid crystal displays and the role of dielectric biaxiality". In: *Displays* 14.2 (Apr. 1993), pp. 86–93. ISSN: 0141-9382. DOI: https://doi.org/10.1016/0141-9382(93)90075-G. URL: https://www.sciencedirect.com/science/article/pii/014193829390075G.

[51] Antonio Martínez-García et al. "Operational modes of a ferroelectric LCoS modulator for displaying binary polarization, amplitude, and phase diffraction gratings". In: *Appl. Opt.* 48.15 (May 2009), pp. 2903–2914. ISSN: 2155-3165. DOI: 10.1364/AO.48.002903. URL: http://ao.osa.org/abstract.cfm?URI=ao-48-15-2903.

[52] Tian Hao, Ruogu Zhou, and Guoliang Xing. "COBRA: Color Barcode Streaming for Smartphone Systems". In: *Proceedings of the 10th International Conference on Mobile Systems, Applications, and Services*. MobiSys '12. Low Wood Bay, Lake District, UK: ACM, 2012, pp. 85–98. DOI: 10.1145/2307636.2307645. URL: https://doi.org/10.1145/2307636.2307645.

[53] Ouyang Zhang et al. “ERSCC: Enable Efficient and Reliable Screen-Camera Communication”. In: *Proceedings of the Twentieth ACM International Symposium on Mobile Ad Hoc Networking and Computing*. Mobihoc ’19. Catania, Italy: ACM, 2019, pp. 281–290. DOI: 10.1145/3323679.3326526. URL: https://doi.org/10.1145/3323679.3326526.

[54] Seyed Keyarash Ghiasi, Marco A. Zúñiga Zamalloa, and Koen Langendoen. “A Principled Design for Passive Light Communication”. In: *Proceedings of the 27th Annual International Conference on Mobile Computing and Networking*. MobiCom ’21. New Orleans, Louisiana: ACM, 2021, pp. 121–133. DOI: 10.1145/3447993.3448629. URL: https://doi.org/10.1145/3447993.3448629.

[55] Chun-Ling Chan, Hsin-Mu Tsai, and Kate Ching-Ju Lin. “POLI: Long-Range Visible Light Communications Using Polarized Light Intensity Modulation”. In: *Proceedings of the 15th Annual International Conference on Mobile Systems, Applications, and Services*. MobiSys ’17. Niagara Falls, New York, USA: ACM, 2017, pp. 109–120. DOI: 10.1145/3081333.3081353. URL: https://doi.org/10.1145/3081333.3081353.

[56] Zhao Tian et al. “PolarTag: Invisible Data with Light Polarization”. In: *Proceedings of the 21st International Workshop on Mobile Computing Systems and Applications*. HotMobile ’20. Austin, TX, USA: ACM, 2020, pp. 74–79. DOI: 10.1145/3376897.3377854. URL: https://doi.org/10.1145/3376897.3377854.

[57] Anran Wang et al. “Enhancing Reliability to Boost the Throughput over Screen-Camera Links”. In: *Proceedings of the 20th Annual International Conference on Mobile Computing and Networking*. MobiCom ’14. Maui, Hawaii, USA: ACM, 2014, pp. 41–52. DOI: 10.1145/2639108.2639135. URL: https://doi.org/10.1145/2639108.2639135.

[58] Mostafa Izz et al. “Uber-in-light: Unobtrusive visible light communication leveraging complementary color channel”. In: *IEEE INFOCOM 2016-The 35th Annual IEEE International Conference on Computer Communications*. INFOCOM ’16. San Francisco, CA, USA: IEEE, 2016, pp. 1–9. DOI: 10.1109/INFOCOM.2016.7524513. URL: https://doi.org/10.1109/INFOCOM.2016.7524513.

[59] Harald Haas. *Wireless data from every light bulb*. Accessed: 30/10/2023. 2011. URL: https://www.ted.com/talks/harald_haas_wireless_data_from_every_light_bulb.

[60] Michael F Holick. “Sunlight and vitamin D for bone health and prevention of autoimmune diseases, cancers, and cardiovascular disease23”. In: *The American Journal of Clinical Nutrition* 80.6 (2004), 1678S–1688S. ISSN: 0002-9165. DOI: https://doi.org/10.1093/ajcn/80.6.1678S. URL: https://www.sciencedirect.com/science/article/pii/S0002916522037674.

[61] Jennifer A. Veitch and Anca D. Galasiu. *The Physiological and Psychological Effects of Windows, Daylight, and View at Home: Review and Research Agenda*. eng. Tech. rep. National Research Council of Canada, Feb. 2012. DOI: 10.4224/20375039. URL: https://doi.org/10.4224/20375039.

[62] Ying-Chih Cheng, Yu-Chen Huang, and Wei-Lieh Huang. “The effect of vitamin D supplement on negative emotions: A systematic review and meta-analysis”. In: *Depression and Anxiety* 37.6 (2020), pp. 549–564. DOI: https://doi.org/10.1002/da.23025. eprint: https://onlinelibrary.wiley.com/doi/pdf/10.1002/da.23025. URL: https://onlinelibrary.wiley.com/doi/abs/10.1002/da.23025.

[63] Cary Cooper. “Human spaces report: Biophilic design in the workplace”. In: *Interface* (2014), pp. 1–36.

[64] Lisa Heschong, Roger L Wright, and Stacia Okura. “Daylighting impacts on human performance in school”. In: *Journal of the Illuminating Engineering Society* 31.2 (2002), pp. 101–114.

[65] Mahmoud Eid El-saggan et al. “A Review of the Evolution of Daylighting Applications and Systems Over Time for Green Buildings”. In: *International Journal of Applied Energy Systems* 5.2 (2023), pp. 31–47.

[66] Sergio Altomonte. “Daylight for energy savings and psycho-physiological well-being in sustainable built environments”. In: *Journal of sustainable development* 1.3 (2008), pp. 3–16.

[67] Frank Sharp et al. “The use and environmental impact of daylighting”. In: *Journal of Cleaner Production* 85 (2014). Special Volume: Making Progress Towards More Sustainable Societies through Lean and Green Initiatives, pp. 462–471. ISSN: 0959-6526. DOI: https://doi.org/10.1016/j.jclepro.2014.03.092. URL: https://www.sciencedirect.com/science/article/pii/S0959652614003254.

[68] Jifeng Song, Bizuayehu Bogale Dessie, and Longyu Gao. “Analysis and Comparison of Daylighting Technologies: Light Pipe, Optical Fiber, and Heliostat”. In: *Sustainability* 15.14 (2023). ISSN: 2071-1050. DOI: 10.3390/su151411044. URL: https://www.mdpi.com/2071-1050/15/14/11044.

[69] C. Sapia. “Daylighting in buildings: Developments of sunlight addressing by optical fiber”. In: *Solar Energy* 89 (2013), pp. 113–121. ISSN: 0038-092X. DOI: https://doi.org/10.1016/j.solener.2012.12.003. URL: https://www.sciencedirect.com/science/article/pii/S0038092X12004185.

[70] Lucio Claudio Andreani et al. “Silicon solar cells: toward the efficiency limits”. In: *Advances in Physics: X* 4.1 (2019), p. 1548305. DOI: 10.1080/23746149.2018.1548305. eprint: https://doi.org/10.1080/23746149.2018.1548305. URL: https://doi.org/10.1080/23746149.2018.1548305.

[71] L. M. Fraas, W. R. Pyle, and P. R. Ryason. “Concentrated and piped sunlight for indoor illumination”. In: *Appl. Opt.* 22.4 (Feb. 1983), pp. 578–582. DOI: 10.1364/AO.22.000578. URL: https://opg.optica.org/ao/abstract.cfm?URI=ao-22-4-578.

5

[72] Jeong Tai Kim and Gon Kim. "Overview and new developments in optical daylighting systems for building a healthy indoor environment". In: *Building and Environment* 45.2 (2010). 1st International Symposium on Sustainable Healthy Buildings, pp. 256–269. ISSN: 0360-1323. DOI: https://doi.org/10.1016/j.buildenv.2009.08.024. URL: https://www.sciencedirect.com/science/article/pii/S0360132309002315.

[73] Sihua Shao, Abdallah Khreishah, and Hany Elgala. "Pixelated VLC-Backscattering for Self-Charging Indoor IoT Devices". In: *IEEE Photonics Technology Letters* 29.2 (2017), pp. 177–180. DOI: 10.1109/LPT.2016.2631946.

[74] Jun-Tae Kim et al. "Active Systems". In: *ZEMCH: Toward the Delivery of Zero Energy Mass Custom Homes*. Ed. by Masa Noguchi. Cham: Springer International Publishing, 2016, pp. 237–274. DOI: 10.1007/978-3-319-31967-4_9. URL: https://doi.org/10.1007/978-3-319-31967-4_9.

[75] Parans Solar Lightning AB. *Parans Solar Lightning System*. Accessed: 30/10/2023. 2022. URL: https://parans.com/.

[76] Himawari Solar Lighting System Laforet Engineeing Co. JP. *Lightning solution*. Accessed: 30/10/2023. 2022. URL: https://himawarisolar.com/.

[77] Georg Rademacher et al. "10.66 Peta-Bit/s Transmission over a 38-Core-Three-Mode Fiber". In: *Optical Fiber Communication Conference (OFC) 2020*. Optica Publishing Group, 2020, Th3H.1. DOI: 10.1364/OFC.2020.Th3H.1. URL: https://opg.optica.org/abstract.cfm?URI=OFC-2020-Th3H.1.

[78] Motoi Kodama and Shinichiro Haruyama. "Pulse Width Modulated Visible Light Communication using Digital Micro-mirror Device Projector for Voice Information Guidance System". In: *2019 IEEE 9th Annual Computing and Communication Workshop and Conference (CCWC)*. 2019, pp. 0793–0799. DOI: 10.1109/CCWC.2019.8666577.

[79] Texas Instruments Incorporated. *TI DLP® Module 2000 EVM User's Guide*. Accessed: 30/10/2023. 2021. URL: https://www.ti.com/lit/ug/dlpu089/dlpu089.pdf.

[80] Jifeng Song et al. "Application of highly concentrated sunlight transmission and daylighting indoor via plastic optical fibers with comprehensive cooling approaches". In: *Renewable Energy* 180 (2021), pp. 1391–1404. ISSN: 0960-1481. DOI: https://doi.org/10.1016/j.renene.2021.08.112. URL: https://www.sciencedirect.com/science/article/pii/S0960148121012805.

[81] Srikant Devaraj and Pankaj C. Patel. "Taxicab tipping and sunlight". In: *PLOS ONE* 12.6 (June 2017), pp. 1–16. DOI: 10.1371/journal.pone.0179193. URL: https://doi.org/10.1371/journal.pone.0179193.

[82] Iman Abdalla, Michael B. Rahaim, and Thomas D.C. Little. "Dynamic FOV visible light communications receiver for dense optical networks". In: *IET Communications* 13.7 (2019), pp. 822–830. DOI: https://doi.org/10.1049/iet-com.2018.5784. eprint: https://ietresearch.onlinelibrary.wiley.com/doi/pdf/10.1049/iet-com.2018.5784. URL: https://ietresearch.onlinelibrary.wiley.com/doi/abs/10.1049/iet-com.2018.5784.

[83] Seyed Keyarash Ghiasi et al. “SpectraLux: Towards Exploiting the Full Spectrum with Passive VLC”. In: *Proceedings of the 22nd International Conference on Information Processing in Sensor Networks*. IPSN ’23. San Antonio, TX, USA: Association for Computing Machinery, 2023, pp. 274–287. ISBN: 9798400701184. DOI: 10.1145/3583120.3586966. URL: https://doi.org/10.1145/3583120.3586966.

[84] Dana Dudley, Walter M. Duncan, and John Slaughter. “Emerging digital micromirror device (DMD) applications”. In: *MOEMS Display and Imaging Systems*. Ed. by Hakan Urey. Vol. 4985. International Society for Optics and Photonics. SPIE, 2003, pp. 14–25. DOI: 10.1117/12.480761. URL: https://doi.org/10.1117/12.480761.

[85] Monia Ghobadi et al. “ProjecToR: Agile Reconfigurable Data Center Interconnect”. In: *Proceedings of the 2016 ACM SIGCOMM Conference*. SIGCOMM ’16. Florianopolis, Brazil: Association for Computing Machinery, 2016, pp. 216–229. ISBN: 9781450341936. DOI: 10.1145/2934872.2934911. URL: https://doi.org/10.1145/2934872.2934911.

[86] Motoi Kodama and Shinichiro Haruyama. “Visible Light Communication using Two Different Polarized DMD Projectors for Seamless Location Services”. In: *Proceedings of the Fifth International Conference on Network, Communication and Computing*. ICNCC ’16. Kyoto, Japan: Association for Computing Machinery, 2016, pp. 272–276. ISBN: 9781450347938. DOI: 10.1145/3033288.3033336. URL: https://doi.org/10.1145/3033288.3033336.

[87] Charles J. Carver et al. “Sunflower: locating underwater robots from the air”. In: *Proceedings of the 20th Annual International Conference on Mobile Systems, Applications and Services*. MobiSys ’22. Portland, Oregon: Association for Computing Machinery, 2022, pp. 14–27. ISBN: 9781450391856. DOI: 10.1145/3498361.3539773. URL: https://doi.org/10.1145/3498361.3539773.

[88] Sahar Ammar et al. “Design and Analysis of LCD-Based Modulator for Passive Sunlight Communications”. In: *IEEE Photonics Journal* 14.5 (2022), pp. 1–17. DOI: 10.1109/JPHOT.2022.3200833.

[89] Javier Talavante, Borja Genoves Guzman, and Domenico Giustiniano. “Rethinking LiFi for Carbon Neutral Sunlight-based Communication”. In: *2023 21st Mediterranean Communication and Computer Networking Conference (MedComNet)*. 2023, pp. 53–60. DOI: 10.1109/MedComNet58619.2023.10168863.

[90] Chung-Yi Li et al. “White-lighting and WDM-VLC system using transmission gratings and an engineered diffuser”. In: *Opt. Lett.* 45.22 (Nov. 2020), pp. 6206–6209. DOI: 10.1364/OL.409843. URL: https://opg.optica.org/ol/abstract.cfm?URI=ol-45-22-6206.

[91] Lu Cui et al. “Analysis of the Multichannel WDM-VLC Communication System”. In: *J. Lightwave Technol.* 34.24 (Dec. 2016), pp. 5627–5634. URL: https://opg.optica.org/jlt/abstract.cfm?URI=jlt-34-24-5627.

[92] M.T. Rahman and Rajendran Parthiban. “Modeling and analysis of multi-channel gigabit class CWDM-VLC system”. In: *Optics Communications* 460 (2020), p. 125141. ISSN: 0030-4018. DOI: https://doi.org/10.1016/j.optcom.2019.125141. URL: https://www.sciencedirect.com/science/article/pii/S003040181931137X.

[93] Mario Poljak. *How much electricity (power) does a wi-fi router use?* Accessed: 30/10/2023. May 2021. URL: https://www.thehomehacksdiy.com/how-much-electricity-power-does-a-wi-fi-router-use/.

[94] L. Teixeira et al. “Review of LED drivers for Visible Light Communication”. In: *IECON 2019 - 45th Annual Conference of the IEEE Industrial Electronics Society*. Vol. 1. 2019, pp. 4274–4279. DOI: 10.1109/IECON.2019.8927340.

[95] Ambiq. *Apollo Plus SoC Datasheet*. Accessed: 30/10/2023. 2022. URL: https://ambiq.com/wp-content/uploads/2022/03/Apollo4-Plus-SoC-Datasheet.pdf.

[96] Fayzatul Ashmera Binti Merdan, Siva Priya Thiagarajah, and Katrina Dambul. “Non-line of sight visible light communications: A technical and application based survey”. In: *Optik* 259 (2022), p. 168982. ISSN: 0030-4026. DOI: https://doi.org/10.1016/j.ijleo.2022.168982. URL: https://www.sciencedirect.com/science/article/pii/S0030402622003588.

[97] Vipul Dixit and Atul Kumar. “Performance analysis of non-line of sight visible light communication systems”. In: *Optics Communications* 459 (2020), p. 125008. ISSN: 0030-4018. DOI: https://doi.org/10.1016/j.optcom.2019.125008. URL: https://www.sciencedirect.com/science/article/pii/S003040181931065X.

[98] Chung-Yi Li et al. “White-lighting and WDM-VLC system using transmission gratings and an engineered diffuser”. In: *Opt. Lett.* 45.22 (Nov. 2020), pp. 6206–6209. DOI: 10.1364/OL.409843. URL: https://opg.optica.org/ol/abstract.cfm?URI=ol-45-22-6206.

[99] Borja Genoves Guzman et al. “Prototyping Visible Light Communication for the Internet of Things Using OpenVLC”. In: *IEEE Communications Magazine* 61.5 (2023), pp. 122–128. DOI: 10.1109/MCOM.001.2200642.

[100] Kenuo Xu et al. “Low-Latency Visible Light Backscatter Networking with Retro-MUMIMO”. In: *Proceedings of the 20th ACM Conference on Embedded Networked Sensor Systems*. SenSys ’22. Boston, Massachusetts, USA: Association for Computing Machinery, 2023, pp. 448–461. ISBN: 9781450398862. DOI: 10.1145/3560905.3568507. URL: https://doi.org/10.1145/3560905.3568507.

[101] Ioannis Papakonstantinou, Mark Portnoi, and Michael G. Debije. “The Hidden Potential of Luminescent Solar Concentrators”. In: *Advanced Energy Materials* 11.3 (2021), p. 2002883. DOI: https://doi.org/10.1002/aenm.202002883. eprint: https://onlinelibrary.wiley.com/doi/pdf/10.1002/aenm.202002883. URL: https://onlinelibrary.wiley.com/doi/abs/10.1002/aenm.202002883.

[102] Bryce S. Richards and Ian A. Howard. “Luminescent solar concentrators for building integrated photovoltaics: opportunities and challenges”. In: *Energy Environ. Sci.* 16 (8 2023), pp. 3214–3239. DOI: 10.1039/D3EE00331K. URL: http://dx.doi.org/10.1039/D3EE00331K.

[103] Mehran Rafiee et al. “An overview of various configurations of Luminescent Solar Concentrators for photovoltaic applications”. In: *Optical Materials* 91 (2019), pp. 212–227. ISSN: 0925-3467. DOI: https://doi.org/10.1016/j.optmat.2019.01.007. URL: https://www.sciencedirect.com/science/article/pii/S092534671930028X.

[104] Haiguang Zhao. “Refractive index dependent optical property of carbon dots integrated luminescent solar concentrators”. In: *Journal of Luminescence* 211 (2019), pp. 150–156. ISSN: 0022-2313. DOI: https://doi.org/10.1016/j.jlumin.2019.03.039. URL: https://www.sciencedirect.com/science/article/pii/S0022231318323780.

[105] Guiju Liu et al. “Role of refractive index in highly efficient laminated luminescent solar concentrators”. In: *Nano Energy* 70 (2020), p. 104470. ISSN: 2211-2855. DOI: https://doi.org/10.1016/j.nanoen.2020.104470. URL: https://www.sciencedirect.com/science/article/pii/S2211285520300264.

[106] Haley C. Bauser et al. “Photonic Crystal Waveguides for >90% Light Trapping Efficiency in Luminescent Solar Concentrators”. In: *ACS Photonics* 7.8 (2020), pp. 2122–2131. DOI: 10.1021/acsphotonics.0c00593. eprint: https://doi.org/10.1021/acsphotonics.0c00593. URL: https://doi.org/10.1021/acsphotonics.0c00593.

[107] Alberto Jiménez-Solano et al. “Design and realization of transparent solar modules based on luminescent solar concentrators integrating nanostructured photonic crystals”. en. In: *Prog. Photovolt.* 23.12 (Dec. 2015), pp. 1785–1792.

[108] Barry McKenna and Rachel C. Evans. “Towards Efficient Spectral Converters through Materials Design for Luminescent Solar Devices”. In: *Advanced Materials* 29.28 (2017), p. 1606491. DOI: https://doi.org/10.1002/adma.201606491. eprint: https://onlinelibrary.wiley.com/doi/pdf/10.1002/adma.201606491. URL: https://onlinelibrary.wiley.com/doi/abs/10.1002/adma.201606491.

[109] Marika Savarese et al. “Fluorescence Lifetimes and Quantum Yields of Rhodamine Derivatives: New Insights from Theory and Experiment”. In: *The Journal of Physical Chemistry A* 116.28 (2012). PMID: 22667332, pp. 7491–7497. DOI: 10.1021/jp3021485. eprint: https://doi.org/10.1021/jp3021485. URL: https://doi.org/10.1021/jp3021485.

[110] Loredana Protesescu et al. “Nanocrystals of Cesium Lead Halide Perovskites (CsPbX3, X = Cl, Br, and I): Novel Optoelectronic Materials Showing Bright Emission with Wide Color Gamut”. In: *Nano Letters* 15.6 (2015). PMID: 25633588, pp. 3692–3696. DOI: 10.1021/nl5048779. eprint: https://doi.org/10.1021/nl5048779. URL: https://doi.org/10.1021/nl5048779.

[111] Ataberk Aksoy, Ömer Yıldız, and Sait Eser Karlık. “Comparative Analysis of End Device and Field Test Device Measurements for RSSI, SNR and SF Performance Parameters in an Indoor LoRaWAN Network”. In: *Wireless Personal Communications* 134.1 (2024), pp. 339–360.

[112] Y. Tanaka, S. Haruyama, and M. Nakagawa. “Wireless optical transmissions with white colored LED for wireless home links”. In: *11th IEEE International Symposium on Personal Indoor and Mobile Radio Communications. PIMRC 2000. Proceedings (Cat. No.00TH8525)*. Vol. 2. 2000, 1325–1329 vol.2. DOI: 10.1109/PIMRC.2000.881634.

[113] Velmenni. *Li-Fi Dongle and Access Point*. Accessed: 29/04/2024. 2023. URL: https://www.velmenni.com/lifi-dongle-access-points.

[114] N. Aste et al. “Performance analysis of a large-area luminescent solar concentrator module”. In: *Renewable Energy* 76 (2015), pp. 330–337. ISSN: 0960-1481. DOI: https://doi.org/10.1016/j.renene.2014.11.026. URL: https://www.sciencedirect.com/science/article/pii/S0960148114007411.

[115] Jun Zhang et al. “Optimization of large-size glass laminated luminescent solar concentrators”. In: *Solar Energy* 117 (2015), pp. 260–267. ISSN: 0038-092X. DOI: https://doi.org/10.1016/j.solener.2015.05.004. URL: https://www.sciencedirect.com/science/article/pii/S0038092X15002273.

[116] Yimu Zhao and Richard R. Lunt. “Transparent Luminescent Solar Concentrators for Large-Area Solar Windows Enabled by Massive Stokes-Shift Nanocluster Phosphors”. In: *Advanced Energy Materials* 3.9 (2013), pp. 1143–1148. DOI: https://doi.org/10.1002/aenm.201300173.

[117] A. Kerrouche et al. “Luminescent solar concentrators: From experimental validation of 3D ray-tracing simulations to coloured stained-glass windows for BIPV”. In: *Solar Energy Materials and Solar Cells* 122 (2014), pp. 99–106. ISSN: 0927-0248. DOI: https://doi.org/10.1016/j.solmat.2013.11.026. URL: https://www.sciencedirect.com/science/article/pii/S0927024813006107.

[118] Matthew R. Bergren et al. “High-Performance CuInS2 Quantum Dot Laminated Glass Luminescent Solar Concentrators for Windows”. In: *ACS Energy Letters* 3.3 (2018), pp. 520–525. DOI: 10.1021/acsenergylett.7b01346. eprint: https://doi.org/10.1021/acsenergylett.7b01346. URL: https://doi.org/10.1021/acsenergylett.7b01346.

[119] Mikhail Vasiliev et al. “Semi-Transparent Energy-Harvesting Solar Concentrator Windows Employing Infrared Transmission-Enhanced Glass and Large-Area Microstructured Diffractive Elements”. In: *Photonics* 5.3 (2018). ISSN: 2304-6732. DOI: 10.3390/photonics5030025. URL: https://www.mdpi.com/2304-6732/5/3/25.

[120] Jeroen A. H. P. Sol et al. “Multistate Luminescent Solar Concentrator “Smart” Windows”. In: *Advanced Energy Materials* 8.12 (2018). Cited by: 80; All Open Access, Green Open Access, Hybrid Gold Open Access. DOI: 10.1002/aenm.201702922. URL: https://www.scopus.com/inward/record.uri?eid=2-s2.0-

85040791523&doi=10.1002%2faenm.201702922&partnerID=40&md5=1e6755a886d7c230338eec832ae08a9b.

[121] Fahad Mateen et al. “Nitrogen-doped carbon quantum dot based luminescent solar concentrator coupled with polymer dispersed liquid crystal device for smart management of solar spectrum”. In: *Solar Energy* 178 (2019), pp. 48–55. ISSN: 0038-092X. DOI: https://doi.org/10.1016/j.solener.2018.12.013. URL: https://www.sciencedirect.com/science/article/pii/S0038092X18311897.

[122] Nikolay S. Makarov et al. “Fiber-Coupled Luminescent Concentrators for Medical Diagnostics, Agriculture, and Telecommunications”. In: *ACS Nano* 13.8 (2019). PMID: 31291097, pp. 9112–9121. DOI: 10.1021/acsnano.9b03335. eprint: https://doi.org/10.1021/acsnano.9b03335. URL: https://doi.org/10.1021/acsnano.9b03335.

[123] Pavlos P. Manousiadis et al. “Wide field-of-view fluorescent antenna for visible light communications beyond the étendue limit”. In: *Optica* 3.7 (July 2016), pp. 702–706. DOI: 10.1364/OPTICA.3.000702. URL: https://opg.optica.org/optica/abstract.cfm?URI=optica-3-7-702.

[124] Yurong Dong et al. “Nanopatterned luminescent concentrators for visible light communications”. In: *Opt. Express* 25.18 (Sept. 2017), pp. 21926–21934. DOI: 10.1364/OE.25.021926. URL: https://opg.optica.org/oe/abstract.cfm?URI=oe-25-18-21926.

[125] T. Peyronel et al. “Luminescent detector for free-space optical communication”. In: *Optica* 3.7 (July 2016), pp. 787–792. DOI: 10.1364/OPTICA.3.000787. URL: https://opg.optica.org/optica/abstract.cfm?URI=optica-3-7-787.

[126] Pavlos P. Manousiadis et al. “Optical Antennas for Wavelength Division Multiplexing in Visible Light Communications beyond the Étendue Limit”. In: *Advanced Optical Materials* 8.4 (2020), p. 1901139. DOI: https://doi.org/10.1002/adom.201901139. eprint: https://onlinelibrary.wiley.com/doi/pdf/10.1002/adom.201901139. URL: https://onlinelibrary.wiley.com/doi/abs/10.1002/adom.201901139.

[127] Zehang Wu. “Designing an optical link between a micro-display and a smartphone camera”. In: (2021). URL: http://resolver.tudelft.nl/uuid:99f57016-e503-4bda-b1ac-d47a64a1e7d8.

[128] Seyed Keyarash Ghiasi, Marco Kaldenbach, and Marco Zuniga. *Passive Screen-to-Camera Communication*. 2024. arXiv: 2403.16185.